Testing the Standard Model: Parity-Violating Asymmetry in Electron-Proton Scattering at Low Momentum Transfer

Christophe Match

A Thesis submitted to the Faculty of Graduate Studies of
The University of Manitoba
in partial fulfillment of the requirements for the degree of

MASTER OF SCIENCE

Department of Physics & Astronomy
University of Manitoba
Winnipeg, MB

Abstract

Fundamental interactions between electrons and protons, coupling between photons and Z bosons, and the underlying substructure of the proton, can all be probed through scattering experiments designed to measure the parity-violating asymmetry due to a mixing of electromagnetic and weak forces. Our research involves testing the limits of the Standard Model in search of new physics, by comparing high precision theoretical predictions of this asymmetry, along with the proton's weak charge and the weak mixing angle, to recent experimental measurements. We were ultimately able to achieve results consistent with experimental observations, by accounting for radiative corrections beyond single boson exchange. Our calculations include up to first-order Feynman diagrams containing 1 loop integrals, soft-photon bremsstrahlung, and we account for additional box diagram corrections. We also consider the addition of a new weakly-interacting dark Z boson (Z') to the Standard Model, and investigate how it affects the calculated asymmetry.

Contents

List of Figures

List of Tables

1 Introduction & Motivation

Our research is part of an effort by the broader subatomic physics community to understand the fundamental characteristics of particles and their interactions [3]. Currently, the Standard Model of particle physics encompasses the knowledge in this field, developed over the last 60 years. As modern technologies and improved experimental techniques develop, our measurements become more precise, and may show inconsistencies or new phenomena that are not included in our models. Therefore, the precision of theoretical models will also need to be improved in order to explain the experimental measurements.

The goal of our research is to improve the accuracy of predictions for the fundamental interactions between electrons and protons. The Standard Model describes matter at the smallest accessible scales, and this research will require detailed, precise calculations of the interaction properties at a foundational level. Fundamental particles are grouped into two types: leptons (i.e. electron, muon, tau, and corresponding three types of neutrinos) and quarks (i.e. constituents of hadrons, including proton and neutron). In this model, interactions are described as a particle exchange, in which forces are mediated by exchange-particles called gauge particles. Each of these interactions involves a mathematical expression with a parameter that gauges the strength of the interaction, and may be represented using so-called Feynman diagrams. The interaction strength varies with the energies of the interacting particles,

and these variations should be precisely theoretically calculated as well as experimentally measured. The variations are due to interactions in which multiple gauge particles are exchanged, and are called radiative corrections. The full theoretical calculations should account for radiative corrections to the leptonic and hadronic currents, as well as bremsstrahlung.

Electron scattering experiments are commonly used to investigate the target substructure, and to probe specific interactions at the sub-atomic level. The mixing of both the electromagnetic force and the parity-violating weak force creates an asymmetry, resulting in different reaction cross sections (i.e. probabilities) depending on the helicity of incident electrons. The fundamental weak charge of the proton can be measured indirectly by taking advantage of this difference in the interaction cross sections (i.e. parity-violating asymmetry), and is highly sensitive to new physics. Any observed inconsistency between the Standard Model predictions and experimental results could expose new types of particles and their unique characteristics. So, numerous research groups have an interest in calculating radiative corrections and testing the predictive power of the Standard Model. Many scattering experiment analyses have used the expressions outlined by Mo & Tsai [4], which were later updated and refined by Maximon & Tjon [5]. The calculation of parity-violating asymmetry observed in various scattering experiments has been thoroughly addressed [6, 7, 8], including the one-loop corrections [9, 10, 11], bremsstrahlung effects [12, 13], and up

to two-loop corrections [14, 15, 16, 17, 18].

Our research includes calculations of interactions between electrons and protons (i.e. electromagnetic and weak forces), with up to first-order Feynman diagrams. In order to achieve incredibly high accuracy and precision in our calculations of interaction probabilities (i.e. parity-violating asymmetry), the proton's weak charge, and ultimately the weak mixing angle, we must include additional radiative corrections. The leptonic vertex correction, the boson self-energy, and soft-photon bremsstrahlung are all explicitly calculated, and we account for the γZ box corrections (two-loop diagrams) in our final results, which are shown to be consistent with recent experimental measurements within the expected range of uncertainty. These calculations provide direct insight into the electro-weak interaction and the coupling strength between the photon and Z-boson gauge particles, as well as the proton structure form factors. The Q-weak experiment (A Precision Test of the Standard Model and Determination of the Weak Charges of the Quarks through Parity-Violating Electron Scattering) [1] at Jefferson Lab has measured the parity-violating asymmetry (A_{PV}) in polarized electron-proton scattering. Similarly, the P2 experiment [19] at Johannes Gutenberg University Mainz is scheduled to repeat the measurement at a lower energy. Specifically, the determination of the protons weak charge and the weak mixing angle will be extremely precise at very low momentum transfer and forward scattering angles. Electro-weak calculations are currently being carried out by independent research

groups (J. Erler et al. [20], Aleksejevs et al. [21]) using two different renormalization schemes, namely MS and OS schemes respectively. Our research will focus on one-loop calculations in the on-shell (OS) scheme, and involves radiative corrections to the leptonic current, parameterizing the relevant hadronic form factors, and systematically calculating the various Feynman diagrams. We also investigate how the addition of a new exchange boson (Z) affects the calculated asymmetry (A_{PV}) for polarized electron-proton scattering.

2 Background & Theory

In this section we will present the underlying theory used in our calculations, and review relevant work in the field for context. We first go through the types of fundamental particles and interactions in the Standard Model, then introduce scattering experiments and measurement of cross sections. We further discuss the importance of parity and intrinsic spin specifically for probing the weak interaction. Finally we review two recent scattering experiments, Q-Weak and P2, designed as precision tests of Standard Model predictions for the weak charge of the proton.

2.1 Standard Model of Particle Physics

A basic theoretical framework is required in order to describe nature at the most fundamental level, and to explain observed physical phenomena. The Standard Model (SM) of particle physics was developed in the 1970s, collecting and incorporating everything known about subatomic interactions, and providing insight into how the laws of physics are structured at the smallest possible scales. The SM provides the basis for all known particles and physical forces by classifying the fundamental units of matter into distinct categories, and describing their interactions as particle exchanges. Fundamental particles in the SM account for everything seen in our universe and are collectively grouped into two distinct types. Fermions are 'matter' particles with half-integer spin, while bosons are 'force-carrier' particles with integer spin (Higgs

boson being a special case). The idea that everything we see around us is composed of very small indivisible units of matter was introduced a long time ago in Greek philosophy. It was only more recently that the existence of the subatomic particles was confirmed, as J.J. Thomson was able to characterize the electron in 1897 and Rutherford discovered the positively charged heavy nucleus at the center of atoms in 1911.

We further distinguish two important types of fermions, leptons and quarks, which are the elementary building blocks of the universe and make up all observable matter. Both of these groups consist of 3 pairs of particles, termed first, second, and third generations based on their relative stability (i.e. mass). Unstable particles in the third generation will eventually decay into the more stable first generation particles. The first generation lepton is the electron (e), followed by the muon (μ), and finally the tau (τ), all of which carry a negative elementary charge of -1. Each of these is paired with a corresponding type of neutrino (ν_e, ν_μ, ν_τ) which are significantly less massive than the other leptons and carry no electric charge. Quarks are the constituents of hadrons, including the proton and neutron, and are governed by quantum chromodynamics (QCD) due to experiencing the strong force. The first pair of quarks is up & down, then charm & strange, and finally top & bottom. In addition to the 6 types of leptons and 6 types of quarks, each has a corresponding anti-particle which shares the same mass as the original particle, but all internal quantum numbers are

inverted (i.e. charge conjugation). Due to the half-integer spin of fermions, they are forbidden by the Pauli exclusion principal from occupying the same point in quantum space. In other words, no two indistinguishable fermions may share the same set of quantum numbers at any given time. Practically, this means electrons in the same vicinity must occupy different energy levels (orbitals) or maintain different quantum spin numbers.

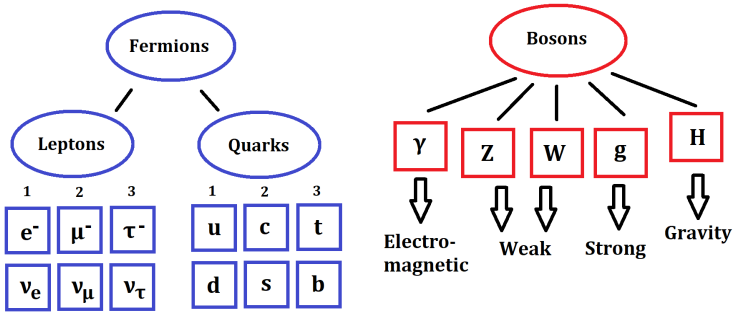

Fig. 1: Fundamental particles in the standard model, categorized into 3 generations of leptons and quarks, and all gauge bosons responsible for mediating the 4 physical forces.

The four fundamental interactions included in the SM are the strong force, electromagnetic (EM) force, weak force, and gravity, listed in order of decreasing strength. Both the EM force and gravity are infinitely ranged, while the strong and weak forces are generally on the scale of nuclear distances. According to the SM, all fundamental interactions are due to the exchange of a virtual gauge boson, which can discretely carry and transfer momentum and energy between particles. In terms of quantum field theory (QFT), fermions are producing and interacting through four fundamental force fields, while bosons are the quantized units of these interacting fields. Virtual

bosons are effectively force carriers that exist only as a means for the interaction. Since each type of field interacts differently, we can define a dimensionless coupling constant for each type of boson based on the strength of the interaction. These fundamental constants of nature are useful for characterizing different particles and predicting how they will interact with each force field. For example, the fine structure constant (α) is the dimensionless coupling parameter used to gauge the strength of the EM force.

The EM force acts between electrically charged particles, and the corresponding exchange boson is the massless photon. The weak force is responsible for the decay of left-handed quarks and leptons, and is mediated by the W and Z bosons. The strong force specifically binds quarks together according to QCD, and is controlled by the exchange of the gluon. Finally, gravity is the least understood of the fundamental forces, acting between all massive particles, and is thought to be governed by the Higgs graviton. The Higgs boson is a special type of 'carrier' for the Higgs field, which is responsible for generating mass in all particles through spontaneous symmetry breaking. Almost all of the bosons are electrically neutral, except for the W boson which can either carry a charge of +1 or -1. Unlike fermions, bosons are not limited by the Pauli exclusion principal and therefore many bosons can occupy the same quantum state at the same time.

The SM is the most precise theoretical tool to date for predicting how particles

interact at the sub-atomic level. Notably, the unification of electromagnetism and the weak interaction is entirely self-consistent and the theory accurately describes all associated experimental phenomena. Although the EM force is much stronger than the weak force due to the mass of the exchange bosons, both interactions must be taken into account for the extreme precision required to compare with experimental results. The predictive power of the theory, combined with the characterization of various particle interactions, allows for new technological developments and revelations in other fields such as astronomy or chemistry. The online database at http://pdg.lbl.gov summarizes all known particle properties and fundamental coupling constants.

2.2 Cross Section & Fermi's Golden Rule

In order to probe the particle - field interactions, we design high-energy scattering experiments, where an incoming beam of particles is accelerated to collide with target particles, and we observe the spatial distribution of scattered particles. The probability of finding specific particles due to the interaction is directly related to the experimental cross section (σ). This interaction probability depends on the type and number of target particles per unit area, and the cross section also depends on the flux of incoming particles (incoming particles per unit area per unit time). The rate is simply defined as number of interactions per unit time, and can be expressed in

terms of the transition probability (i.e. Hamiltonian).

$$\sigma = \frac{Interaction\ Rate}{\#Targets \times Incoming\ Flux} \tag{1}$$

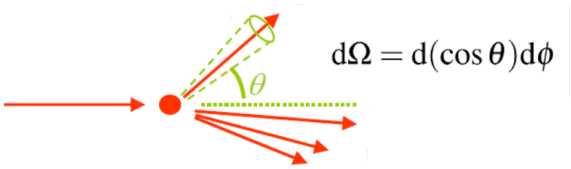

Fig. 2: Schematic description of particle beam scattering from a target, and an element of the solid angle.

The total cross section for the interaction is actually a sum over the entire angular distribution of the scattered particles.

$$\sigma = \int \frac{d\sigma}{d\Omega} d\Omega \tag{2}$$

In order to relate the physical quantity measured in scattering experiments to our theoretical model, we use Fermi's Golden Rule as stated in eqn. 3.

$$\omega = 2\pi\delta(E_f - E_i)|T|^2 d\rho_f \tag{3}$$

This interaction rate (ω) includes the transition amplitude squared, and the delta function ensures energy conservation for elastic scattering.The matrix element (T) corresponds to the transition from initial to final quantum eigenstates of the system,

using the interaction Hamiltonian. The density of final states ($d\rho_f$) accounts for the finite volume of phase space (V), and thus finite number of energy eigenstates, in which particles could be found after scattering. We can determine the flux of incoming particles (I), and the cross section σ can then be calculated and compared to the experimental measurement, by using controlled experimental parameters such as beam energy and detector resolution.

$$T = \langle \psi_f | \hat{H}_I | \psi_i \rangle \tag{4a}$$

$$d\rho_f = \frac{V}{(2\pi)^3} k_f E_f dE_f d\Omega \tag{4b}$$

$$I = \frac{k_i}{V E_i} \tag{4c}$$

$$\frac{d\sigma}{d\Omega} = \frac{\omega}{I} = \frac{V^2}{4\pi^2} |T|^2 E_i^2 dE_f \tag{4d}$$

In this example, we can look at elastic scattering of electrons off a stationary point charge (Z), and get an analytic expression for the Mott cross section. For simplicity we can neglect the electron mass and target recoil. The interaction Hamiltonian used for the following equation was simply for the electromagnetic interaction (i.e.

Coulomb potential).

$$|T|^2 = \frac{Z^2 e^4}{V^2 Q^4} |\mathcal{M}|^2 \tag{5a}$$

$$Q^2 = 4k^2 \sin^2(\theta/2) \tag{5b}$$

$$\frac{d\sigma}{d\Omega} = \frac{Z^2 E_i^2 \alpha^2}{4k^4 \sin^4(\theta/2)} |\mathcal{M}|^2 dE_f \tag{5c}$$

The transition rate can be expressed in terms of the Feynman amplitude squared (i.e. probability) associated with the relevant interaction. The total cross section for a scattering process involves the sum of all contributing Feynman amplitudes, including higher order terms (i.e. radiative corrections). However, the interaction probability decreases with more massive virtual particles being exchanged, so we can approximate the total cross section accurately using a finite set of the Feynman amplitudes. The cross section for the electron-proton interaction could be calculated fairly accurately using just the one Feynman diagram for the photon exchange. However, this provides no insight into the weak force interaction or couplings with the neutral Z boson.

2.3 Helicity & Parity Violation

A parity inversion can be thought of as a total spatial inversion, or a transformation of all 3 spatial coordinates (x,y,z). The intrinsic spin of a particle is parity-conserving, but the direction of travel flips under the transformation. In 1956, theoretical physi-

cists Lee and Yang proposed an experiment to test parity conservation of the weak interaction. The experiment, conducted by Wu et al. in the same year, investigated the decay of cobalt-60 atoms in a uniform magnetic field, producing a electron - electron antineutrino pair. Unexpectedly, the electrons were emitted preferentially in the direction opposite to the fixes nuclear spin, confirming parity-violation in the weak interaction. The orientation of spin with respect to the direction of travel determines the helicity of particles, which would be inverted under parity transformation. For a scattering experiment, the incoming electrons can be given a net positive or negative helicity, and the beam is said to be longitudinally polarized (analogous to circular polarization for photons). It is now well-known that the weak force is uniquely parity violating, meaning that the exchange of the Z boson has a preference for a particular helicity (spin orientation) of interacting particles. More specifically, only left-handed particles are subject to the weak force, when the intrinsic spin is opposite the direction of travel.

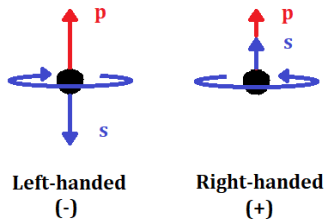

Fig. 3: Schematic description of positive and negative particle helicity, showing relative directions of momentum (p) in red and spin (s) in blue.

In order to extract the elusive features of the weak force, we can take advantage

of the parity violation by re-performing the experiment with the polarization of the incident electron beam flipped. In this way, we obtain two different cross sections, one for the right-handed interaction and one for the left-handed interaction. By calculating the difference between them, we are effectively removing the influence of any purely parity-conserving interactions (namely the dominant EM force) and highlighting the weak interaction terms in the final result. When normalized, this is termed the parity-violating asymmetry, and is a very small quantity due to the relative strength of the weak force. At tree-level, we can see in eqn. 7 that the parity-violating asymmetry numerator is determined by the interference-terms, involving both photon and Z boson exchange. This is in contrast to the individual cross sections in eqn. 6, which are dominated by the stronger EM interaction. Typically, the quadratic contributions from the Z boson exchange diagram can be neglected as they are relatively small. The higher order one-loop Feynman diagrams become necessary in order to accurately predict the asymmetry in our case.

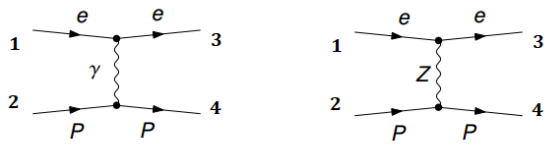

Fig. 4: Tree level Feynman diagrams for both electromagnetic and weak forces mediating the electron-proton interaction.

$$\begin{aligned}\sigma &\propto |\mathcal{M}_\gamma + \mathcal{M}_Z|^2 \\ &\propto |\mathcal{M}_\gamma|^2 + |\mathcal{M}_Z|^2 + 2Re(\mathcal{M}_\gamma^\dagger \cdot \mathcal{M}_Z) \approx |\mathcal{M}_\gamma|^2\end{aligned} \tag{6}$$

$$A_{PV} = \frac{\sigma_R - \sigma_L}{\sigma_R + \sigma_L} \propto \frac{2Re(\mathcal{M}_\gamma^\dagger \cdot \mathcal{M}_Z)_R - 2Re(\mathcal{M}_\gamma^\dagger \cdot \mathcal{M}_Z)_L}{2|\mathcal{M}_\gamma|^2} \tag{7}$$

2.4 Experimental Tests & Precision Calculation

Ultimately, we are seeking to either confirm the accuracy of the SM for specific interactions, or discover new physics beyond the existing SM framework. There are many questions left unsolved in the SM such as the abundance of matter over anti-matter, the full mechanism for gravity, and the existence of new fundamental particles (e.g. dark matter). In order to test a theory precisely, we need to measure fundamental physical quantities with extreme accuracy, and compare with theoretical predictions. If the calculation and measurement error bars are made small enough, then our theoretical models can be exposed as incomplete or as incredibly precise depending on if the results agree.

The weak charge of the proton is a fundamental coupling parameter that could be sensitive to new physics and is also precisely predicted by the SM. The weak mixing angle (a.k.a. Weinberg angle) unifies the EM and weak interactions by defining the re-

lation between their fundamental coupling constants, and therefore is directly related to the weak charge of all particles in the SM. The energy/momentum dependence of the weak mixing angle (θ_W) has been measured (fig. 5) but not to high precision at the TeV scale. This variation of θ_W can be explained by considering higher order radiative corrections in the theory, where more virtual particles are exchanged and produced/annihilated. Since the full interaction amplitude depends on the sum of all physically indistinguishable processes, including the entire set of radiative corrections would account for this energy dependence. Since the quantities measured at low energies are relatively small, we can use perturbation theory up to a specified order of accuracy to solve for interaction amplitudes, without including an infinite set of radiative corrections.

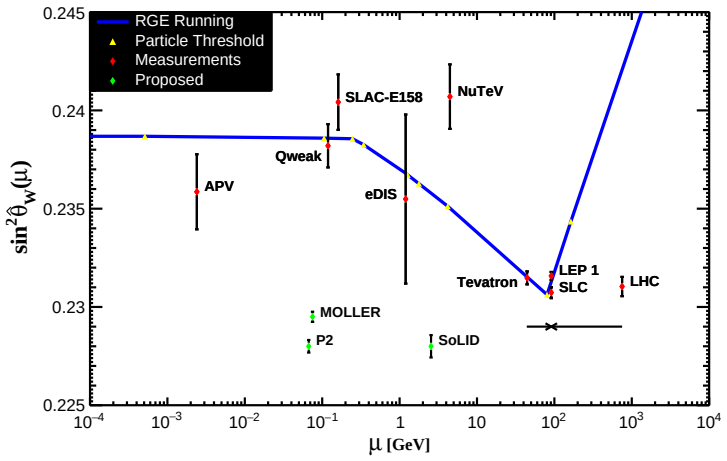

Fig. 5: Collection of experimental results and theoretical predictions for the energy dependence of $sin^2(\theta_W)$. Figure taken with persmission from Jens Erler

The weak charge of the proton (Q_W^p) can be measured indirectly, through the parity-violating asymmetry of the electron-proton interaction cross-section. In the SM, the weak charge is defined by θ_W at zero energy and momentum transfer, as seen in the tree-level (zeroth order) equation. 8. At vanishingly small momentum transfer, we can extrapolate results of the asymmetry in order to approximate the proton weak charge, according to eqn. 9. However, at higher energies, the proton structure form factors, embedded within $\mathcal{B}(\theta, Q^2)$, are necessary to relate the experimental asymmetry and the SM theory predictions. Multiple experiments, including Q-Weak and P2, are designed specifically to take advantage of parity-violation and extract features of the protons weak charge at low energies and with high precision.

$$Q_W^p = 1 - 4\sin^2\theta_W(Q^2 = 0) \tag{8}$$

$$A_{PV} = -\frac{G_F Q^2}{4\pi\alpha\sqrt{2}}\left(Q_W^p + Q^2\mathcal{B}(Q^2)\right) \tag{9}$$

2.4.1 Q-Weak

The Q-Weak experiment at Jefferson National Laboratory completed data collection in 2012, and the final results were published in 2018 after a thorough analysis process [1]. In order to get an experimental result for the parity-violating asymmetry, we measure the right and left handed cross sections for polarized electrons scattering elastically from liquid hydrogen at specific angles. We minimize unwanted

inelastic scattering by probing the interaction with low-momentum transfer. Also, we can reduce contributions from the proton substructure by scattering at forward angles. Collimators and polarimeters are used to set predetermined kinematics and to produce a narrowly focused beam of highly polarized electrons. The electron beam is accelerated with high current around a track to attain the desired energy, and then directed towards the intended target. Elastically scattered electrons which fall within the desired range of angles are then selected out using the spectrometer, made up of a large toroidal magnet, in order to deflect the electrons towards the detector. Finally, as the scattered electrons are redirected and passed through a layer of quartz, Cerenkov radiation is emitted and then collected by photo-multiplier tubes for analysis. With the measurement of parity-violating asymmetry (A_{PV}) and momentum transfer (Q^2), we can extract the weak charge of the proton and the weak mixing angle, according to equations 8 and 9, by neglecting the Q^4 terms since we are dealing with low energies and forward scattering angles. The relevant experimental parameters set by the equipment and design are listed in table 1.

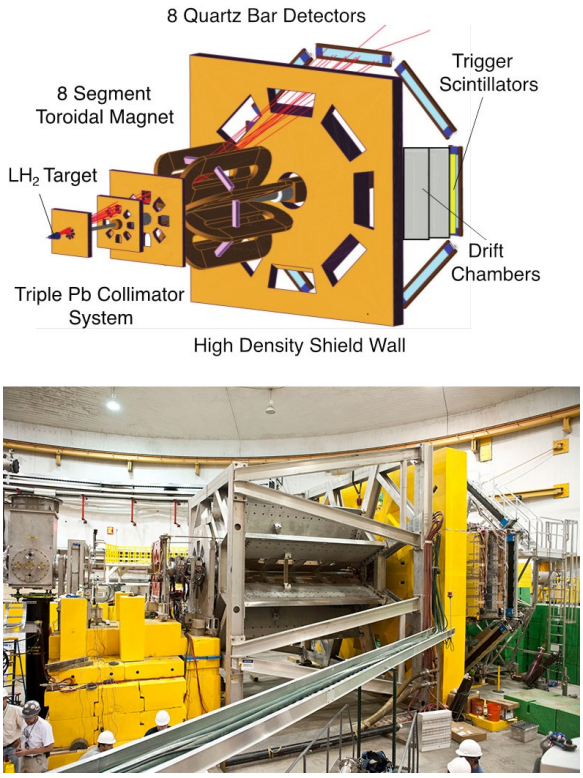

Fig. 6: Illustration (top) and actual picture (bottom) of the Q-Weak experimental setup in Hall C of of Jefferson Lab. Images taken from www.jlab.org

Central Scattering Angle	$7.9° \pm 3°$
Phi Acceptance	49% of 2π
Average Q^2	$0.0249 \pm 0.0006 GeV^2$
Beam Energy	$1.154 \pm 0.003 GeV$
Beam Current	$145 - 180 \mu$A
Beam Polarization	0.89 ± 0.018
Target Power	$2.5 kW$

Table 1: List of Q-Weak experimental parameters, as listed in [1]

The motivation for the Q-Weak experiment was to determine the weak charge of the proton to within $\pm 4\%$ uncertainty, which roughly translates to an uncertainty of 10 ppb in the measured asymmetry. Since the measured parity-violating asymme-

try is relatively small (on the scale of ppb), instrument precision and control of all systematic effects are crucial in order to get high accuracy in the results. Numerous small factors could influence the measurement and must be taken into account, such as polarization of the electron beam, density fluctuation in the liquid hydrogen target, symmetry in spectrometer magnet, and background noise in the detectors. The experimental measurements were ultimately successful, and after a lengthy analysis of the data, both statistical and systematic uncertainties were precisely determined for the parity-violating asymmetry. The final results and uncertainties are compiled in table 2 below.

Parity-Violating Asymmetry	-226.5 ppb
Statistical Uncertainty	$\pm$7.3 ppb
Systematic Uncertainty	$\pm$5.8 ppb
Proton Weak Charge	0.0719 ± 0.0045
$\sin^2\theta_W(Q^2 = 0)$	0.2382 ± 0.0011

Table 2: Final Q-Weak experimental results and calculated uncertainties [1] for the measured parity-violating asymmetry in electron-proton scattering, as well as the weak charge of the proton and the weak mixing angle.

Q-Weak is most precise measurement of the asymmetry, at the lowest q^2, compared to all other completed experiments. The precision and proximity to zero momentum transfer allows for accurate extrapolation to determine the protons weak charge, and for the ability to compare with the SM predictions.

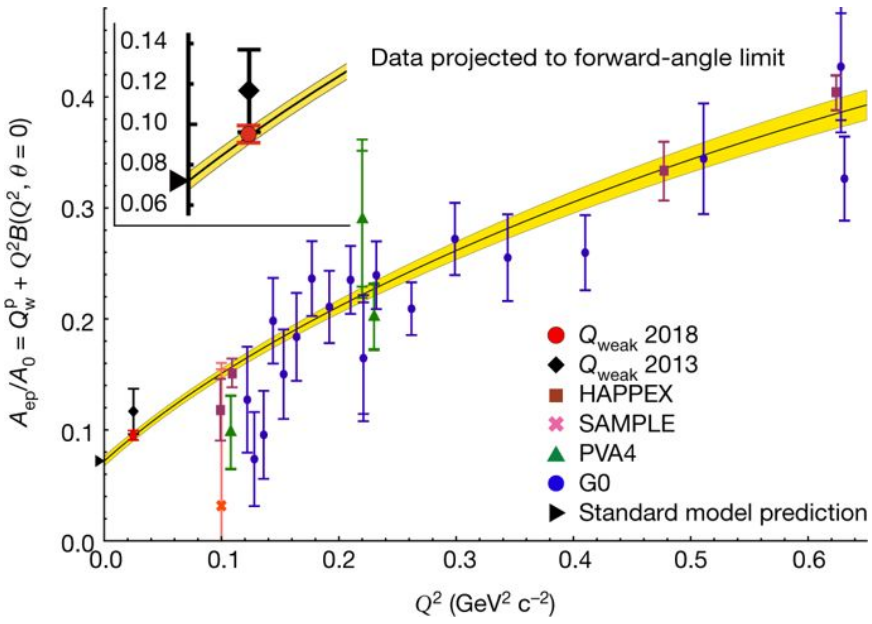

Fig. 7: Collection of experimental results for the reduced asymmetry, corresponding to eqn. 9, plotted against the momentum transfer. The standard model prediction is shown as a solid line, and the weak charge of the proton is at the intercept. Figure taken from [1]

2.4.2 P2

The P2 experiment [19] will make use of the new Mainz Energy Recovery Superconducting Accelerator (MESA) in order to measure the proton's weak charge and the weak mixing angle, through the parity-violating asymmetry in electron scattering from liquid hydrogen. The basis for this experiment is to improve the accuracy and precision of the Q-Weak measurements, by lowering the beam energy and thus the momentum transfer, closer to where the weak charge is defined. Also at lower energies, the higher order radiative corrections, such as box diagrams, will contribute much less to the interaction. In this way, other experiments could be complimented

by the low energy results in order to provide a full and accurate description of the Q^2 dependence. The experimental set-up is very similar to that of Q-Weak since the measurement process is the same. However, the new equipment will be designed with different parameters in mind, and will of course be tuned to get the most accurate results possible. The most notable improvements include a solenoid-spectrometer with 100% phi-acceptance, an atomic H trap polarimeter, a high power target with extremely low noise level, and newly updated detectors within the spectrometer.

Central Scattering Angle	$35^\circ \pm 20^\circ$
Phi Acceptance	2π
Average Q^2	$0.0045 GeV^2$
Beam Energy	$0.155 GeV$
Beam Current	150μA
Beam Polarization	0.85
Target Power	$4.0 kW$

Table 3: List of expected P2 experimental parameters

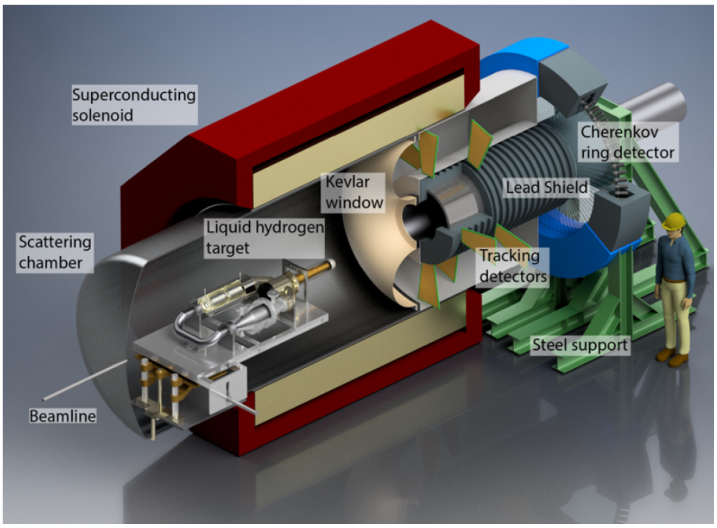

Fig. 8: Simulated drawing of the proposed experimental setup, at the MESA facility. Figure taken from the P2 critical design report [19]

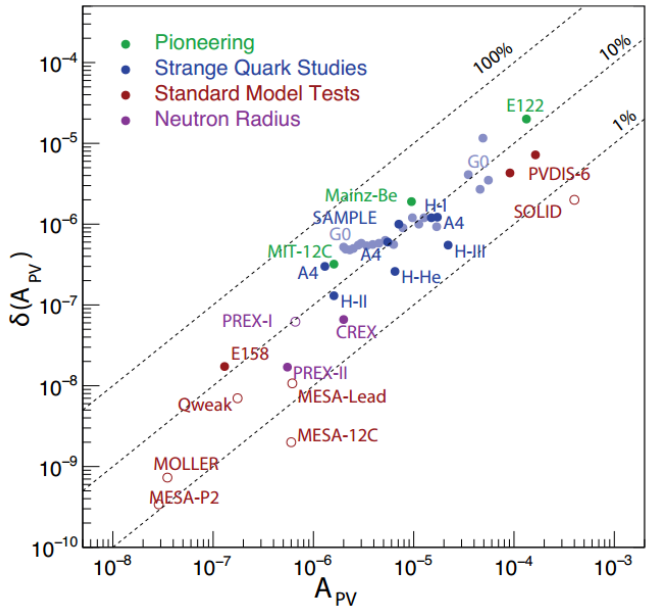

Fig. 9: Collection of experimental results for the parity-violating asymmetry, plotted against the corresponding estimated uncertainty. The diagonal dashed lines indicate to what percent the asymmetry is accurately determined, and the colored legend indicates the specific nature of the parity-violating scattering experiment. Figure taken from the P2 critical design report [19]

The main goal for the P2 experiment is to measure the weak mixing angle $\sin^2\theta_W$ to a precision of 0.14% at very low momentum transfer and beam energy [22]. As the energies are relatively low, the hadronic contributions and two-loop interactions are negligible, and the parity-violating asymmetry is very sensitive to the weak charge of the proton. As in the Q-Weak experiment, the experimentally observed quantity is so small that the results could be significantly affected by systematic effects in the equipment, so extreme precision and reliable instruments are required to ensure high accuracy. The construction at MESA is still ongoing for the P2 experiment, but there are preliminary designs and simulations made up to predict the experimental results and foresee any major issues. Above in table 3 we listed the proposed experimental parameters as reported in [19], and the average parity-violating asymmetry is expected to be $< A_{PV} >= 39.94 \pm 0.56$ ppb.

3 Calculations & Methods

Our goal is to use specific theories and models to probe the fundamental forces between elementary particles. Since we are interested in the weak force, we want to understand the Z boson coupling with electrons and protons, and predict the results of experimental tests precisely. As described in the previous section, the experimental results are in the form of cross sections (probabilities) which characterize the interaction, and ultimately we extract the parity-violating asymmetry. Starting from only the Feynman diagrams, we can use our theoretical tools to calculate the relevant cross sections and the asymmetry. In addition to the tree-level diagrams with a single boson exchange between scattered particles, there are higher-order diagrams called radiative corrections which should also be included in the full calculations. We will only consider up to first-order diagrams containing just 1 loop, which already involve high-order tensor integrals that need to be decomposed. We use reasonable approximations and assumptions throughout the numerical evaluation, in order to balance computational efficiency and accuracy of the results. We are using computer software Mathematica 9.0 (Wolfram Research, Inc.) to carry out the high-level calculations, which could not reasonably be completed on paper.

3.1 Feynman Rules

In order to determine the Feynman amplitude $\mathcal{M}$ used in calculating the cross section of a particular scattering process, we use a set of rules associated with the Feynman diagram for that process [23]. This allows for a procedural treatment of any diagram by breaking down the process into 3 components: external lines (particles), internal lines (propagators), and vertices (interactions). Feynman diagrams are a useful graphical representation of the scattering process, but also represent a mathematical expression used in calculating the transition amplitude. External lines (real particles) represent either dirac spinors in the case of fermions, or polarization vectors in the case of bosons. The arrow indicates the direction of momentum in the case of particles, and the opposite direction for anti-particles. Internal lines (virtual particles) are the propagators for the interaction, and have vertices at both ends. The explicit diagrams and Feynman rules for internal and external lines are well known and are placed in the appendix. A full description of the Feynman rules can be readily found in various textbooks [24, 25].

Vertices are where 3 lines intersect, and represent the interaction between particles. Each vertex requires an additional factor and depends on the coupling of the particle to the propagator. When the interacting particle is not point-like (e.g. proton), the vertex factors can be modified by form factors to account for the underlying physical substructure. As protons are made up of quarks, these semi-empirical form factors

are effectively used in place of higher level quantum chromodynamics calculations.

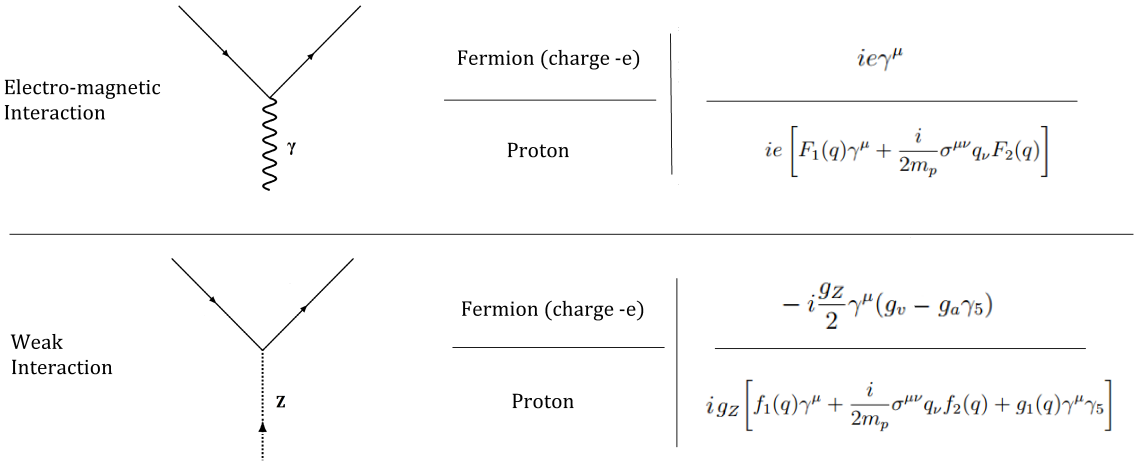

Fig. 10: Vertex factors associated with the E-M and Weak interactions for both the electron and proton.

$$g_Z = \frac{e}{\sin\theta_W \cos\theta_W} \tag{10a}$$

$$g_v = I_3 + 2\sin^2\theta_W \tag{10b}$$

$$g_a = I_3 \tag{10c}$$

$$\cos\theta_W = \frac{m_W}{m_Z} \tag{10d}$$

$$\sigma^{\mu\nu} = \frac{i}{2}(\gamma^{\mu}\gamma^{\nu} - \gamma^{\nu}\gamma^{\mu}) \tag{10e}$$

Here, I_3 refers to the 3rd component of the isospin (i.e. projection into the direction of motion), which for the electron is -1/2. Also, e is the elementary charge, and θ_W is the

weak mixing angle (i.e. Weinberg angle) which describes a fundamental relationship between the EM and weak forces, and relates the Z and W boson masses. Finally, q is the momentum transfer between interacting particles carried by the exchange boson, and can be defined as the difference between initial and final momenta of one of the scattered particles. The following values used for the proton, Z and W boson masses were obtained from http://pdg.lbl.gov (2018).

$$m_p = 0.938272081 GeV$$

$$m_Z = 91.1876 GeV$$

$$m_W = 80.379 GeV$$

We approximate the proton as a point particle, and make use of structural form factors $(F_1, F_2, f_1, f_2, g_1)$ to account for the underlying physics of quarks. F_1 and F_2 are known as the Dirac and Pauli form factors, and are related to the Fourier transform of charge and magnetization densities, respectively. Magnetic and electric form factors (G) are calculated in part using available experimental data for the proton and neutron, taken from [26] and [27] section 5.2, respectively. Strangeness form factors were taken from [27] section 5.3. In the following subscript notation, N denotes neutron, M and E denote magnetic and electric, and S is used to denote strangeness form factors. For the following numerical values, we have chosen to use the kinematics (i.e average momentum transfer) from the Q-Weak experiment, but

the full expressions for all form factors can be found in the appendix (Mathematica Code section 7.2).

$$q^2 = -T = 0.0249 GeV^2$$

$$\tau = \frac{-T}{4m_p^2} = 0.00709537$$

$$G_M = 2.60619 \qquad G_E = 0.933166$$

$$G_{MN} = -1.76319 \qquad G_{EN} = 0.0146635$$

$$G_{MS} = 0.0672367 \qquad G_{ES} = 0.0020677$$

$$F_1 = \frac{\tau G_M + G_E}{1+\tau} \qquad F_2 = \frac{G_M - G_E}{1+\tau} \tag{11a}$$

$$F_{1N} = \frac{\tau G_{MN} + G_{EN}}{1+\tau} \qquad F_{2N} = \frac{G_{MN} - G_{EN}}{1+\tau} \tag{11b}$$

$$F_{1S} = \frac{\tau G_{MS} + G_{ES}}{1+\tau} \qquad F_{2S} = \frac{G_{MS} - G_{ES}}{1+\tau} \tag{11c}$$

$$f_1 = (\frac{1}{2} - \sin^2\theta_W)\frac{F_1 - F_{1N}}{2} - \sin^2\theta_W \frac{F_1 + F_{1N}}{2} - \frac{1}{4}F_{1S} \tag{11d}$$

$$f_2 = (\frac{1}{2} - \sin^2\theta_W)\frac{F_2 - F_{2N}}{2} - \sin^2\theta_W \frac{F_2 + F_{2N}}{2} - \frac{1}{4}F_{2S} \tag{11e}$$

$$g_1 = \frac{1.267}{4(1 - T/1.014^2)^2} \tag{11f}$$

There are a few additional factors needed to account for energy conservation which are usually omitted until numerical calculation is required. For every vertex

and internal line present in the Feynman diagram, we must integrate over the 4-momentum of the virtual particle and include the corresponding factors. Outgoing momenta (denoted using arrows) are given a negative sign. For a specific example on calculating the Feynman amplitudes from diagrams using these rules, we explicitly show our calculation in the Results & Analysis section (5.1).

3.2 Tensor Decomposition

Tensor decomposition [28, 9] is a useful technique when dealing with general one-loop tensor integrals $T^N_{\mu_1...\mu_n}$ which appear in the Feynman amplitude for loop diagrams.

$$T^N_{\mu_1...\mu_n}(k_1...k_{N-1}, m_1...m_{N-1}) = \int \frac{q_{\mu_1}...q_{\mu_n}}{\mathcal{D}_0\mathcal{D}_1...\mathcal{D}_{N-1}} d^D q \tag{12}$$

$$\mathcal{D}_0 = q^2 - \lambda^2$$

$$\mathcal{D}_i = (q + k_i)^2 - m_i^2$$

In shorthand notation we can write $T^1_{\mu_1...\mu_n} = A_{\mu_1...\mu_n}$, $T^2_{\mu_1...\mu_n} = B_{\mu_1...\mu_n}$, etc... where N denotes the number of denominators multiplied together.

The denominators $\mathcal{D}$ arise from propagators within the loop, and the momenta in the numerator come from the propagators or the vertex factors. Unlike tree level processes where the momenta of internal lines are set by total momentum conservation, the momenta within the loop must be integrated over to account for all possible

distributions. By reducing the complicated tensor integrals down to scalar integrals, we can solve them using well-known numerical methods [29]. As described by Peskin & Schroeder [24], the integrals can be solved using a simple procedure which involves Feynman parameters, variable replacements, and Wick rotation. The first few scalar integrals are given below in eqn. 13.

$$A_0(\lambda) = \int \frac{1}{\mathcal{D}_0} d^D q \tag{13a}$$

$$A_0(k_i, m_i) = \int \frac{1}{\mathcal{D}_i} d^D q \tag{13b}$$

$$B_0(k_i, m_i, \lambda) = \int \frac{1}{\mathcal{D}_0 \mathcal{D}_i} d^D q \tag{13c}$$

$$C_0(k_j, m_j, k_i, m_i, \lambda) = \int \frac{1}{\mathcal{D}_0 \mathcal{D}_i \mathcal{D}_j} d^D q \tag{13d}$$

The tensor decomposition technique [28, 9] allows us to rewrite the integrals as linear combinations of coefficient functions that may easily be reduced into basic expressions. Effectively, we rewrite the tensor integral in terms of basic scalar integrals using linear algebra techniques. There are numerous methods and computational algorithms designed for solving complicated integrals, both numerically and analytically [30, 31, 32]. Examples of how to further reduce the tensor integrals to basic expressions will be given in the next subsection (Radiative Corrections). Some useful tensor decomposition expressions are given in eqn. 14.

$$B_\mu = \int \frac{q_\mu}{\mathcal{D}_0 \mathcal{D}_1} d^D q = k_{1\mu} b_1 \tag{14a}$$

$$B_{\mu\nu} = \int \frac{q_\mu q_\nu}{\mathcal{D}_0 \mathcal{D}_1} d^D q = g_{\mu\nu} b_{00} + k_{1\mu} k_{1\nu} b_{11} \tag{14b}$$

$$C_\mu = \int \frac{q_\mu}{\mathcal{D}_0 \mathcal{D}_1 \mathcal{D}_2} d^D q = \sum_{i=1}^{2} k_{i\mu} c_i \tag{14c}$$

$$C_{\mu\nu} = \int \frac{q_\mu q_\nu}{\mathcal{D}_0 \mathcal{D}_1 \mathcal{D}_2} d^D q = g_{\mu\nu} c_{00} + \sum_{i,j=1}^{2} k_{i\mu} k_{j\nu} c_{ij} \tag{14d}$$

$$C_{\mu\nu\delta} = \int \frac{q_\mu q_\nu q_\delta}{\mathcal{D}_0 \mathcal{D}_1 \mathcal{D}_2} d^D q = \sum_{i=1}^{2} (g_{\mu\nu} k_{i\delta} + g_{\nu\delta} k_{i\mu} + g_{\mu\delta} k_{i\nu}) c_{00i} + \sum_{i,j,p=1}^{2} k_{i\mu} k_{j\nu} k_{p\delta} c_{ijp} \tag{14e}$$

The trick is to further contract the integral with a useful expression, such as the metric tensor $g_{\mu\nu}$ or wavenumber k_1^μ, in order to reduce the entire expression into a simpler form. The goal is to solve for the coefficients in terms of known scalar integrals, and then replace them in the original tensor decomposition formula.

3.3 Radiative Corrections

As our theoretical models and calculations are never exact, we use perturbation theory to estimate quantities to a known accuracy depending on the level of calculation. The series of Feynman diagrams for a specific scattering process are derived by starting from a single boson exchange (tree-level diagram) and adding

leading order corrections from contributing processes. These so-called radiative corrections would include the exchange of multiple bosons, pair creation/annihilation, and bremsstrahlung. As the cross section for a scattering process involves the sum of all contributing Feynman amplitudes, the parity violating asymmetry will also depend on the level of calculation.

3.3.1 Boson Self-Energy

The self energy diagram represents the decay of an propagator into two virtual particles, which subsequently recombine to reform the propagator. The momenta around the loop must be integrated over, as they are not fixed by total momentum conservation.

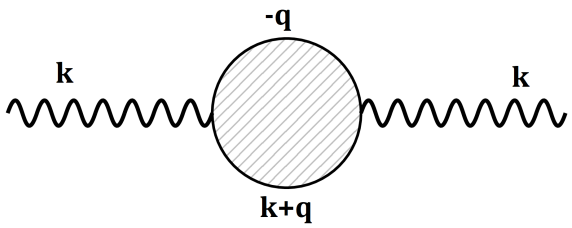

Fig. 11: Truncated Feynman diagram for one-loop QED self-energy

Using the above diagram and the Feynman rules in section 4.1, we can write down

a truncated amplitude for the self-energy loop.

$$\begin{aligned}
&\int d^D q (ie\gamma^\mu) \frac{i(-\not{q} + m_1)}{q^2 - m_1^2} (ie\gamma^\nu) \frac{i(\not{k} + \not{q} + m_2)}{(k+q)^2 - m_2^2} \\
&\propto \int d^D q \frac{\gamma^\mu(-\not{q} + m_1)\gamma^\nu(\not{k} + \not{q} + m_2)}{(q^2 - m_1^2)[(k+q)^2 - m_2^2]} \\
&\propto \int d^D q \frac{\gamma^\mu(-\not{q} + m_1)\gamma^\nu(\not{k} + \not{q} + m_2)}{\mathcal{D}_0 \mathcal{D}_2}
\end{aligned} \tag{15}$$

The numerator can be expanded into terms grouped by order of q.

$$\begin{aligned}
\gamma^\mu(-\not{q} + m_1)\gamma^\nu(\not{k} + \not{q} + m_2) =& m_1 m_2 \gamma^\mu\gamma^\nu + m_1\gamma^\mu\gamma^\nu\not{k} \\
&+ m_1\gamma^\mu\gamma^\nu\not{q} - \gamma^\mu\not{q}\gamma^\nu\not{k} - m_2\gamma^\mu\not{q}\gamma^\nu \\
&- \gamma^\mu\not{q}\gamma^\nu\not{q}
\end{aligned} \tag{16}$$

We can clearly see that the integral consists of three types of tensor integrals $B_0, B_\alpha, B_{\alpha\beta}$. So we need to reduce B_α and $B_{\alpha\beta}$ using the tensor decomposition expressions from eqn. 14, and then express the coefficients in terms of basic scalar integrals. We first contract B_α with k^α in order to reduce the expression.

$$\begin{aligned}
k^\alpha B_\alpha = k^2 b_2 &= \int \frac{k^\alpha q_\alpha}{\mathcal{D}_0 \mathcal{D}_2} d^D q \\
&= \frac{1}{2} \int \frac{[(k+q)^2 - m_2^2] - (k^2 - m_2^2) - (q^2 - m_1^2) - m_1^2}{(q^2 - m_1^2)[(k+q)^2 - m_2^2]} d^D q \\
&= \frac{1}{2} \left[\int \frac{1}{\mathcal{D}_0} d^D q - (k^2 - m_2^2 + m_1^2) \int \frac{1}{\mathcal{D}_0 \mathcal{D}_2} d^D q - \int \frac{1}{\mathcal{D}_2} d^D q \right]
\end{aligned}$$

$$\therefore b_2 = \frac{1}{2k^2}[A_0(m_1) - (k^2 - m_2^2 + m_1^2)B_0(k, m_2, m_1) - A_0(k, m_2)] \tag{17}$$

Now we want to contract $B_{\alpha\beta}$ first with the metric tensor $g^{\alpha\beta}$ and then with k^α to get a set of two reduced equations.

$$\begin{aligned} g^{\alpha\beta}B_{\alpha\beta} = 4b_{00} + k^2 b_{22} &= \int \frac{(q^2 - m_1^2) + m_1^2}{\mathcal{D}_0\mathcal{D}_2} d^D q \\ &= \int \frac{1}{\mathcal{D}_2} d^D q + m_1^2 \int \frac{1}{\mathcal{D}_0\mathcal{D}_2} d^D q \\ &= A_0(k, m_2) + m_1^2 B_0(k, m_2, m_1) \end{aligned}$$

$$\begin{aligned} k^\alpha B_{\alpha\beta} = k_\beta b_{00} + k^2 k_\beta b_{22} &= \int \frac{(k^\alpha q_\alpha) q_\beta}{\mathcal{D}_0\mathcal{D}_2} d^D q \\ &= \frac{1}{2}\int q_\beta \frac{[(k+q)^2 - m_2^2] - (k^2 - m_2^2) - (q^2 - m_1^2) - m_1^2}{(q^2 - m_1^2)[(k+q)^2 - m_2^2]} d^D q \\ &= \frac{1}{2}\left[\int \frac{q_\beta}{\cancel{\mathcal{D}_0}} \cancel{d^D q} - (k^2 - m_2^2 + m_1^2)\int \frac{q_\beta}{\mathcal{D}_0\mathcal{D}_2} d^D q - \int \frac{q_\beta}{\mathcal{D}_2} d^D q\right] \\ &= -\frac{1}{2}(k^2 - m_2^2 + m_1^2)k_\beta b_2 - \frac{1}{2}\int \frac{q_\beta}{(k+q)^2 - m_2^2} d^D q \\ &= -\frac{1}{2}(k^2 - m_2^2 + m_1^2)k_\beta b_2 - \frac{1}{2}\int \frac{q_\beta - k_\beta}{q^2 - m_2^2} d^D q \\ &= -\frac{1}{2}(k^2 - m_2^2 + m_1^2)k_\beta b_2 + \frac{1}{2}k_\beta A_0(m_2) \end{aligned}$$

Where we have used the substitution $q_\beta \to q_\beta - k_\beta$ which does not affect the integration variable. With the system of two reduced equations we can easily solve for the two

remaining coefficients.

$$\therefore b_{00} = \frac{1}{6}\left(2A_0(k, m_2) - A_0(m_2) + (k^2 - m_2^2 + m_1^2)b_2\right) + \frac{1}{3}m_1^2 B_0(k, m_2, m_1) \quad (18)$$

$$\therefore b_{22} = \frac{1}{k^2}(A_0(k, m_2) + m_1^2 B_0(k, m_2, m_1) - 4b_{00}) \quad (19)$$

3.3.2 Vertex Correction

The vertex correction represents the change in particle response to the incoming field. At the one-loop level, this results in a three-point integral represented by a triangle graph.

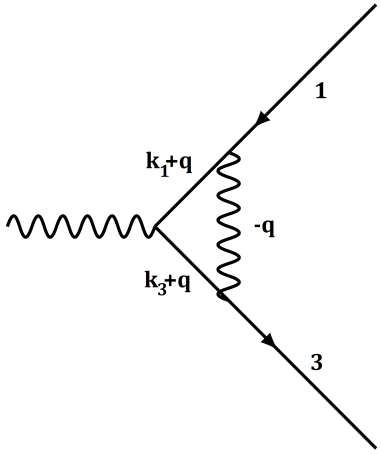

Fig. 12: Truncated Feynman diagram for one-loop QED vertex correction

As seen in the Feynman diagram, there is an additional propagator which forms a loop between the two external lines. The truncated amplitude for the one-loop vertex

correction can be written according to the Feynman rules.

$$\begin{aligned}
&\int d^D q (ie\gamma^\mu) \frac{i(\not{k}_3 + \not{q} + m)}{(k_3+q)^2 - m^2} (ie\gamma^\delta) \frac{i(\not{k}_1 + \not{q} + m)}{(k_1+q)^2 - m^2} \left(\frac{-ig_{\mu\nu}}{q^2 - \lambda^2} \right) (ie\gamma^\nu) \\
&\propto \int d^D q \frac{\gamma^\mu(\not{k}_3 + \not{q} + m)\gamma^\delta(\not{k}_1 + \not{q} + m)\gamma_\mu}{(q^2-\lambda^2)[(k_1+q)^2 - m^2][(k_3+q)^2 - m^2]} \\
&\propto \int d^D q \frac{\gamma^\mu(\not{k}_3 + \not{q} + m)\gamma^\delta(\not{k}_1 + \not{q} + m)\gamma_\mu}{\mathcal{D}_0 \mathcal{D}_1 \mathcal{D}_3}
\end{aligned} \tag{20}$$

The numerator can be expanded into terms grouped by order of q.

$$\begin{aligned}
\gamma^\mu(\not{k}_3 + \not{q} + m)\gamma^\delta(\not{k}_1 + \not{q} + m)\gamma_\mu =& m^2\gamma^\mu\gamma^\delta\gamma_\mu + m\gamma^\mu\not{k}_3\gamma^\delta\gamma_\mu + m\gamma^\mu\gamma^\delta\not{k}_1\gamma_\mu + \gamma^\mu\not{k}_3\gamma^\delta\not{k}_1\gamma_\mu \\
&+ m\gamma^\mu\not{q}\gamma^\delta\gamma_\mu + m\gamma^\mu\gamma^\delta\not{q}\gamma_\mu + \gamma^\mu\not{q}\gamma^\delta\not{k}_1\gamma_\mu + \gamma^\mu\not{k}_3\gamma^\delta\not{q}\gamma_\mu \\
&+ \gamma^\mu\not{q}\gamma^\delta\not{q}\gamma_\mu
\end{aligned} \tag{21}$$

We can directly see that the integral consists of three types of tensor integrals $C_0, C_\alpha, C_{\alpha\beta}$. So we need to reduce C_α and $C_{\alpha\beta}$ using the tensor decomposition expressions from eqn. 14. We first contract C_α with k_1^α and k_3^α in order to reduce the expression. For this case, we have $k_1^2 = k_3^2 = m^2$.

$$C_\alpha = k_{1\alpha}c_1 + k_{3\alpha}c_3$$

$$
\begin{aligned}
k_1^\alpha C_\alpha = m^2 c_1 + k_1^\alpha k_{3\alpha} c_3 &= \int \frac{k_1^\alpha q_\alpha}{\mathcal{D}_0 \mathcal{D}_1 \mathcal{D}_3} d^D q \\
&= \frac{1}{2} \int \frac{[(k_1+q)^2 - m^2] - \cancel{(k_1^2 - m^2)} - q^2}{\mathcal{D}_0 [(k_1+q)^2 - m^2] \mathcal{D}_3} d^D q \\
&= \frac{1}{2} \int \left[\frac{1}{\mathcal{D}_0 \mathcal{D}_3} - \frac{q^2 - \lambda^2}{\mathcal{D}_0 \mathcal{D}_1 \mathcal{D}_3} - \frac{\lambda^2}{\mathcal{D}_0 \mathcal{D}_1 \mathcal{D}_3} \right] d^D q \\
&= \frac{1}{2} \left[B_0(k_3, m, \lambda) - B_0(k_3 - k_1, m, m) - \lambda^2 C_0(k_3, m, k_1, m, \lambda) \right] \\
&\equiv S_1
\end{aligned}
$$

$$
\begin{aligned}
k_3^\alpha C_\alpha = k_3^\alpha k_{1\alpha} c_1 + m^2 c_3 &= \int \frac{k_3^\alpha q_\alpha}{\mathcal{D}_0 \mathcal{D}_1 \mathcal{D}_3} d^D q \\
&= \frac{1}{2} \int \frac{[(k_3+q)^2 - m^2] - \cancel{(k_3^2 - m^2)} - q^2}{\mathcal{D}_0 \mathcal{D}_1 [(k_3+q)^2 - m^2]} d^D q \\
&= \frac{1}{2} \int \left[\frac{1}{\mathcal{D}_0 \mathcal{D}_1} - \frac{q^2 - \lambda^2}{\mathcal{D}_0 \mathcal{D}_1 \mathcal{D}_3} - \frac{\lambda^2}{\mathcal{D}_0 \mathcal{D}_1 \mathcal{D}_3} \right] d^D q \\
&= \frac{1}{2} \left[B_0(k_1, m, \lambda) - B_0(k_3 - k_1, m, m) - \lambda^2 C_0(k_3, m, k_1, m, \lambda) \right] \\
&\equiv S_3
\end{aligned}
$$

By solving this this system of 2 equations, we can express the coefficients in terms of the basic scalar integrals.

$$
G = \begin{vmatrix} m^2 & k_1 \cdot k_3 \\ k_1 \cdot k_3 & m^2 \end{vmatrix} = m^4 - (k_1 \cdot k_3)^2
$$

$$
\therefore c_1 = \frac{\begin{vmatrix} S_1 & k_1 \cdot k_3 \\ S_3 & m^2 \end{vmatrix}}{G} = \frac{m^2 S_1 - k_1 \cdot k_3 S_3}{m^4 - (k_1 \cdot k_3)^2} \tag{22}
$$

$$\therefore c_3 = \frac{\begin{vmatrix} m^2 & S_1 \\ k_1 \cdot k_3 & S_3 \end{vmatrix}}{G} = \frac{m^2 S_3 - k_1 \cdot k_3 S_1}{m^4 - (k_1 \cdot k_3)^2} \tag{23}$$

Now, we want to contract $C_{\alpha\beta}$ with the metric tensor $g^{\alpha\beta}$, $k_1^\alpha k_1^\beta$, $k_3^\alpha k_3^\beta$, and $k_1^\alpha k_3^\beta$ in order to get a set of reduced equations. We already know that $c_{13} = c_{31}$ since $k_1^2 = k_3^2 = m^2$, so we have just four unknown coefficients. In the following notation, $(k_1 k_3)$ represents the dot product $k_1 \cdot k_3$, and b_3 refers back to eqn. 17 with variables (k, m_2, m_1) replaced as indicated.

$$C_{\alpha\beta} = g_{\alpha\beta} c_{00} + k_{1\alpha} k_{1\beta} c_{11} + k_{3\alpha} k_{3\beta} c_{33} + (k_{1\alpha} k_{3\beta} + k_{1\beta} k_{3\alpha}) c_{13}$$

$$\begin{aligned} g^{\alpha\beta} C_{\alpha\beta} &= 4c_{00} + m^2 c_{11} + m^2 c_{33} + 2(k_1 k_3) c_{13} \\ &= \int \frac{(q^2 - \lambda^2) + \lambda^2}{\mathcal{D}_0 \mathcal{D}_1 \mathcal{D}_3} d^D q \\ &= \int \frac{1}{\mathcal{D}_1 \mathcal{D}_3} d^D q + \lambda^2 \int \frac{1}{\mathcal{D}_0 \mathcal{D}_1 \mathcal{D}_3} d^D q \\ &= B_0(k_3 - k_1, m, m) + \lambda^2 C_0(k_3, m, k_1, m, \lambda) \\ &\equiv T_{00} \end{aligned} \tag{24}$$

$$
\begin{aligned}
k_1^\alpha k_1^\beta C_{\alpha\beta} &= m^2 c_{00} + m^4 c_{11} + (k_1 k_3)^2 c_{33} + 2m^2 (k_1 k_3) c_{13} \\
&= \int \frac{(k_1 q)^2}{\mathcal{D}_0 \mathcal{D}_1 \mathcal{D}_3} d^D q \\
&= \frac{1}{2} \int \left[\frac{(k_1 q)}{\mathcal{D}_0 \mathcal{D}_3} - \frac{(k_1 q)(q^2 - \lambda^2)}{\mathcal{D}_0 \mathcal{D}_1 \mathcal{D}_3} - \frac{(k_1 q)\lambda^2}{\mathcal{D}_0 \mathcal{D}_1 \mathcal{D}_3} \right] d^D q \\
&= \frac{1}{4} \int \left[\frac{2 k_1^\alpha q_\alpha}{\mathcal{D}_0 \mathcal{D}_3} - \frac{\mathcal{D}_1 - q^2}{\mathcal{D}_1 \mathcal{D}_3} - \lambda^2 \frac{\mathcal{D}_1 - q^2}{\mathcal{D}_0 \mathcal{D}_1 \mathcal{D}_3} \right] d^D q \\
&= \frac{1}{2} (k_1 k_3) b_2(k_3, m, \lambda) \\
&\quad - \frac{1}{4} \int \left[\frac{1}{\mathcal{D}_3} - \frac{\mathcal{D}_1 + 2(k_1 q)}{\mathcal{D}_1 \mathcal{D}_3} \right] d^D q - \frac{\lambda^2}{4} \int \left[\frac{1}{\mathcal{D}_0 \mathcal{D}_3} - \frac{(q^2 - \lambda^2) + \lambda^2}{\mathcal{D}_0 \mathcal{D}_1 \mathcal{D}_3} \right] d^D q \\
&= \frac{1}{2} (k_1 k_3) b_2(k_3, m, \lambda) \\
&\quad + \frac{k_{1\alpha}}{2} \int \left[\frac{q^\alpha}{\mathcal{D}_1 \mathcal{D}_3} \right] d^D q - \frac{\lambda^2}{4} \int \left[\frac{1}{\mathcal{D}_0 \mathcal{D}_3} - \frac{1}{\mathcal{D}_1 \mathcal{D}_3} - \frac{\lambda^2}{\mathcal{D}_0 \mathcal{D}_1 \mathcal{D}_3} \right] d^D q \\
&= \frac{1}{2} (k_1 k_3) b_2(k_3, m, \lambda) + \frac{1}{2} \left[(k_1 k_3) - m^2 \right] b_2(k_3 - k_1, m, m) - \frac{m^2}{2} B_0(k_3 - k_1, m, m) \\
&\quad - \frac{\lambda^2}{4} \left[B_0(k_3, m, \lambda) - B_0(k_3 - k_1, m, m) - \lambda^2 C_0(k_3, m, k_1, m, \lambda) \right] \\
&\equiv T_{11}
\end{aligned}
\tag{25}
$$

Using almost the same exact procedure, we can also determine the following:

$$
\begin{aligned}
k_3^\alpha k_3^\beta C_{\alpha\beta} &= m^2 c_{00} + (k_1 k_3)^2 c_{11} + m^4 c_{33} + 2m^2 (k_1 k_3) c_{13} \\
&= \int \frac{(k_3 q)^2}{\mathcal{D}_0 \mathcal{D}_1 \mathcal{D}_3} d^D q \\
&= \frac{1}{4} \int \left[\frac{2 k_3^\alpha q_\alpha}{\mathcal{D}_0 \mathcal{D}_1} - \frac{\mathcal{D}_3 - q^2}{\mathcal{D}_1 \mathcal{D}_3} - \lambda^2 \frac{\mathcal{D}_3 - q^2}{\mathcal{D}_0 \mathcal{D}_1 \mathcal{D}_3} \right] d^D q \\
&= \frac{1}{2} (k_1 k_3) b_2(k_1, m, \lambda) \\
&\quad - \frac{1}{4} \int \left[\frac{1}{\mathcal{D}_1} - \frac{\mathcal{D}_3 + 2(k_3 q)}{\mathcal{D}_1 \mathcal{D}_3} \right] d^D q - \frac{\lambda^2}{4} \int \left[\frac{1}{\mathcal{D}_0 \mathcal{D}_1} - \frac{(q^2 - \lambda^2) + \lambda^2}{\mathcal{D}_0 \mathcal{D}_1 \mathcal{D}_3} \right] d^D q \\
&= \frac{1}{2} (k_1 k_3) b_2(k_1, m, \lambda) + \frac{1}{2} \left[(k_1 k_3) - m^2 \right] b_2(k_1 - k_3, m, m) - \frac{m^2}{2} B_0(k_1 - k_3, m, m) \\
&\quad - \frac{\lambda^2}{4} \left[B_0(k_1, m, \lambda) - B_0(k_1 - k_3, m, m) - \lambda^2 C_0(k_3, m, k_1, m, \lambda) \right] \\
&\equiv T_{33}
\end{aligned}
\tag{26}
$$

$$
\begin{aligned}
k_1^\alpha k_3^\beta C_{\alpha\beta} &= (k_1k_3)c_{00} + m^2(k_1k_3)(c_{11}+c_{33}) + [m^4+(k_1k_3)^2]c_{13} \\
&= \int \frac{(k_1q)(k_3q)}{\mathcal{D}_0\mathcal{D}_1\mathcal{D}_3} d^Dq \\
&= \frac{1}{2}\int \left[\frac{(k_3q)}{\mathcal{D}_0\mathcal{D}_3} - \frac{(k_3q)(q^2-\lambda^2)}{\mathcal{D}_0\mathcal{D}_1\mathcal{D}_3} - \frac{(k_3q)\lambda^2}{\mathcal{D}_0\mathcal{D}_1\mathcal{D}_3}\right] d^Dq \\
&= \frac{1}{2}m^2 b_2(k_3,m,\lambda) - \frac{1}{4}\int \left[\frac{1}{\mathcal{D}_1} - \frac{\mathcal{D}_3+2(k_3q)}{\mathcal{D}_1\mathcal{D}_3}\right] d^Dq - \frac{\lambda^2}{4}\int \left[\frac{1}{\mathcal{D}_0\mathcal{D}_1} - \frac{(q^2-\lambda^2)+\lambda^2}{\mathcal{D}_0\mathcal{D}_1\mathcal{D}_3}\right] d^Dq \\
&= \frac{1}{2}m^2 b_2(k_3,m,\lambda) + \frac{1}{2}\left[(k_1k_3)-m^2\right] b_2(k_1-k_3,m,m) - \frac{m^2}{2}B_0(k_1-k_3,m,m) \\
&\quad - \frac{\lambda^2}{4}\left[B_0(k_1,m,\lambda) - B_0(k_1-k_3,m,m) - \lambda^2 C_0(k_3,m,k_1,m,\lambda)\right] \\
&\equiv T_{13}
\end{aligned}
\tag{27}
$$

Finally, using the 4 equations (24-27) we can build a system of equations and solve for $c_{00}, c_{11}, c_{33}, c_{13}$ using Cramer's rule, as shown previously for c_1 and c_3.

3.3.3 Bremsstrahlung

We consider the radiative corrections due to low energy (soft) photon bremsstrahlung from only the electronic current. Bremsstrahlung is considered a $2 \to 3$ process in which the emitted photons energy should be integrated over possible values. Using the soft-photon approximation [4], we limit the energy of emitted photons below a threshold (dE), such that the bremsstrahlung cross section can be reasonably calculated as a $2 \to 2$ tree-level process with a multiplicative factor.

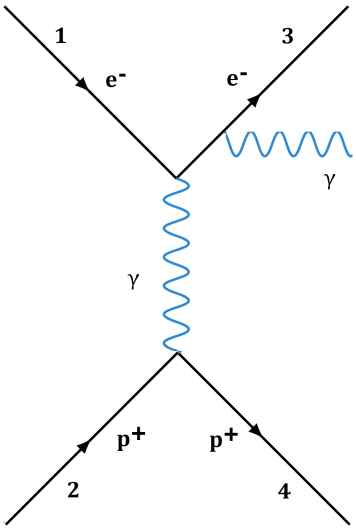

Fig. 13: Feynman diagram for bremsstrahlung

$$|\mathcal{M}_B|^2 = |\mathcal{M}_{Tree}|^2 B \tag{28}$$

In order to carry out the necessary integrals, a fictitious photon mass is included in the calculations which ends up appearing in the bremsstralung cross section. When we take the limit of the photon mass approaching 0, the cross section blows up to infinity, meaning the cross section is divergent. However, since we should consider all first order radiative corrections together in calculating the final cross section, we can remove this divergence by considering the vertex correction which cancels the photon mass out from the final result. Using the standard approach from Hooft and Veltman [29] and adjusting for our specific case of electron proton scattering, we can

investigate the structure of the bremsstrahlung factor.

$$B = \frac{\alpha}{4\pi^2}\left[-m^2 Z(1) - m^2 Z(3) + 2k_n(1)\cdot k_n(3) R(1,3)\right] \tag{29}$$

$$Z(j) = \frac{2\pi}{m^2}\left[\ln(\frac{4dE^2}{\lambda}) - \frac{2x(j)}{\sqrt{x(j)^2 - m^2\Lambda}}\ln(\frac{\beta(j)}{m\sqrt{\Lambda}})\right] \tag{30a}$$

$$\beta(j) = x(j) + \sqrt{x(j)^2 - m^2\Lambda} \tag{30b}$$

$$x(j) = k_n(j)\cdot k_n(3) + k_n(j)\cdot k_n(4) \tag{30c}$$

$$\Lambda = m^2 + m_p^2 + 2k_n(3)\cdot k_n(4) \tag{30d}$$

$$\gamma(1,3) = \sqrt{(k_n(1)\cdot k_n(3))^2 - m^4} \tag{30e}$$

$$\Omega(1,3) = \frac{k_n(1)\cdot k_n(3) + \gamma(1,3)}{m^2} \tag{30f}$$

$$S(1,3) = \Omega(1,3)x(1) - x(3) \tag{30g}$$

$$\begin{aligned} R(1,3) = \frac{2\pi}{\gamma(1,3)}\Big[& \ln(\frac{4dE^2}{\lambda})\ln(\Omega(1,3)) \\ & + \ln(\frac{\beta(1)}{m\sqrt{\Lambda}})^2 - \ln(\frac{\beta(3)}{m\sqrt{\Lambda}})^2 \\ & + Li_2(1 - \frac{\beta(1)S(1,3)}{\Lambda\gamma(1,3)}) + Li_2(1 - \frac{m^2 S(1,3)}{\beta(1)\gamma(1,3)}) \\ & - Li_2(1 - \frac{\beta(3)S(1,3)}{\Omega(1,3)\Lambda\gamma(1,3)}) - Li_2(1 - \frac{m^2 S(1,3)}{\Omega(1,3)\beta(3)\gamma(1,3)})\Big] \end{aligned}$$

Here, α is the fine structure constant, and the Li_2 function is known as the dilogarithm

(a.k.a. Spence function), whose properties are summarized in [33]. Using reasonable approximations (e.g. neglecting electron mass) and by checking the values numerically for our specific case, we were able to reduce the expression for the bremsstrahlung factor to a much simpler form.

$$\beta(j) \approx 2x(j) \tag{31a}$$

$$x(j) \approx k_n(j) \cdot k_n(4) \tag{31b}$$

$$x(3) \approx x(1) \tag{31c}$$

$$\Lambda \approx m_p^2 + 2x(1) \tag{31d}$$

$$\gamma(1,3) \approx k_n(1) \cdot k_n(3) \tag{31e}$$

$$Z(j) \approx \frac{2\pi}{m^2}\left[\ln(\frac{4dE^2}{\lambda}) - 2\ln(\frac{2x(j)}{m\sqrt{\Lambda}})\right] \tag{31f}$$

$$S(1,3) \approx \frac{2k_n(1) \cdot k_n(3)}{m^2}x(1) \approx \frac{\beta(1)\gamma(1,3)}{m^2} \tag{31g}$$

$$\begin{aligned} R(1,3) \approx \frac{2\pi}{\gamma(1,3)}\Big[& \ln(\frac{4dE^2}{\lambda})\ln(\frac{2k_n(1) \cdot k_n(3)}{m^2}) \\ & + Li_2(1 - \frac{4x(1)^2}{m^2\Lambda}) \\ & - Li_2(1 - \frac{4x(1)^2}{2k_n(1) \cdot k_n(3)\Lambda}) - Li_2(1 - \frac{m^2}{2k_n(1) \cdot k_n(3)})\Big] \end{aligned}$$

We can further reduce the bremsstrahlung factor using connections to the Mandel-

stram variables (s, T, u) [34].

$$
\begin{aligned}
B \approx \frac{\alpha}{4\pi^2}(4\pi)\Bigg[& -\ln(\frac{4dE^2}{\lambda}) + \ln(\frac{4x(j)^2}{m^2\Lambda}) \\
& + \ln(\frac{4dE^2}{\lambda})\ln(\frac{2k_n(1)\cdot k_n(3)}{m^2}) \\
& + Li_2(1 - \frac{4x(1)^2}{m^2\Lambda}) \\
& - Li_2(1 - \frac{4x(1)^2}{2k_n(1)\cdot k_n(3)\Lambda}) - Li_2(1 - \frac{m^2}{2k_n(1)\cdot k_n(3)})\Bigg]
\end{aligned}
\tag{32}
$$

$$\Lambda \approx s \tag{33a}$$

$$T = -Q^2 \approx -2k_n(1)\cdot k_n(3) \tag{33b}$$

$$4x(1)^2 \approx (s - m_p^2)^2 \approx \frac{(s - T - u)^2}{4} \tag{33c}$$

$$
\begin{aligned}
B \approx \frac{\alpha}{\pi}\Bigg[& \ln(\frac{4dE^2}{\lambda})\ln(\frac{-T}{em^2}) + \ln(\frac{(s - m_p^2)^2}{m^2 s}) \\
& + Li_2(1 - \frac{(s - m_p^2)^2}{m^2 s}) - Li_2(1 + \frac{(s - m_p^2)^2}{Ts}) - \frac{\pi^2}{6}\Bigg]
\end{aligned}
\tag{34}
$$

As we use a cut-off for the soft-photon energy (dE) as the upper limit in the integral, this parameter appears in the final cross section. This parameter could be eliminated by including the hard-photon bremsstrahlung [12], where the lower limit of the photon energy would be set by this threshold (dE). We have chosen to ignore the hard-photon bremsstrahlung, but can choose a cut-off value (dE) based on the acceptance of the

spectrometer in a given experimental setup. Alternatively, we have found a useful mathematical replacement that takes advantage of the first order expansion of e^{δ} and eliminates the dependence on this parameter, detailed in the Results & Analysis section (5.2). This exponential scaling of the total cross sections (eqn. 66) is a reasonably good approximation at low momentum transfer.

3.4 Renormalization

In order to deal with the divergent integrals in the one-loop Feynman amplitude, we require a renormalization scheme to obtain a finite result. These divergences are due to integration over the infinite number of states within a loop (i.e. summation over all possible Feynman diagrams). Generally, we first identify a set of fundamental parameters (e.g. particle masses, coupling constants) and embed the appropriate divergences, which are selected exactly to cancel the divergences in the relevant loop-integrals. The parameters are then renormalized in such a way to restore their physical meaning and are again finite and measurable. Using on-shell multiplicative renormalization [9, 21, 35], we employ specific conditions to cancel the divergences and obtain the corresponding counter-terms. The on-shell condition forces the energy-momentum relations (i.e. classical equations of motion) to be satisfied for all particles. The mass 'shell' is simply a hyperboloid in energy-momentum space which describes the equations of motion 35. Mass can be defined as the radius

of this 4-dimensional 'shell', such that a particular mass could have various different combinations of energy and momenta that still satisfy the on-shell conditions.

$$E^2 - |p|^2c^2 = m^2c^4 \tag{35}$$

We can first start with the standard QED lagrangian which describes the interaction:

$$\mathcal{L}^o_{QED} = \overline{\psi_o}(i\partial\!\!\!/ - e_o\mathcal{A}\!\!\!/^o - m_o)\psi_o - \frac{1}{4}(\partial_\mu \mathcal{A}^o_\nu - \partial_\nu \mathcal{A}^o_\mu)^2 \tag{36}$$

Then we employ the multiplicative renormalization to the fermion field ψ, electric charge e, mass m, and boson field $\mathcal{A}$ in order to renormalize the lagrangian (denoted by $\widehat{}$). We are using the Taylor expansion to first order in order to get the one-loop counter terms.

$$Z_i = 1 + \delta Z_i \tag{37a}$$

$$\psi_o \to \sqrt{Z_\psi}\psi \tag{37b}$$

$$e_o \to Z_e e \tag{37c}$$

$$m_o \to Z_m m \tag{37d}$$

$$\mathcal{A}^o_\mu \to \sqrt{Z_\gamma}\mathcal{A}_\mu \tag{37e}$$

$$\begin{aligned}\widehat{\mathcal{L}}_{QED} =&(1+\delta Z_\psi)\overline{\psi}\Big(i\partial\!\!\!/ - (1+\delta Z_e)e(1+\frac{1}{2}\delta Z_\gamma)\mathcal{A}\!\!\!/ - (1+\delta Z_m)m\Big)\psi \\ &- \frac{1}{4}(1+\frac{1}{2}\delta Z_\gamma)^2(\partial_\mu \mathcal{A}_\nu - \partial_\nu \mathcal{A}_\mu)^2\end{aligned} \tag{38}$$

From here, we can already separate out the counter terms by comparing to the original lagrangian in eqn. 36, and we can group the relevant counter terms together based on the type of correction.

$$\begin{aligned}\widehat{\mathcal{L}}_{QED} =&\overline{\psi}(i\partial\!\!\!/ - e\mathcal{A}\!\!\!/ - m)\psi - \frac{1}{4}(\partial_\mu \mathcal{A}_\nu - \partial_\nu \mathcal{A}_\mu)^2 \\ &+ \delta Z_\psi \overline{\psi}(i\partial\!\!\!/ - e\mathcal{A}\!\!\!/ - m)\psi + \overline{\psi}(-\delta Z_e)e\mathcal{A}\!\!\!/\psi \\ &+ \overline{\psi}(-\frac{1}{2}\delta Z_\gamma)e\mathcal{A}\!\!\!/\psi + \overline{\psi}(-\delta Z_m)m\psi \\ &- \frac{1}{4}\delta Z_\gamma(\partial_\mu \mathcal{A}_\nu - \partial_\nu \mathcal{A}_\mu)^2\end{aligned} \tag{39}$$

We would expect the vertex corrections to account for interaction terms, namely those containing $e\mathcal{A}\!\!\!/$. While the photon self-energy accounts for terms with $\mathcal{A}_m u^2$, and the fermion self-energy includes terms with the fermion mass or partial derivative of ψ. The renormalized coupling after including counter terms would be of the structure $\widehat{\Gamma}_\mu = \Gamma_\mu + \delta\Gamma_\mu$

$$\text{Vertex} \rightarrow \delta\Gamma_\mu = -ie\gamma_\mu(\delta Z_e + \frac{1}{2}\delta Z_\gamma + \delta Z_\psi) \tag{40a}$$

$$\text{Photon Self-Energy} \rightarrow \delta\Pi_{\gamma\gamma} = -ig_{\mu\nu}k^2\delta Z_\gamma \tag{40b}$$

$$\text{Fermion Self-Energy} \rightarrow \delta\Sigma_{ff} = k\!\!\!/\delta Z_\psi - m(\delta Z_\psi + \delta Z_m) \tag{40c}$$

The on-shell conditions are as follows, where $\widehat{\ }$ again denotes the renormalized version. 1. Photon self-energy (i.e. vacuum polarization)

$$\widehat{\Sigma}_{\gamma\gamma}|_{k^2=0} = 0 \tag{41a}$$

$$\frac{\partial\widehat{\Sigma}_{\gamma\gamma}}{\partial k^2}|_{k^2=0} = 0 \tag{41b}$$

2. Fermion self-energy

$$\lim_{\not{k}\to m} \frac{\widehat{\Sigma}_{ff}}{\not{k} - m} u(k) = 0 \tag{42a}$$

$$\widehat{\Sigma}_{ff}|_{\not{k}=m} = 0 \tag{42b}$$

3. Vertex correction, in the limit of vanishing momentum transfer

$$\widehat{\Gamma}^{ff\gamma}_{\mu}|_{q^2=0} = ie\gamma_{\mu} \tag{43}$$

4. Ward-Takahashi identity

$$\Gamma^{ff\gamma}_{\mu}|_{q^2=0} = -ie\frac{\partial\Sigma(\not{k})}{\partial k_{\mu}}|_{\not{k}=m} \tag{44}$$

Starting with the vacuum polarization tensor, we can isolate the renormalized

photon self-energy.

$$\widehat{\Pi}_{\gamma\gamma} = -ig_{\mu\nu}\Sigma_{\gamma\gamma} - ig_{\mu\nu}k^2\delta Z_\gamma \tag{45a}$$

$$\widehat{\Sigma}_{\gamma\gamma} = \Sigma_{\gamma\gamma} + k^2\delta Z_\gamma \tag{45b}$$

Now using the on-shell renormalization conditions (eqn. 41) we get:

$$0 = \Sigma_{\gamma\gamma}|_{k^2=0} \tag{46a}$$

$$0 = \frac{\partial\Sigma_{\gamma\gamma}}{\partial k^2}|_{k^2=0} + \delta Z_\gamma \tag{46b}$$

$$\therefore \boxed{\widehat{\Sigma}_{\gamma\gamma} = \Sigma_{\gamma\gamma} - k^2\frac{\partial\Sigma_{\gamma\gamma}}{\partial k^2}|_{k^2=0}} \tag{46c}$$

Moving on to the vertex renormalization, the total coupling includes the tree-level and one-loop corrections, which can be approximated using the Dirac and Pauli form factors.

$$\begin{aligned}\widehat{\Gamma}^{ff\gamma}_\mu = &- ie\gamma_\mu + ie\big(\gamma_\mu F_1 + \frac{i}{2m}\sigma_{\mu\nu}q^\nu F_2\big) \\ &- ie\gamma_\mu(\delta Z_e + \frac{1}{2}\delta Z_\gamma + \delta Z_\psi)\end{aligned} \tag{47}$$

Using the renormalization condition (eqn. 43) and some simple rearranging we get:

$$0 = ie\gamma_\mu F_1|_{q^2=0} - ie\gamma_\mu(\delta Z_e + \frac{1}{2}\delta Z_\gamma + \delta Z_\psi) \tag{48a}$$

$$\therefore \boxed{F_1|_{q^2=0} = \delta Z_e + \frac{1}{2}\delta Z_\gamma + \delta Z_\psi} \tag{48b}$$

Finally, for the fermion self-energy, we will separate this term into the vector (v) and scalar (s) parts of the interaction.

$$\Sigma_{ff} = \not{k}\Sigma_v + m\Sigma_s \tag{49a}$$

$$\frac{\partial \Sigma_{ff}}{\partial k_\mu} = \gamma_\mu \Sigma_v + \not{k} 2k_\mu \frac{\partial \Sigma_v}{\partial k^2} + m 2k_\mu \frac{\partial \Sigma_s}{\partial k^2} \tag{49b}$$

$$\therefore \frac{\partial \Sigma_{ff}}{\partial k_\mu}|_{\not{k}=m} = \gamma_\mu \Sigma_v + 2m^2\gamma_\mu \left(\frac{\partial \Sigma_v}{\partial k^2} + \frac{\partial \Sigma_s}{\partial k^2} \right) |_{k^2=m^2} \tag{49c}$$

Then we can make use of the Ward-Takahashi identity (eqn. 44) with $\Sigma_{ff}(\not{k})$ and the one-loop correction for $\Gamma^{ff\gamma}_\mu$.

$$ie\gamma_\mu \left[\Sigma_v + 2m^2 \left(\frac{\partial \Sigma_v}{\partial k^2} + \frac{\partial \Sigma_s}{\partial k^2} \right) \right] |_{k^2=m^2} = -ie\gamma_\mu F_1|_{q^2=0} \tag{50}$$

Now we use L'Hopital rule with the first renormalization condition from eqn. 42 in

order to get:

$$\rightarrow \frac{\partial \widehat{\Sigma}_{ff}}{\partial \not{k}}|_{\not{k}=m} = 0 \tag{51a}$$

$$\widehat{\Sigma}_{ff} = \not{k}\Sigma_v + m\Sigma_s + \not{k}\delta Z_\psi - m(\delta Z_\psi + \delta Z_m) \tag{51b}$$

$$\therefore 0 = \left[\Sigma_v + 2m^2\left(\frac{\partial \Sigma_v}{\partial k^2} + \frac{\partial \Sigma_s}{\partial k^2}\right)\right]|_{k^2=m^2} + \delta Z_\psi \tag{51c}$$

Combing the previous two results from 50 and 51 we get a useful relation:

$$\boxed{\delta Z_\psi = -\frac{\partial \Sigma_{ff}}{\partial \not{k}}|_{\not{k}=m} = F_1|_{q^2=0}} \tag{52}$$

So, we can now go back to our result from eqn. 48 and combine with eqn. 46 b.

$$F_1|_{q^2=0} = \delta Z_e + \frac{1}{2}\delta Z_\gamma + F_1|_{q^2=0} \tag{53a}$$

$$\therefore \boxed{\delta Z_e = -\frac{1}{2}\delta Z_\gamma = \frac{1}{2}\frac{\partial \Sigma_{\gamma\gamma}}{\partial k^2}|_{k^2=0}} \tag{53b}$$

Finally, using the second renormalization condition from eqn. 41 we get:

$$\widehat{\Sigma}_{ff}|_{\not{k}=m} = m\Sigma_v|_{k^2=m^2} + m\Sigma_s|_{k^2=m^2} + m\delta Z_\psi - m(\delta Z_\psi + \delta Z_m) = 0 \tag{54a}$$

$$\therefore \boxed{m\delta Z_m = m\Big[\Sigma_v + \Sigma_s\Big]|_{k^2=m^2} = \Sigma_{ff}|_{\not{k}=m}} \tag{54b}$$

3.5 Mathematica Code

We primarily use three packages within Mathematica, which are all available directly from http://www.feynarts.de, for calculating the various cross sections required for the one-loop asymmetry. FeynArts [36, 37] is used to create and visualize Feynman diagrams, including those for counter terms, then generate the corresponding Feynman amplitudes. The procedure is to identify all possible interaction topologies and combinations of fields based on the input provided, then apply Feynman rules to the diagrams and extract the amplitudes. This procedure is described schematically in the FeynArts 3.9 user guide [38], as included below.

2 Roadmap of *FeynArts*

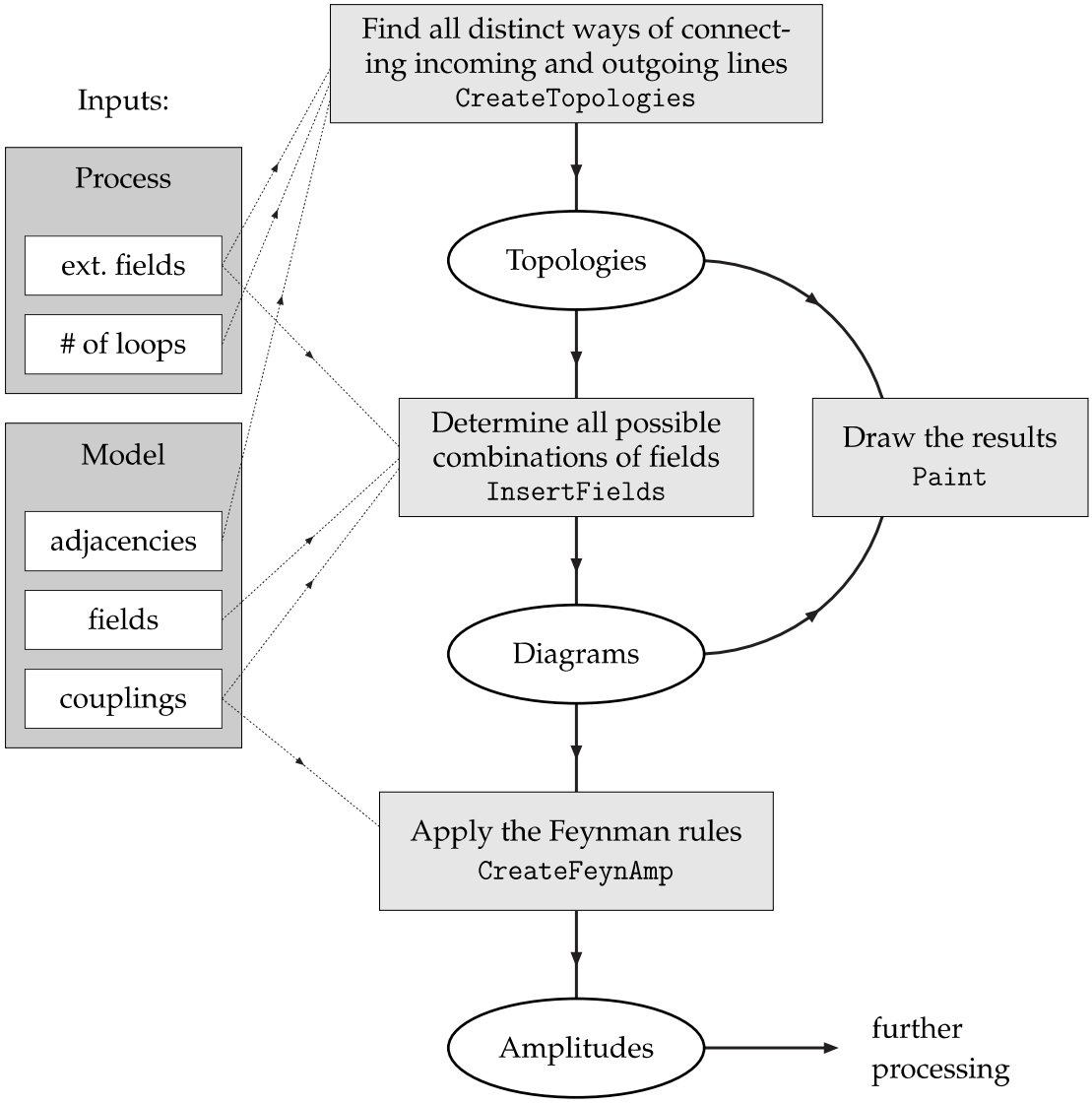

FormCalc [39, 40] is used with FeynArts to carry out the analytical evaluation of Feynman diagrams, the simplification of algebraic expressions and the conversion of computational output to a generic C code for processing. The benefit here is that the internal functions of FormCalc are performed in FORM, so calculations of large polynomial expressions are very quick, and simplified results are returned to user-friendly Mathematica for further analysis. LoopTools [41] is eventually used to numerically evaluate the scalar and tensor one-loop integrals, using the Passarino-Veltman reduction scheme [31, 29].

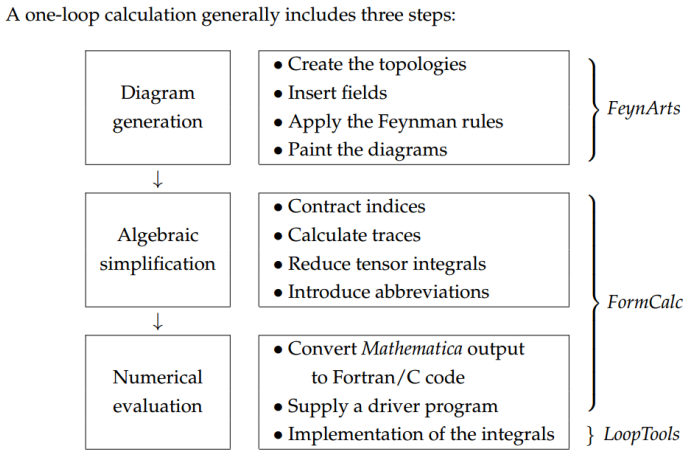

Fig. 14: Schematic description of a generic one-loop calculation procedure, taken from the FormCalc user guide [40]

A separate model file which stores all particle information and couplings can be modified, as to include new particles or implement new models entirely. In our case, we added the proton as an elementary particle in the model, and implemented the necessary couplings using form factors to account for proton substructure. The full

list of relevant parameters used in our calculations, including all masses and couplings, are detailed in the appendix (section 7.2) along with essential parts of the script used in order to calculate the one-loop cross sections.

4 Results & Analysis

We explicitly calculate the parity-violating asymmetry, using computational techniques detailed in the previous section, with kinetics set to match experimental tests of the electron-proton interaction. Using experimental parameters from Q-Weak and P2 experiments, we are able to calculate the expected results based on our theoretical models and compare to real experimental measurements. As the experiments are extremely precise and have small calculated uncertainties, we also need our theory to predict results with high precision in order to determine its validity. We begin by examining the two tree-level Feynman diagrams which contribute to the electron-proton interaction in these scattering experiments, and by extracting an analytic expression for the tree-level parity-violating asymmetry. Then we look at final results from the one-loop level calculations done in Mathematica, and discuss the individual contributions from radiative corrections and bremsstrahlung, as well as important assumptions made throughout. The full list of Feynman diagrams used in our one-loop calculations includes all boson self-energy graphs and lepton vertex correction triangle graphs, explicitly shown in the appendix. We will also extract the weak charge of the proton from the energy dependence of the final corrected asymmetry, and calculate the weak mixing angle. Finally, we consider a new exchange particle (Z') in our theoretical model, and analyze the effects on our calculated one-loop asymmetry.

4.1 Electron-Proton Scattering

The scattering experiments involve a polarized beam of electrons incident on a liquid hydrogen target. First, we are specifically interested in two tree-level Feynman diagrams, which involve electron-proton interactions mediated by the electromagnetic (EM) and weak forces. As the EM interaction is much stronger than the weak interaction, we expect the Feynman amplitude for the tree-level process to mainly be due to the exchange of a photon.

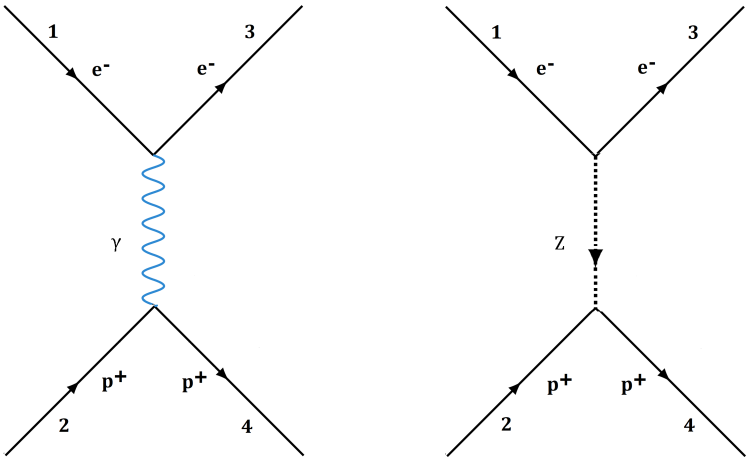

Fig. 15: Tree level Feynman diagrams for both electromagnetic and weak forces mediating the electron-proton interaction.

The total Feynman amplitude ($\mathcal{M}_{Total}$) for the scattering process is the sum of all physically indistinguishable interaction amplitudes. Importantly, $|\mathcal{M}_{Total}|^2$ and thus the cross section, involves an interference term between the EM and weak forces that is exploited in the parity-violating asymmetry measurement and calculation (eqn.

56). Although the EM force is dominant in the total cross section for the electron-proton interaction, we can effectively cancel out the main contribution by extracting just the parity-violating part. By performing the same experiment with the incident electron beam polarization flipped, we get a pair of cross sections corresponding to the left and right handed interactions. Since the EM interaction is parity conserving, the contributions should be identical to each cross section, and thus cancel exactly. Using the Feynman rules outlined in the Calculations section (4.1), we calculated the parity-violating asymmetry at tree-level, neglecting the quadratic $\mathcal{M}_Z$ terms. We also reasonably assume only photon exchange and an unpolarized electron beam for the denominator. It should be noted that we haven chosen to use the Feynman gauge for convenience in our calculations.

$$\begin{aligned} \sigma \propto |\mathcal{M}_{Total}|^2 &= |\mathcal{M}_\gamma + \mathcal{M}_Z|^2 \\ &= |\mathcal{M}_\gamma|^2 + |\mathcal{M}_Z|^2 + 2Re(\mathcal{M}_\gamma^\dagger \cdot \mathcal{M}_Z) \\ &\approx |\mathcal{M}_\gamma|^2 \end{aligned} \tag{55}$$

$$A = \frac{\sigma_R - \sigma_L}{\sigma_R + \sigma_L} \propto \frac{2Re(\mathcal{M}_\gamma^\dagger \cdot \mathcal{M}_Z)_R - 2Re(\mathcal{M}_\gamma^\dagger \cdot \mathcal{M}_Z)_L}{2|\mathcal{M}_\gamma|^2} \tag{56}$$

First we need to calculate the Feynman amplitude for each interaction individually,

directly from the Feynman rules.

$$\begin{aligned}\mathcal{M}_\gamma &= \overline{u}(3)\left(ie\gamma^\delta\right)u(1)\left(\frac{-ig_{\delta\mu}}{q^2}\right)\overline{u}(4)\left(ie\big[F_1\gamma^\mu + \frac{i}{2m_p}\sigma^{\mu\nu}q_\nu F_2\big]\right)u(2)\\ &= \frac{ie^2}{q^2}\overline{u}(3)\gamma_\mu u(1)\overline{u}(4)\big[F_1\gamma^\mu + \frac{i}{2m_p}\sigma^{\mu\nu}q_\nu F_2\big]u(2)\end{aligned} \tag{57}$$

$$\begin{aligned}\mathcal{M}_Z &= \overline{u}(3)\left(-i\frac{g_Z}{2}\gamma^\beta\big[g_V - g_A\gamma_5\big]\right)u(1)\left(\frac{-ig_{\beta\alpha}}{q^2 - m_Z^2}\right)\\ &\quad\times\overline{u}(4)\left(ig_Z\big[f_1\gamma^\alpha + \frac{i}{2m_p}\sigma^{\alpha\beta}q_\beta f_2 + g_1\gamma^\alpha\gamma_5\big]\right)u(2)\\ &= \frac{-ig_Z^2}{2(q^2 - m_Z^2)}\overline{u}(3)\gamma_\alpha\big[g_V - g_A\gamma_5\big]u(1)\overline{u}(4)\big[f_1\gamma^\alpha + \frac{i}{2m_p}\sigma^{\alpha\beta}q_\beta f_2 + g_1\gamma^\alpha\gamma_5\big]u(2)\end{aligned} \tag{58}$$

Then, in order to construct the numerator in the asymmetry, we calculate the interference term between the two Feynman amplitudes.

$$\begin{aligned}\mathcal{M}_\gamma^\dagger\mathcal{M}_Z &= \frac{-e^2g_Z^2}{2q^2(q^2 - m_Z^2)}\overline{u}(2)\big[F_1\gamma^\mu - \frac{i}{2m_p}\sigma^{\mu\nu}q_\nu F_2\big]u(4)\\ &\quad\times\overline{u}(1)\gamma_\mu u(3)\overline{u}(3)\gamma_\alpha\big[g_V - g_A\gamma_5\big]u(1)\\ &\quad\times\overline{u}(4)\big[f_1\gamma^\alpha + \frac{i}{2m_p}\sigma^{\alpha\beta}q_\beta f_2 + g_1\gamma^\alpha\gamma_5\big]u(2)\\ &= \frac{-e^2g_Z^2}{2q^2(q^2 - m_Z^2)}u(2)\overline{u}(2)\big[F_1\gamma^\mu - \frac{i}{2m_p}\sigma^{\mu\nu}q_\nu F_2\big]u(4)\\ &\quad\times\overline{u}(4)\big[f_1\gamma^\alpha + \frac{i}{2m_p}\sigma^{\alpha\beta}q_\beta f_2 + g_1\gamma^\alpha\gamma_5\big]\\ &\quad\times u(1)\overline{u}(1)\gamma_\mu u(3)\overline{u}(3)\gamma_\alpha\big[g_V - g_A\gamma_5\big]\end{aligned} \tag{59}$$

In order to calculate the total amplitude, we must average the initial proton spin states, and sum over all possible final spins. We can make use of Casimir's trick [24] in order to write the polarization sums as products of traces. The helicity of the initial electron (1) is set by polarization of the beam, so an extra factor is needed in the trace. Here, λ is the helicity, representing either right or left handed polarization (1 or -1 respectively) and s is the helicity reference 4-vector defined as s = (p/m, 0, 0, E/m).

$$\begin{aligned}(\mathcal{M}_\gamma^\dagger \mathcal{M}_Z) &= \frac{1}{2}\sum_{\lambda_2}\sum_{\lambda_3}\sum_{\lambda_4}\mathcal{M}_\gamma^\dagger \mathcal{M}_Z \\ &= \frac{-e^2 g_Z^2}{4q^2(q^2-m_Z^2)}\mathrm{Tr}\Bigg[(\not{p}_2 + m_p)\left(F_1\gamma^\mu - \frac{i}{2m_p}\sigma^{\mu\nu}q_\nu F_2\right) \\ &\qquad \cdot (\not{p}_4 + m_p)\left(f_1\gamma^\alpha + \frac{i}{2m_p}\sigma^{\alpha\beta}q_\beta f_2 + g_1\gamma^\alpha\gamma_5\right)\Bigg] \\ &\qquad \times \mathrm{Tr}\left[\frac{1}{2}(1+\lambda\gamma_5\not{s}_1)(\not{p}_1 + m_e)\gamma_\mu(\not{p}_3 + m_e)\gamma_\alpha\left(g_V - g_A\gamma_5\right)\right]\end{aligned} \tag{60}$$

Finally, we need just need the denominator, so we calculate the quadratic $\mathcal{M}_\gamma$ term.

$$\begin{aligned}
|\mathcal{M}_\gamma|^2 &= \frac{e^4}{q^4}\overline{u}(2)\big[F_1\gamma^\mu - \frac{i}{2m_p}\sigma^{\mu\nu}q_\nu F_2\big]u(4)\overline{u}(1)\gamma_\mu u(3) \\
&\quad \times \overline{u}(3)\gamma_\alpha u(1)\overline{u}(4)\big[F_1\gamma^\alpha + \frac{i}{2m_p}\sigma^{\alpha\beta}q_\beta F_2\big]u(2) \\
&= \frac{e^4}{q^4}u(2)\overline{u}(2)\big[F_1\gamma^\mu - \frac{i}{2m_p}\sigma^{\mu\nu}q_\nu F_2\big]u(4) \\
&\quad \times \overline{u}(4)\big[F_1\gamma^\alpha + \frac{i}{2m_p}\sigma^{\alpha\beta}q_\beta F_2\big] \\
&\quad \times u(1)\overline{u}(1)\gamma_\mu u(3)\overline{u}(3)\gamma_\alpha
\end{aligned} \tag{61}$$

Again, we average the initial spin states, now including the incident electron, and sum over all possible final spins.

$$\begin{aligned}
\big(|\mathcal{M}_\gamma|^2\big) &= \frac{1}{4}\sum_{\lambda_1}\sum_{\lambda_2}\sum_{\lambda_3}\sum_{\lambda_4}|\mathcal{M}_\gamma|^2 \\
&= \frac{e^4}{4q^4}\mathrm{Tr}\Bigg[(\not{p}_2 + m_p)\left(F_1\gamma^\mu - \frac{i}{2m_p}\sigma^{\mu\nu}q_\nu F_2\right) \\
&\qquad \cdot (\not{p}_4 + m_p)\left(F_1\gamma^\alpha + \frac{i}{2m_p}\sigma^{\alpha\beta}q_\beta F_2\right)\Bigg] \\
&\qquad \times \mathrm{Tr}\Big[(\not{p}_1 + m_e)\gamma_\mu(\not{p}_3 + m_e)\gamma_\alpha\Big]
\end{aligned} \tag{62}$$

4.2 One-Loop Parity Violating Asymmetry

Using Mathematica together with the FeynArts packages, we were able to calculate the one-loop radiative corrections to the parity-violating asymmetry (A_{PV})

for electron-proton scattering at low momentum transfer, and compared results with experimental tests. The radiative corrections explicitly included were the boson self-energies and lepton vertex corrections, as well as soft-photon bremsstrahlung (B), all outlined in the Calculations section. Since the radiative corrections themselves are known to be small in comparison to the tree-level diagrams, we neglect the quadratic terms in eqn. 63 and include only the interference terms in the total one-loop cross section (σ_1). As discussed previously, the low-energy bremsstrahlung (eqn. 29) can be included as a multiplicative factor with the tree level cross section (σ_0), with a limiting photon energy of dE (maximum). This limit can also be thought of as the minimum threshold for hard photons, which are not included in the calculation. For the following superscripts, 0 denotes the total tree-level contribution (detailed in the previous section), 1 denotes one-loop corrected part, and R/L denote right and left handed polarization of the incident electron beam when applicable.

$$\sigma_{SelfEnergy} \propto (\mathcal{M}_0^\dagger \mathcal{M}_{SelfEnergy}) \tag{63a}$$

$$\sigma_{Vertex} \propto (\mathcal{M}_0^\dagger \mathcal{M}_{Vertex}) \tag{63b}$$

$$\sigma_1 = \sigma_0(1+B) + 2Re[\sigma_{SelfEnergy}] + 2Re[\sigma_{Vertex}] \tag{64}$$

$$A^0_{PV} = \frac{(\sigma_{0R} - \sigma_{0L})}{2\sigma_0} \tag{65a}$$

$$A^1_{PV} = \frac{(\sigma_{1R} - \sigma_{1L})}{2\sigma_1} \tag{65b}$$

Only the total sum of all possible cross sections can be physically observed in experiment, but we are using various assumptions to ignore many higher order Feynman diagrams. The main contribution to σ_1 is of course the tree-level interactions where a single boson is exchanged, which have the highest probability of occuring during scattering. We include the next to leading order radiative corrections such as soft-photon bremsstrahlung, one-loop vertex triangle diagrams and boson self-energies, which are significantly smaller in magnitude but still important for high accuracy calculations, and we implicitly account for other interactions through structural form factors. However, we omit the explicit proton vertex loops, any external leg corrections, and higher-order Feynman diagrams. Divergences in the calculated one-loop radiative corrections are obviously unphysical, and are a product of our approximations and neglected terms. To our benefit, the infrared divergences (as q^2 approaches zero) found in the one-loop corrections are exactly canceled by those found in the soft-bremsstrahlung correction, yielding a finite final cross section. Since we are using the soft-photon approximation in calculating the bremsstrahlung factor, we will

not be including all the relevant diagrams for which the emitted photon has energy greater than the threshold (dE). This will inevitably lead to a dependence on the floating parameter in the bremsstrahlung factor, and subsequently in the final one-loop asymmetry. Experimentally, this soft-photon limit depends on the acceptance of the spectrometer, and the maximum energy of emitted photons for which the scattered electron could no longer be detected. Using the experimental parameters and equipment specifications, we have estimated the soft-photon limit to be dE = 200MeV for Q-Weak and dE = 50MeV for P2. However, rather than including the hard-photon bremsstrahlung, we can also eliminate the dependence of this added parameter from the parity-violating asymmetry by using an exponential scaling (eqn. 66). We can define the one-loop cross section to be the tree-level cross section, plus some arbitrary multiple (δ) of itself. Since we are expecting the contribution of one loop radiative corrections to be relatively small compared to the tree-level cross section, we can Taylor expand the exponential of δ and approximate to first order. In this way, we can see that the exponential scaling of the one-loop asymmetry (A_{PV}^{1e}) should not significantly alter the final result, but only change the way it is calculated. We can see in fig. 17 that the dependence on the floating parameter dE from the bremsstrahlung factor is completely washed out in this way.

$$\delta = \frac{\sigma_1}{\sigma_0} - 1 \tag{66a}$$

$$\mathrm{e}^{\delta} \approx \delta + 1 \tag{66b}$$

$$A_{PV}^{1e} = \frac{\left(\sigma_{0R} \cdot \mathrm{e}^{\delta_R} - \sigma_{0L} \cdot \mathrm{e}^{\delta_L}\right)}{2\sigma_0 \cdot \mathrm{e}^{\delta}} \approx A_{PV}^{1} \tag{66c}$$

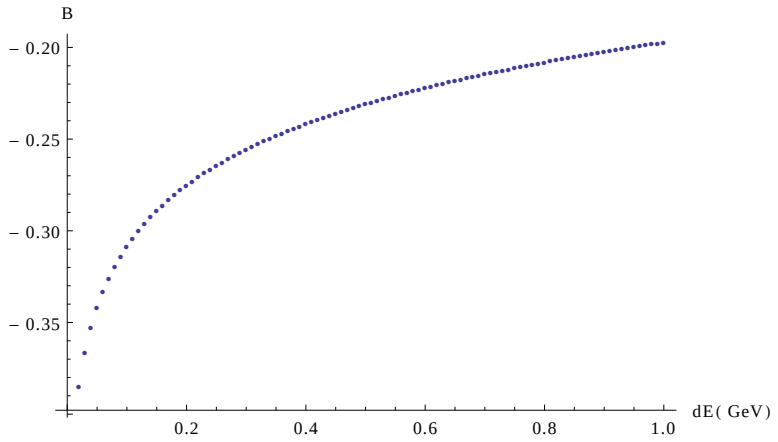

Fig. 16: Dependence on soft-photon energy upper-limit parameter (dE) for the bremsstrahlung factor ($E_{lab} = 1.154GeV$, $\theta = 7.9°$).

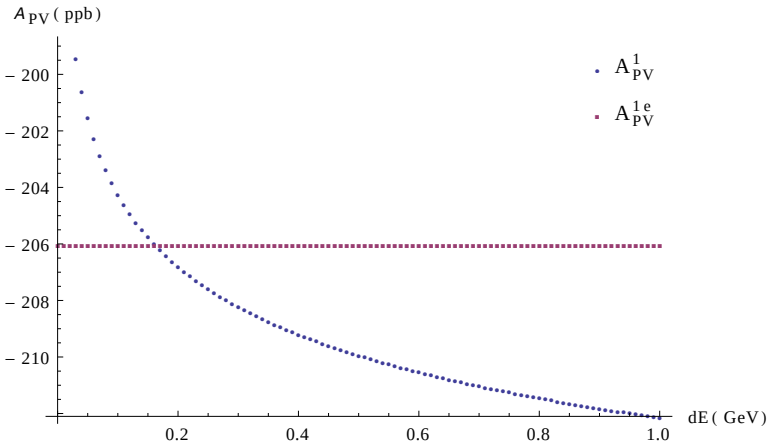

Fig. 17: One-loop parity violating asymmetry, calculated in two different ways, showing the dependence on soft-photon limit parameter dE ($E_{lab} = 1.154GeV$, $\theta = 7.9°$).

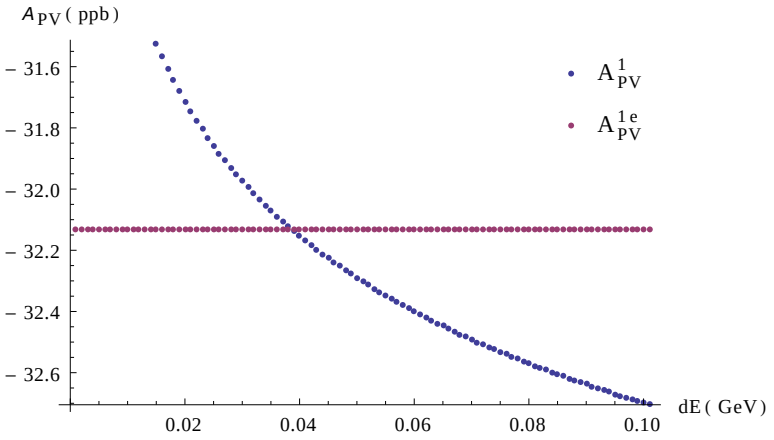

Fig. 18: One-loop parity violating asymmetry, calculated in two different ways, showing the dependence on soft-photon limit parameter dE ($E_{lab} = 0.155GeV$, $\theta = 25.5°$).

Since the parity-violating asymmetry ultimately depends on experimental parameters, namely the momentum transfer between scattered particles ($-Q^2$) and the energy of the incident electron beam (E_{lab}). We have chosen the average momentum transfer in the Q-Weak experiment as a useful starting point, so we have $Q^2 = 0.0249GeV^2$, $\theta = 7.9°$, and $E_{lab} = 1.154GeV$. Similar calculations were also

done using the average P2 experimental parameters, $Q^2 = 0.0045GeV^2$, $\theta = 25.5°$, and $E_{lab} = 0.155GeV$.

$$Q^2 = \frac{4E_{lab}^2 \sin^2\theta}{1 + \frac{2E_{lab}}{M_p}\sin^2\theta} \tag{67}$$

By varying just the angle of detection (θ) for the scattered electrons, we are implicitly changing Q^2 and are able to characterize its dependence in the final asymmetry. We would expect that the parity-violating asymmetry grows in magnitude as the momentum transfer between particles increases, as more interactions become energetically possible. In the following calculations, we varied θ between 2° and 12° in steps of 0.1° when $E_{lab} = 1.154GeV$, and between 15° and 55° in steps of 0.5° when $E_{lab} = 0.155GeV$. We can see in fig. 19 that the first order asymmetry is significantly shifted from the tree-level result, indicating that at least one-loop radiative corrections are necessary to produce accurate results. We can also see that the exponential scaling of the asymmetry (A_{PV}^{1e}) has no significant deviation from the normal one-loop corrected asymmetry (within 0.4%), as expected, but does not depend on the soft-photon limit parameter (dE). The added uncertainty associated with our exponentiation approximation (eqn. 66) is assumed to be small in our final results, since $\delta \approx 0.08 \ll 1$, and the one-loop radiative corrections to the cross sections are relatively small. The difference between the exponential and the first-order Taylor expansion is only 0.003 ($\approx 0.3\%$) for the value of dE in our case.

There will be some uncertainty associated with our final results, due to the var-

ious approximations made throughout the calculations, the chosen renormalization scheme, as well as uncertainties in the input parameters. In order to estimate the precision of our calculations, we can use the observed change in calculated asymmetry when the mass of the W boson (m_W) is varied within a reasonable range ($m_W = 80.379 \pm 0.012$ GeV from http://pdg.lbl.gov). The masses of the Z boson and proton are known to such high precision that the results aren't significantly altered when these parameters are varied within their accepted range of values. Here, we chose a representative set of values for Q^2 and report the change observed in the asymmetry as m_W is varied within the given range (Table 4). We will simply use the variation as the approximate error in our one-loop corrected results. Although the absolute value of uncertainty in the asymmetry grows with increasing Q^2, the relative uncertainty actually decreases. It should be noted that since we have neglected additional sources of error in our final results, we would expect to be slightly underestimating the total uncertainty.

$E_{Lab} = 1.154GeV$		$E_{Lab} = 0.155GeV$	
Q^2 (GeV)	ΔA^1_{PV} ($\pm$ ppb)	Q^2 (GeV)	ΔA^1_{PV} ($\pm$ ppb)
0.001621	0.3	0.001628	0.22
0.003644	0.35	0.002594	0.25
0.006469	0.5	0.003770	0.32
0.010088	0.75	0.005145	0.45
0.014493	1.25	0.006705	0.625
0.019670	1.6	0.008438	0.775
0.025614	2.1	0.010328	0.95
0.032302	2.6	0.012360	1.15
0.039721	3.2	0.014517	1.4
0.047853	3.55	0.016783	1.7
0.056679	4.0	0.019141	1.9

Table 4: Observed change in calculated one-loop asymmetry when m_W is varied from 80.367 - 80.391 GeV at different values of momentum transfer, for both Q-Weak and P2 experimental energies.

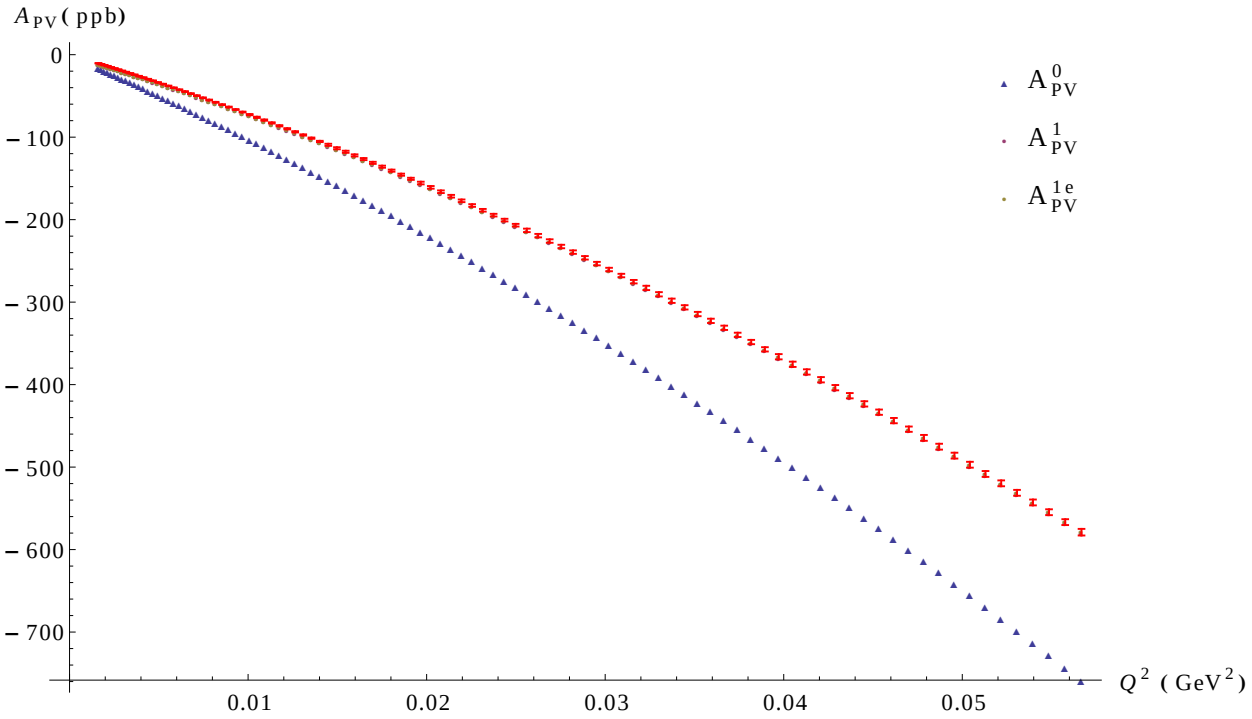

Fig. 19: Tree-level and one-loop calculated parity violating asymmetry, for different values of momentum transfer ($E_{lab} = 1.154GeV$). One-loop results shown with calculated error bars.

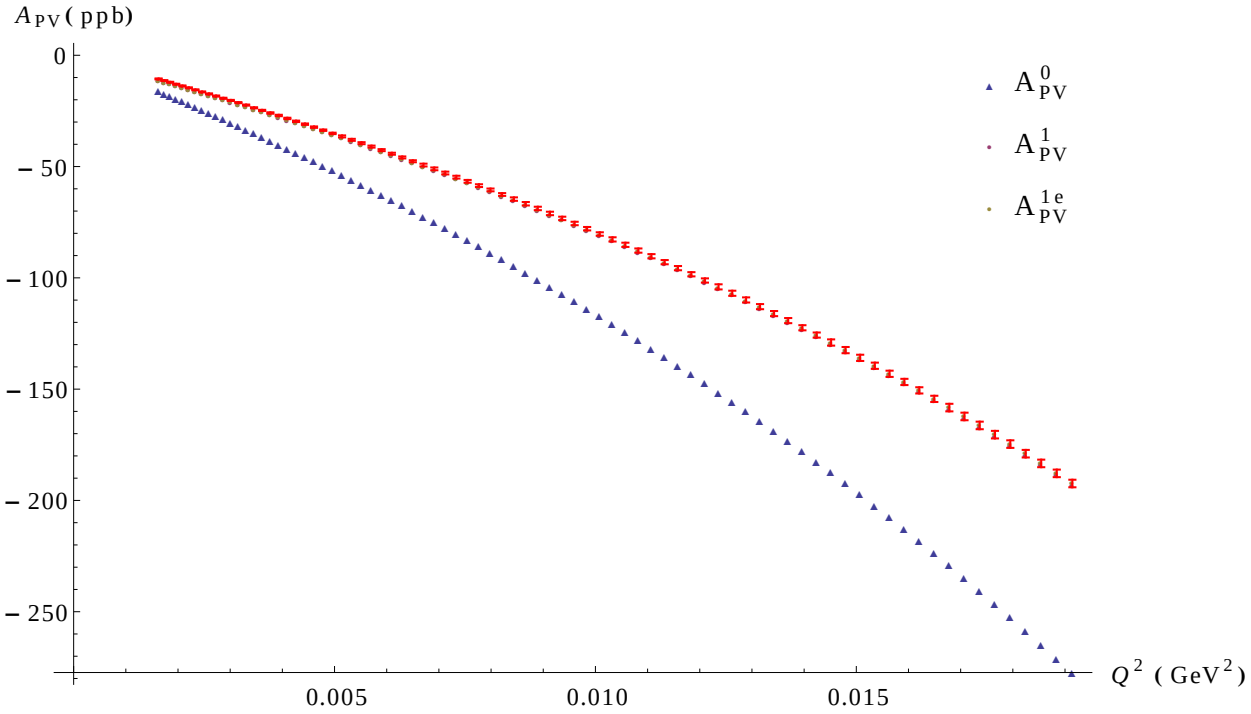

Fig. 20: Tree-level and one-loop calculated parity violating asymmetry, for different values of momentum transfer ($E_{lab} = 0.155GeV$). One-loop results shown with calculated error bars.

In the end, we are looking to uncover fundamental characteristics of the electron-proton interaction, and specifically the parity-violating weak force. The weak charge of the proton (Q_W^p) is determined using the asymmetry measured in the Q-Weak and P2 experiments at low momentum transfer, with semi-empirical form factors which take into account previous experimental data. Due to the high accuracy required in extracting the weak charge from our calculations, we must account for any energy-dependent contributions which would shift the asymmetry with Q^2, such as γ-Z box diagrams (i.e. two-loop radiative corrections) [22]. We include the energy-dependent shift expected in the proton's weak charge (eqn. 69), taking the value of $\Box_{\gamma Z}(E_{Lab})$

from [2] for both Q-Weak and P2 energies. This will also require a correction to the results for parity-violating asymmetry, as seen in eqn. 70, since we didn't include two-loop diagrams explicitly in our calculations. As seen in table 5, the γZ box correction for the P2 results are smaller than for Q-Weak, since at lower energies the two-loop corrections are expected to be less significant.

We can then fit our final corrected asymmetry $A_{PV}^{1^*}$, scaled by A_o, to a straight line (fig. 22) using eqn. 69 in order to extract the proton's weak charge Q_W^p. The $\mathcal{B}$ function is a Q^2 dependent form factor which accounts for hadronic substructure. Since we want to extrapolate down to zero momentum transfer, we can ignore the Q^4 terms and simply fit $\mathcal{B}$ as a constant over a small range. This is a reasonable approach in this case, as the average Q^2 values in Q-Weak and P2 experiments are relatively very small.

$$M_p = 0.938272081 GeV \tag{68a}$$

$$\alpha = \frac{1}{137.035999} \tag{68b}$$

$$G_F = 1.16639 \times 10^{-5} GeV^{-2} \tag{68c}$$

$$A_o = \frac{-G_F Q^2}{4\pi\alpha\sqrt{2}} \tag{68d}$$

$$\frac{A_{PV}^{1^*}}{A_o} = Q_W^p + \Box_{\gamma Z}(E_{Lab}) + Q^2\ \mathcal{B}(Q^2) \tag{69}$$

$$A_{PV}^{1^*} = A_{PV}^1 + A_o\ \Box_{\gamma Z}(E_{Lab}) \tag{70}$$

	Q-Weak	P2
E_{lab} (GeV)	1.154	0.155
$\Box_{\gamma Z}$	0.0054 ± 0.0004	0.0012 ± 0.0001

Table 5: Estimated values for energy-dependent γ-Z box corrections (two-loop diagrams), for both Q-Weak and P2 experimental beam energies. (Values taken from [2]).

By Gaussian error propagation, the uncertainty due to adding γ Z box corrections [2] will propagate to the corrected parity-violating asymmetry $A_{PV}^{1^*}$ through equation 69, leading to eqn. 71. As we are extracting the value of the proton's weak charge by fitting our results for $A_{PV}^{1^*}$ at various Q^2 values and extrapolating down to $Q^2 = 0$, we will use the estimated uncertainty provided by least-squares fitting and χ^2 minimization procedure in Mathematica, which weights the results according to their associated errors. Additionally, we include the uncertainty from γ Z box corrections in the final error for Q_W^p, since the determined intercept value from the fitting is actually the sum of these terms. Ultimately we can see that just from the tree-level equation 8, the weak mixing angle is determined to a higher relative precision than Q_W^p, and we use eqn. 72 to estimate the associated uncertainty.

$$\Delta \frac{A_{PV}^{1^*}}{A_o} = \Delta \frac{A_{PV}^{1}}{A_o} + \Delta_{\Box\gamma Z} \tag{71}$$

$$\Delta \sin^2 \theta_W = \frac{\Delta Q_W^p}{4} \tag{72}$$

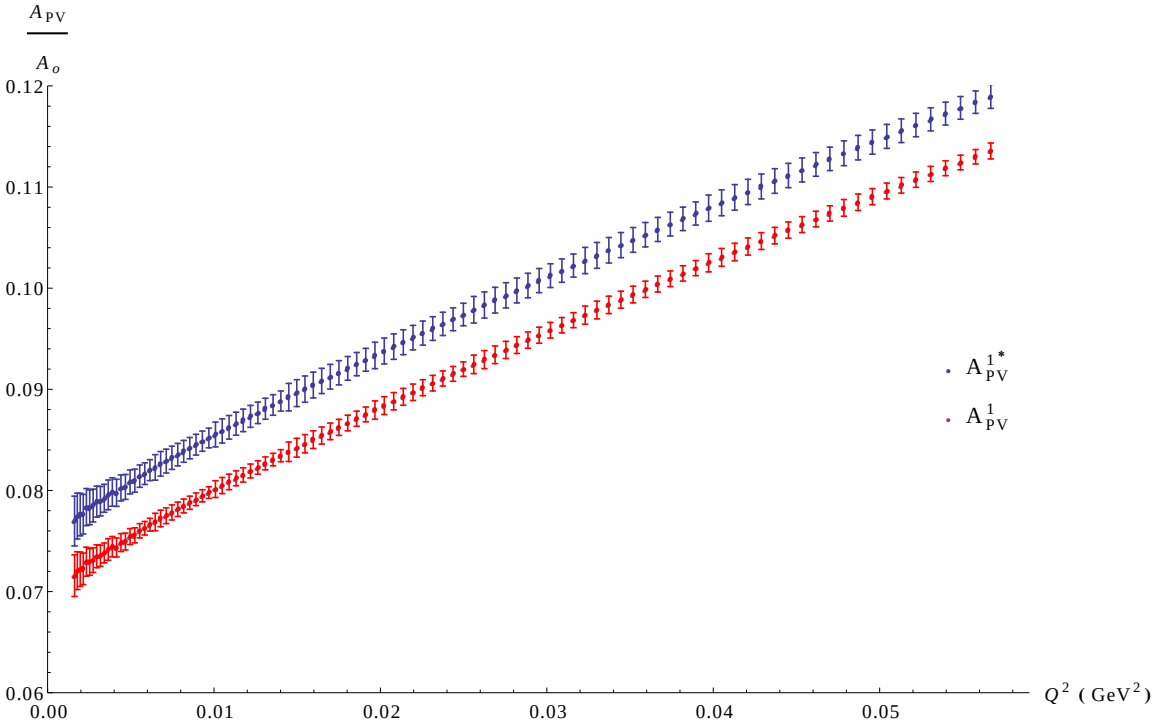

Fig. 21: One-loop and final corrected parity violating asymmetry, scaled by A_o, calculated at various values of momentum transfer ($E_{lab} = 1.154GeV$).

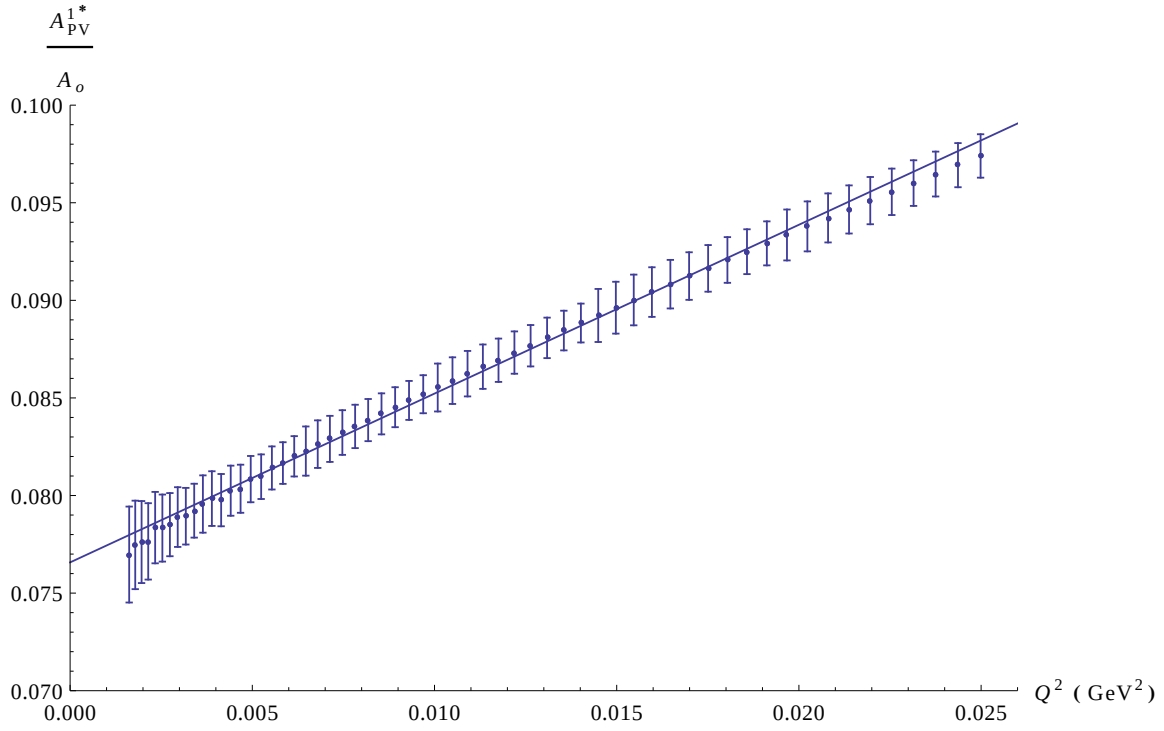

Fig. 22: Final corrected asymmetry, scaled by A_o, with partial linear fit extrapolating to zero momentum transfer corresponding to eqn. 69 ($E_{lab} = 1.154GeV$).

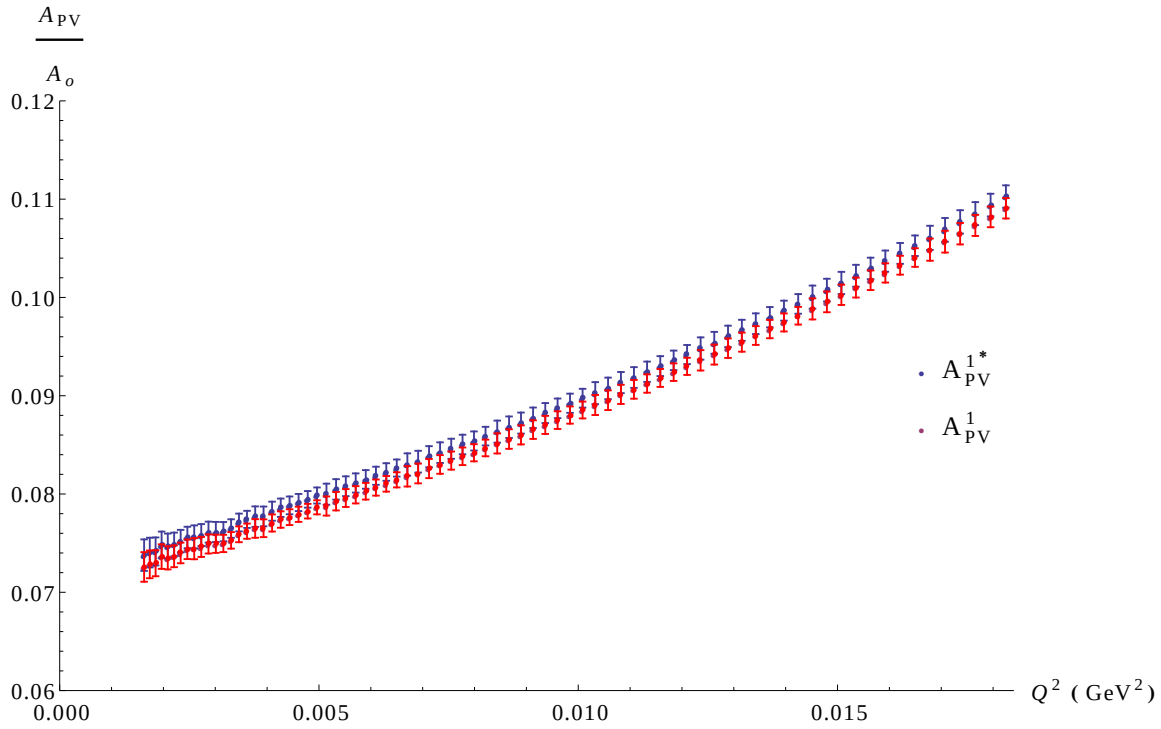

Fig. 23: One-loop and final corrected parity violating asymmetry, scaled by A_o, calculated at various values of momentum transfer ($E_{lab} = 0.155GeV$).

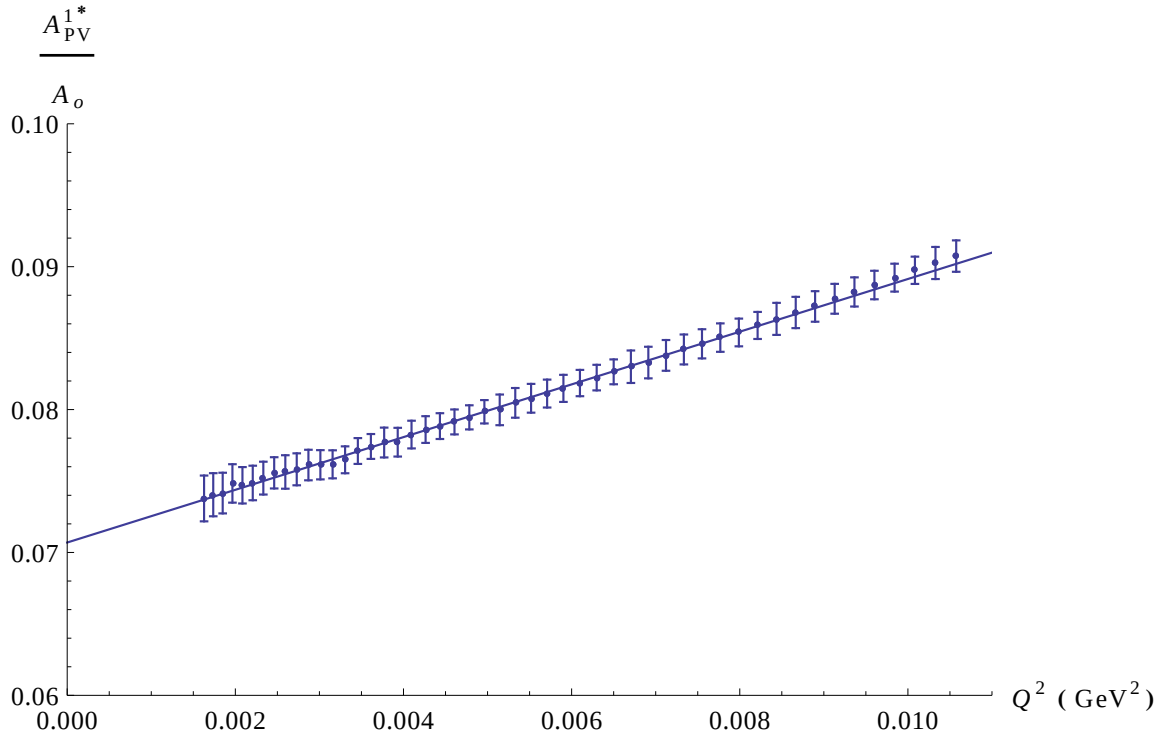

Fig. 24: Final corrected asymmetry, scaled by A_o, with partial linear fit extrapolating to zero momentum transfer corresponding to eqn. 69 ($E_{lab} = 0.155GeV$).

The benefit to measuring Q_W^p is the relatively small size of the coupling and the sensitivity to new physics beyond the standard model, making high precision determinations worthwhile. The underlying physics being probed is the running of the weak mixing angle $\sin^2\theta_W$ which is ultimately related to the proton's weak charge and the hadronic coupling parameters, as shown in eqn. 69 together with eqn. 73. Since the weak charge of the proton happens to be a suppressed quantity in the SM, it has extreme sensitivity to slight changes in the weak mixing angle. We want to account for the additional radiative corrections when calculating $\sin^2\theta_W$ since we

require high accuracy and precision, so rather than the tree level equation, we will use eqn. 73 when calculating the weak mixing angle [1]. In this notation, $\Delta_\Box$ is the energy-independent parts of the WW, ZZ, and γZ box diagram radiative corrections, ρ is the renormalization of neutral to charged current interactions at low energy, Δ_e and Δ'_e are corrections to the electron vertex. (Energy-dependent box corrections were already included in the final asymmetry before fitting).

$$4\sin^2\theta_W(Q^2=0) = 1 - \frac{Q_W^p - \Delta_\Box}{\rho + \Delta_e} + \Delta'_e \tag{73}$$

$\Delta_\Box = 0.02456$	$\rho = 1.00066$
Δ_e = -0.001161	Δ'_e = -0.001411

Table 6: Radiative correction parameters for the weak mixing angle determination, taken from [1].

	Q-Weak	P2
E_{lab} (GeV)	1.154	0.155
dE (GeV)	0.2	0.05
θ (deg)	7.9	25.5
Q^2 (GeV^2)	0.0249	0.0046
A_{PV}^0 (ppb)	-281.2	-47.32
A_{PV}^1 (ppb)	-206.7 ± 1.6	-32.29 ± 0.32
$A_{PV}^{1^*}$ (ppb)	-218.9 ± 2.5	-32.79 ± 0.36
Q_W^p	0.0711 ± 0.0008	0.0695 ± 0.0005
$\sin^2\theta_W(Q^2=0)$	0.2380 ± 0.0002	0.2384 ± 0.0001

Table 7: Tree level, one-loop, and final corrected results for the parity-violating asymmetry, as well as the weak charge of the proton and the weak mixing angle, for both Q-Weak and P2 average experimental parameters.

By comparing our final calculated results with experimental measurements (Table

2), we are ultimately testing the predictive power of the standard model and our methods, to high precision. The measured parity-violating asymmetry is a relatively small quantity (ppb), and is sensitive to new physics associated with the exchange of a Z boson mediating the weak force. So, the first order radiative corrections included along with tree level interactions were necessary to get high accuracy results in the final asymmetry determination. Additionally, we accounted for the energy dependent shift expected in our final results due to two-loop level γZ box corrections. We can see in table 7 that the one-loop corrected asymmetry has a difference of roughly 25% from the tree-level result, and our final results end up within the range of expected uncertainty for the Q-Weak measurement ($A_{PV} = -226.5 \pm 7.3$ ppb) reported in [1]. It should be noted that we did not perform an average over a range of scattering angles, as would be done in the experimental measurement of the asymmetry, but instead chose the average Q^2 value to compute the final results. Since the weak charge of the proton is a fundamental quantity and is defined at zero momentum transfer, the final result would not depend on the kinematics of the experiment. The most precise measurement we have to date is from the Q-Weak experiment ($Q_W^p = 0.0719 \pm 0.0045$), which puts a constraint on our theoretical model. The model should agree with experimental observations within a small range of estimated uncertainty, and the calculations should be high-precision in order to notice any slight discrepancies. Our calculated values for the proton's weak charge (table 7)

are consistent with the experimental measurement within the accepted range of uncertainty, which demonstrates the extreme accuracy of the Standard Model theoretical framework. The same is true for the comparison of our calculated weak mixing angles with the Q-Weak measurement ($\sin^2\theta_W(Q^2 = 0) = 0.2382 \pm 0.0011$), when taking into account the additional radiative corrections, as in equations 69 and 73. As we are using approximate methods, using form factors to account for the substructure of the proton, and only consider effects up to next-to-leading-order (i.e. one loop corrections), we expect that many interactions are left out of our calculations, and there still may be new weakly-interacting particles which are not being accounted for in the SM. However, we can still accurately predict the parity-violating asymmetry and the proton's weak charge using our approximate methods with a precision of about 7%, which is the level of statistical uncertainty in the Q-Weak experimental results. There is a better chance of finding new physics and inconsistencies in the results by narrowing the range of uncertainty and going to lower energies, so the P2 experiment is highly anticipated as the next best evaluation of the SM.

4.3 Z' Boson

In the search for new physics beyond the Standard Model (SM), there is a possibility of discovering particles that were previously unaccounted for. If our high precision theoretical calculations do not account for all experimental findings, it may

be reasonable to assume a new particle or interaction is being left out of the equation [42]. We have considered the so-called 'dark' Z' boson [43] as a possible new addition to the fundamental particles within the SM, and we investigate the effects on the calculated parity-violating asymmetry and weak-charge of the proton. The 'dark' or hidden nature of Z' is due to the possible unseen interactions with dark matter, and also its close relation to the usual Z vector boson, characterized by the mixing term (ϵ_Z) in eqn. 74. Here, we have chosen to constrain the mixing by setting the variable $\delta^2 = 3 \times 10^{-5}$, and we expect the mass of the Z' boson to be relatively small ($M_{Z'} \ll M_Z$) [42]. In terms of coupling, the Z' boson is essentially acts a modified Z boson mediating the weak force, with induced coupling to an electromagnetic current. Referring back to the Feynman rules for fermion and proton coupling in fig. 10 and eqn. 10, we modify each of the electromagnetic and weak interaction contributions with multiplicative factors ϵ and ϵ_Z respectively. Also, referring back to the proton form factors (equation 11) used in our high-precision calculations, we redefine a convenient set for the Z' interaction in eqn. 75. Since ϵ_Z is set by the mass of the Z' particle, we only have two new variables which can be tuned to control the interaction strengths (i.e. ϵ and $M_{Z'}$). By comparing the theoretical predictions with experimental results, we could either confirm or rule out the possibility of a 'dark' Z' boson with specific ranges for these variables.

$$\epsilon_Z = \frac{M_{Z'}}{M_Z}\delta \tag{74}$$

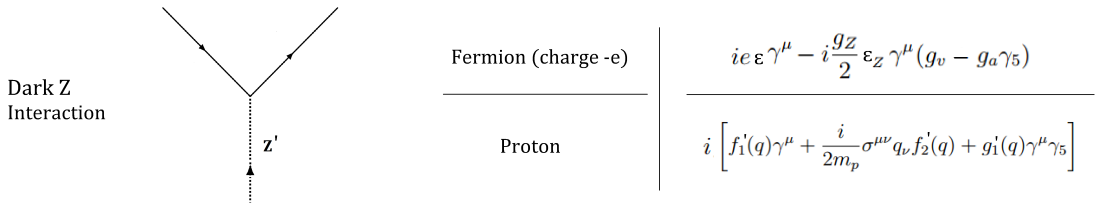

Fig. 25: Vertex factors (coupling) for the new theoretical Z' boson interactions with both the electron and proton.

$$f_1^{'} = e\epsilon F_1 + g_Z\epsilon_Z f_1 \tag{75a}$$

$$f_2^{'} = e\epsilon F_2 + g_Z\epsilon_Z f_2 \tag{75b}$$

$$g_1^{'} = g_Z\epsilon_Z g_1 \tag{75c}$$

As in the previous section, we have chosen to work with the average kinematics from Q-Weak and P2 experiments in order to calculate the parity-violating asymmetry for electron-proton scattering. We used the exact same calculation procedure for the tree level and one-loop corrected asymmetry as the original case, but with Z' interactions included in our model. We have considered 3 different sets of values for the Z' model-dependent parameters in order to investigate the effects of the new boson

included in our calculations. Each set of asymmetry results is labeled alphabetically, and the list of parameters is given below in table 8.

	(a)	(b)	(c)
$M_{Z'}$ (GeV)	1	0.18	6×10^{-4}
ϵ^2	3×10^{-6}	10^{-6}	10^{-2}

Table 8: Z' model parameters, i.e. mass and coupling constant, used for each set of calculations.

We can see by comparison with previous results that for the chosen set of variables, the asymmetry has not significantly changed with the addition of Z'. However, as the momentum transfer approaches zero, the scaled asymmetry ($\frac{A_{PV}}{A_o}$) has very different behaviors depending on the Z' model parameters, as seen in in figures 29 and 31. Since we are extracting the weak charge of the proton (Q_W^p) by extrapolation of this curve, there is high sensitivity to this new weakly interacting Z' boson. When the coupling is made increasingly larger, the scaled asymmetry ($\frac{A_{PV}}{A_o}$) begins to diverge as the momentum transfer approaches zero, producing a nonsensical result for the proton's weak charge. So, high precision experimental measurements and theoretical calculations put constraints on the accepted range of values for Q_W^p, thus limiting the range of reasonable values for ϵ and $M_{Z'}$.

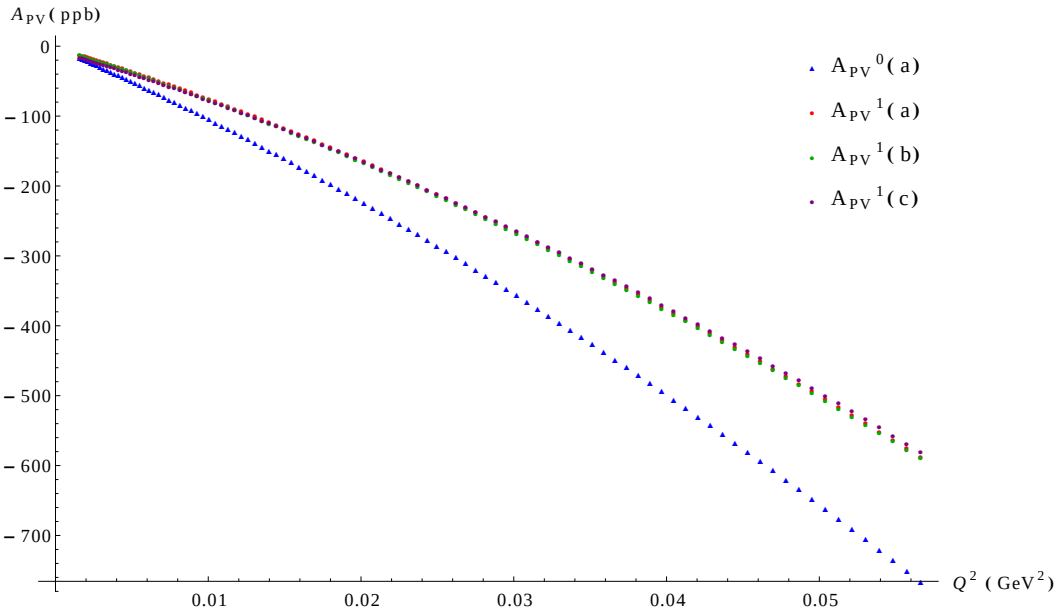

Fig. 26: Tree-level and one-loop calculated parity violating asymmetry, including theoretical Z' boson, for different values of momentum transfer ($E_{lab} = 1.154GeV$).

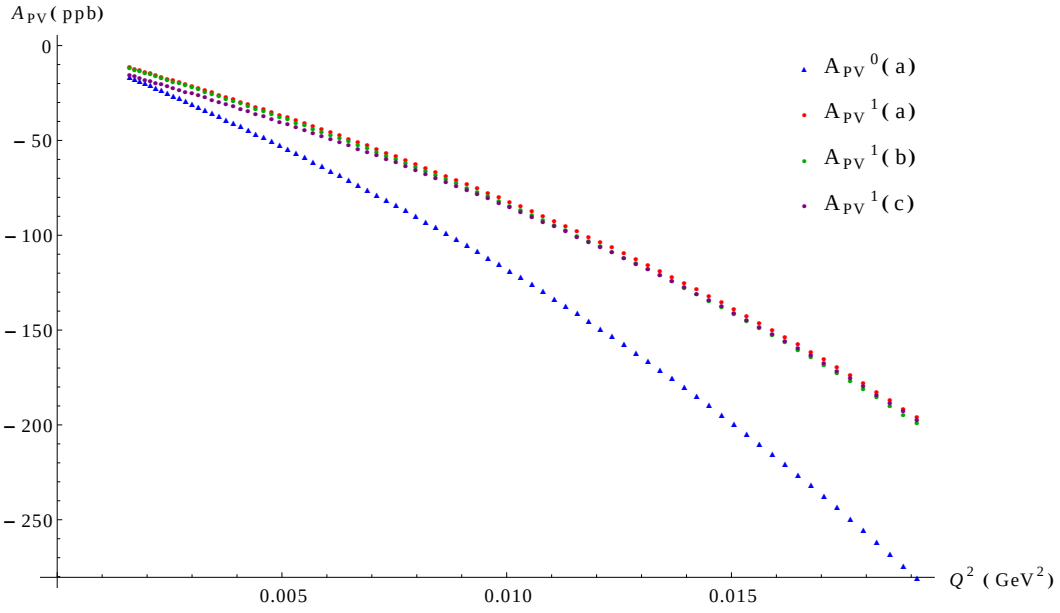

Fig. 27: Tree-level and one-loop calculated parity violating asymmetry, including theoretical Z' boson, for different values of momentum transfer ($E_{lab} = 0.155GeV$).

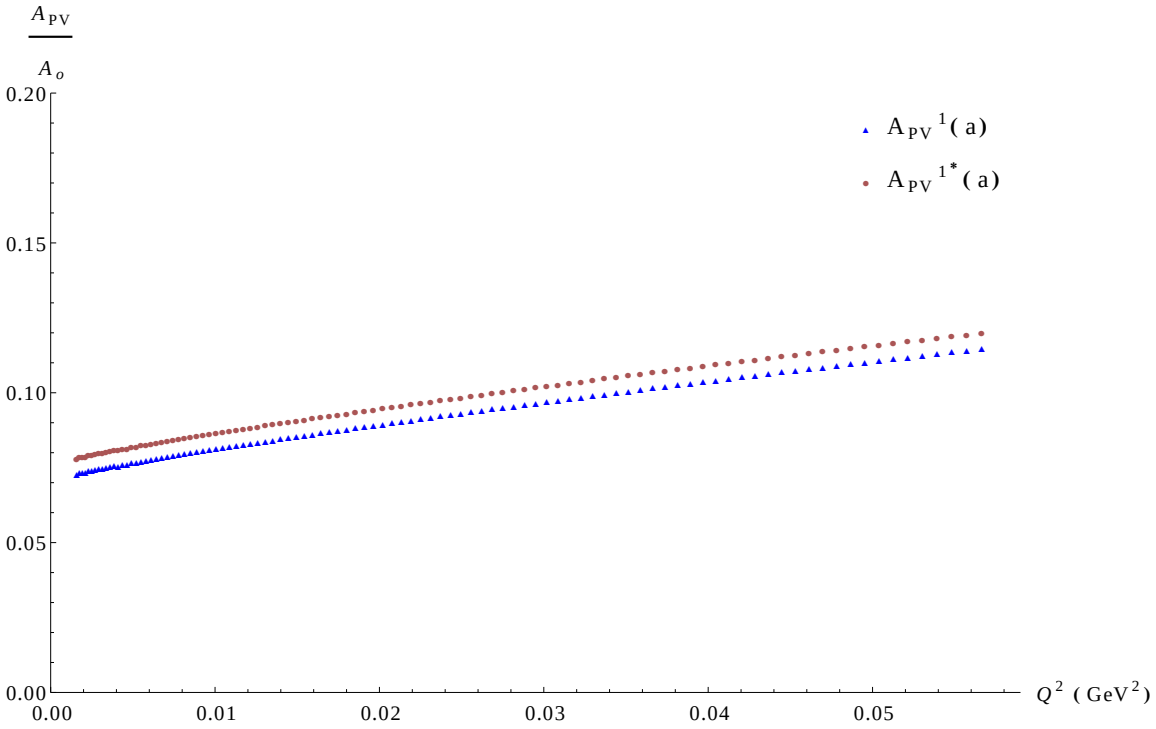

Fig. 28: One-loop and final corrected parity violating asymmetry, scaled by A_o, including theoretical Z' boson, for a range of momentum transfer values ($E_{lab} = 1.154GeV$).

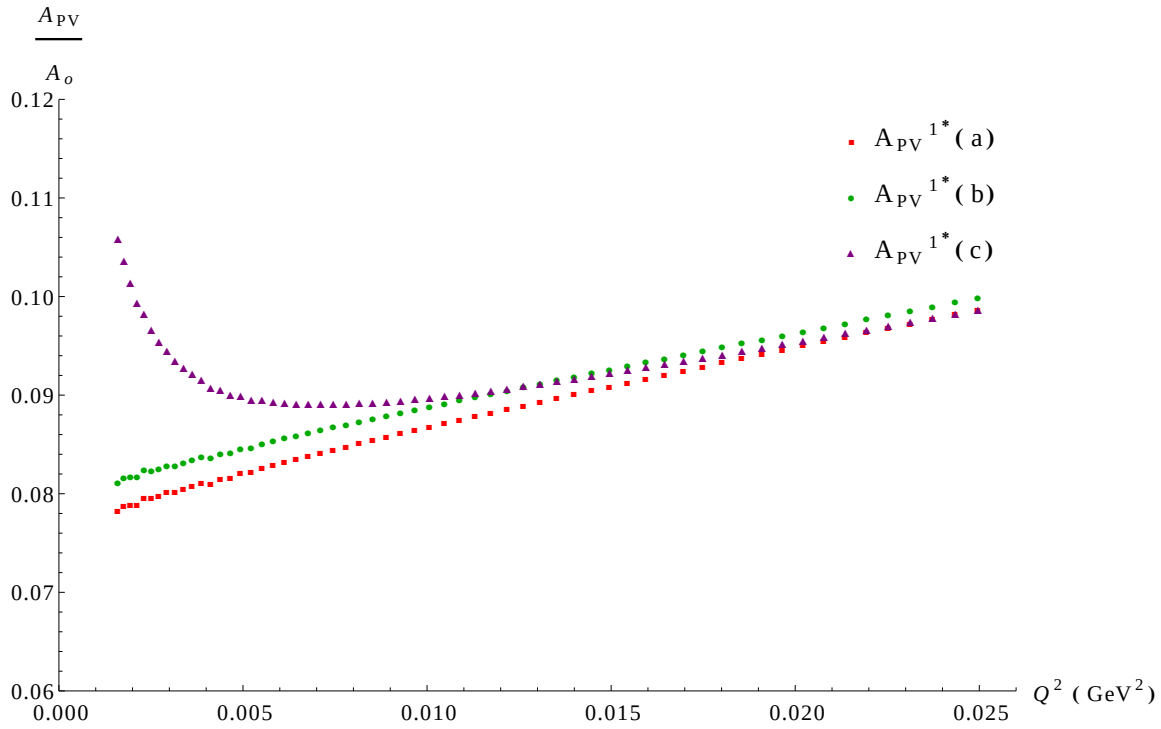

Fig. 29: Final corrected parity violating asymmetry, scaled by A_o, including theoretical Z' boson with 3 sets of input parameters, for a range of momentum transfer values ($E_{lab} = 1.154 GeV$).

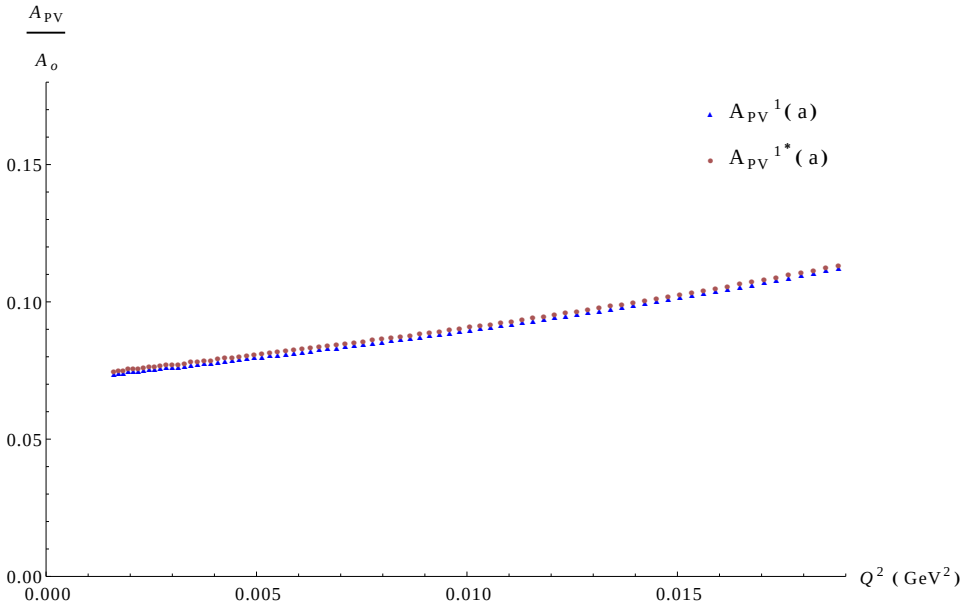

Fig. 30: One-loop and final corrected parity violating asymmetry, scaled by A_o, including theoretical Z' boson, for a range of momentum transfer values ($E_{lab} = 0.155GeV$).

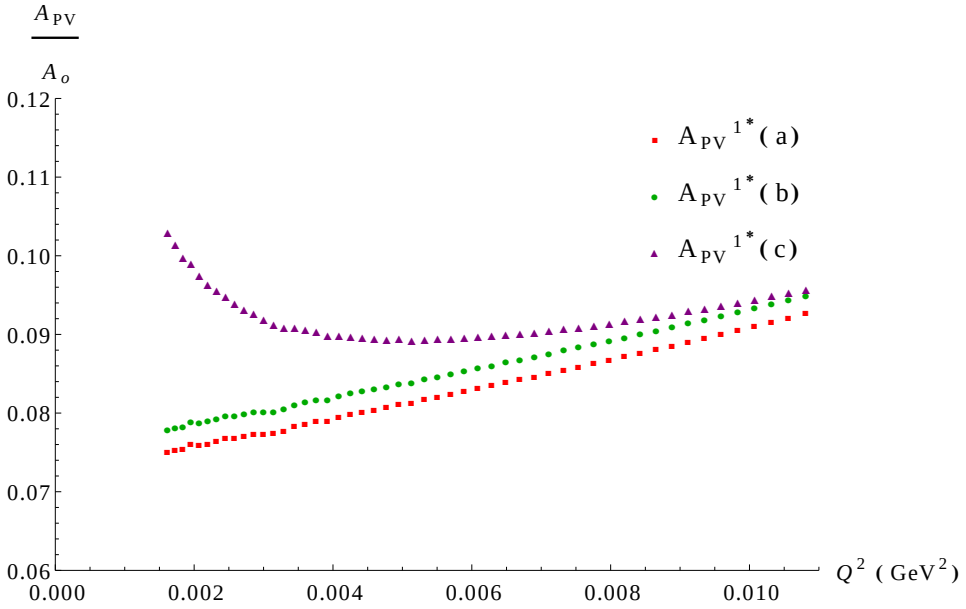

Fig. 31: Final corrected parity violating asymmetry, scaled by A_o, including theoretical Z' boson with 3 sets of input parameters, for a range of momentum transfer values ($E_{lab} = 0.155GeV$).

In order to determine the possible range for both variables which characterize the Z' interactions, we can make a 3-dimensional color plot showing the change in calculated one-loop asymmetry (A^1_{PV}). In this way, each point on the 2-D plane is an individual calculation for the asymmetry, and is colored based on the percent difference relative to the original result without Z' included (table 7). So, points without color agree within 1% of the original value, blue dots represent up to 2% change, green dots represent up to 3.5% change, and red dots represent greater than 3.5% change. These exclusion plots (figures 32 and 33) show that for smaller values of $M_{Z'}$ and ϵ the asymmetry results are not significantly altered, as expected. However, with larger values of mass and coupling constant ϵ, the results for parity-violating asymmetry start to deviate dramatically, and are clearly not in agreement with experimental observations. The most interesting region occurs where the asymmetry is only slightly changed (up to 2%) by the Z' interaction, around $M_{Z'} \approx 0.5GeV$ for a range of small coupling constant values ($\epsilon^2 \approx 10^-6$).

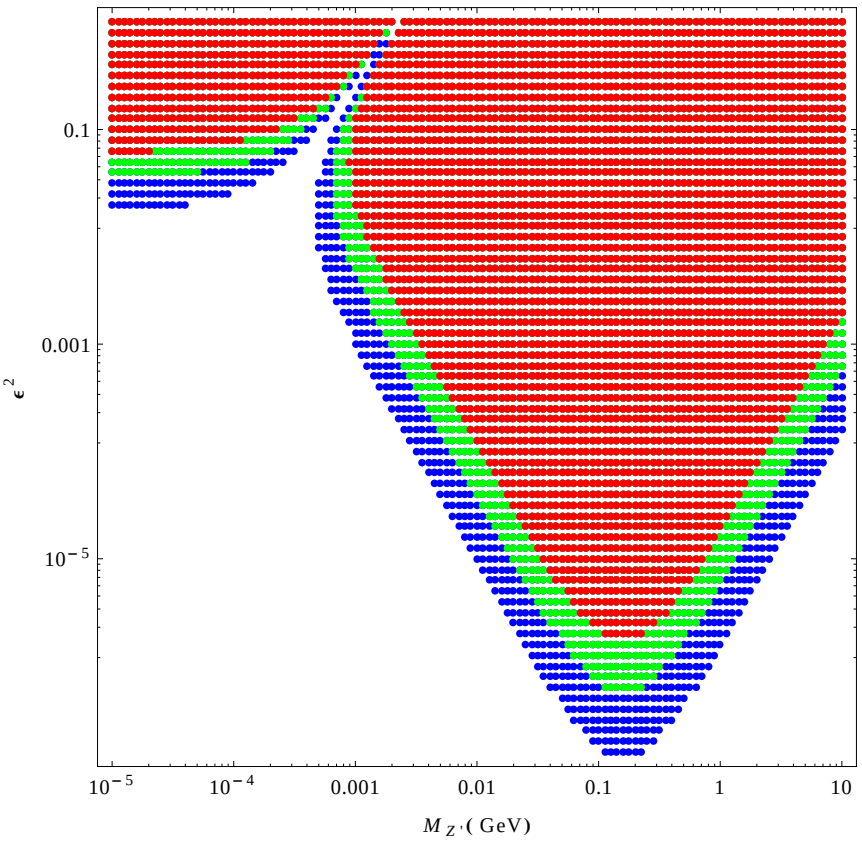

Fig. 32: Exclusion plot for the final corrected asymmetry depending on theoretical Z' boson characteristics (mass and coupling parameters). The colored points (blue, green, red) indicate $> 1\%$, $> 2\%$, and $> 3.5\%$ difference (respectively) with the original calculated asymmetry (A_{PV} = -218.9 ppb) when $E_{lab} = 1.154 GeV$, $\theta = 7.9°$.

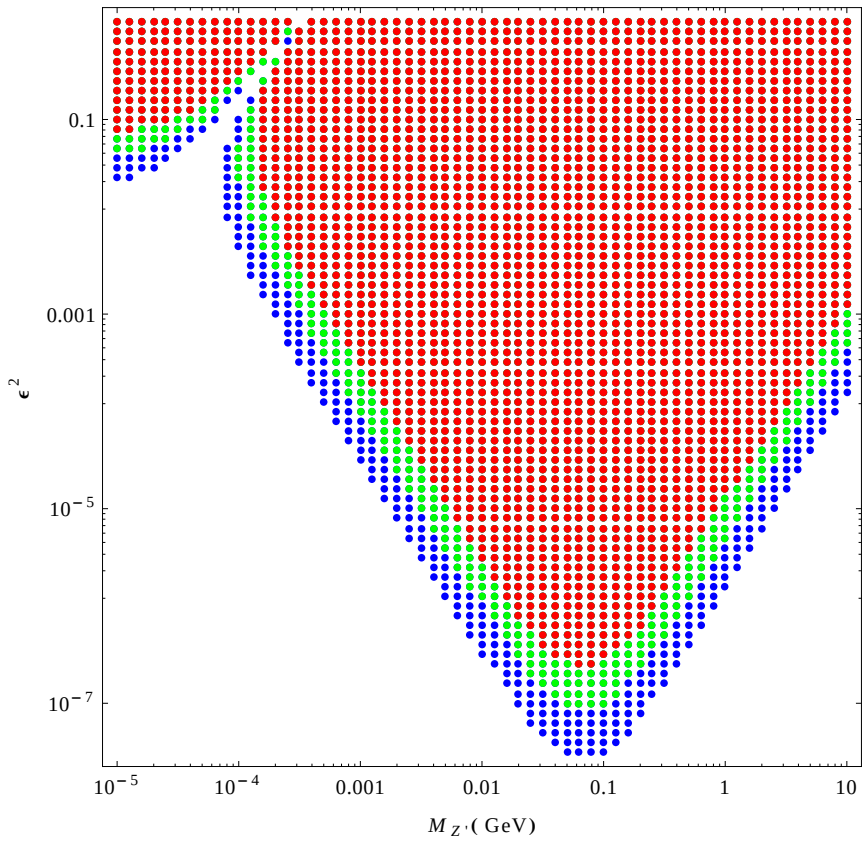

Fig. 33: Exclusion plot for the one-loop parity violating asymmetry depending on theoretical Z' boson characteristics (mass and coupling parameters). The colored points (blue, green, red) indicate $> 1\%$, $> 2\%$, and $> 3.5\%$ difference (respectively) with the original one-loop asymmetry (A_{PV} = -32.79 ppb) when $E_{lab} = 0.155GeV$, $\theta = 25.5°$.

Our high precision calculations combined with the small uncertainties in the Q-Weak and P2 experiments, allows for the exclusion of various combinations of Z' model parameters which produce inconsistent results. For Q-weak, the experimental statistical uncertainty is just over 3%, and the expectation is that precision for the upcoming P2 experiment will be even better due to the chosen kinematics. As previously discussed, the parity violating asymmetry and fundamental weak charge of

the proton are highly sensitive to new physics due to the precise predictions made by the SM, and our theoretical model must ultimately account for all experimental measurements. We can see in figures 29 and 31 that the extrapolation down to $Q^2 = 0$, and thus the value calculated for the proton's weak charge, can change significantly for different values of the Z' parameters even when the asymmetry is not drastically affected. There are various other research groups which have come up with constraints on coupling and mass parameters, in order to enforce agreement with other experimental observations which could fit within the theory.

5 Conclusion

We have reviewed the fundamental concepts of particle physics and the Standard model, and shown the need for high-precision calculations in order to test our theories against ever-improving experimental measurements. Electron scattering experiments are useful for probing specific interactions between particles, and characterizing underlying coupling properties. We can take advantage of the unique parity-violation of the weak force and measure the asymmetry in polarized electron-proton scattering, in order to investigate the exchange of the Z boson, rather than the more dominant electromagnetic (EM) interaction. This measurement has been carried out at low energy in the Q-Weak experiment [1] and will be repeated at even lower energies by the P2 experiment [19], thus providing a need for highly accurate theoretical analysis of the full interaction. Ultimately, using the energy dependence of the asymmetry, we can extract the proton's weak charge (Q_W^p) and the fundamental weak mixing angle (θ_W) which characterizes the mixing of EM and weak forces through their fundamental coupling constants. In our research, we used semi-empirical form factors to account for the substructure of the proton, thus treating it like a point particle. We also accounted for the first order radiative corrections to the asymmetry, using Mathematica software. The FeynArts [36, 37], FormCalc [39, 40], and LoopTools [41] packages were extremely valuable in visualizing and evaluating all relevant Feynman diagrams, and calculating the one-loop integrals. We explicitly include the vertex cor-

rections for the leptonic current, and the boson self-energy loops, which were shown to be necessary in getting accurate results for the relatively small asymmetry. We also crucially account for low energy bremsstrahlung using the soft-photon approximation [4], limiting the energy of emitted photons below a detector limited threshold (dE). We have shown that the dependence on this added parameter in the final asymmetry can be suppressed by using an exponential scaling and a first order Taylor expansion (fig. 17), without significantly altering the calculated asymmetry. We compared the Q^2 dependence of our final results for the tree level and one-loop asymmetry, using the kinetic parameters from Q-weak and P2 experiments (figs. 19, 20). We added an estimate of the γ-Z box (i.e. two-loop) corrections to the proton's weak charge, from [2], in order to account for the shift in asymmetry 70. We were able to determine Q_W^p by fitting the corrected asymmetry to a straight line equation (69), extrapolating down to $Q^2 = 0$ (figs. 22, 24). We require high accuracy and precision in our results for $\sin^2\theta_W$, so we account for additional radiative corrections (eqn. 73) using calculated parameters from [1]. We specifically used the average Q^2 values from the Q-Weak and P2 experiments for our final results in table 7 in order to compare with the experimental measurements. In order to determine the uncertainty in the calculated results, we used the observed change in calculated one-loop asymmetry as the mass parameter for the W boson was varied within a reasonable range, and took the estimated uncertainty for Q_W^p from the least-squares fit statistics. We ultimately

showed that we can accurately calculate the parity-violating asymmetry and the proton's weak charge to high precision using our theoretical model. Finally, we repeated all asymmetry calculations including a theoretical dark Z boson (Z') in our model, with two new variables which can be tuned to control the interaction strengths (i.e. ϵ and $M_{Z'}$). Since Q_W^p happens to be a suppressed quantity, it is highly sensitive to new physics and to variations in the weak mixing angle. We saw that although the values of asymmetry were not drastically altered with the addition of Z', the behaviour of the scaled asymmetry as Q^2 approaches 0 depends greatly on the interaction parameters chosen (figs. 29, 31). We also made exclusion plots (figs. 32, 33) in order to visualize the 2-D parameter space in terms of change to the one-loop corrected asymmetry. There are combinations of ϵ and $M_{Z'}$ which can readily be excluded from possible models, since the calculated asymmetry would be inconsistent with experimental observations. In future work, it will be useful to have full experimental measurements completed for P2, and perhaps an exclusion plot involving the proton's weak charge rather than the asymmetry could be made to explore the coupling parameter phase space, since Q_W^p is more sensitive to the possibility of new physics.

6 Appendix

The following sections provide explicit details on the Mathematica code and methods used in the one-loop calculations of the parity-violating asymmetry. This includes the full list of Feynman diagrams, the soft-photon bremsstrahlung factor calculations, and the underlying FeynArts models.

6.1 Feynman Rules

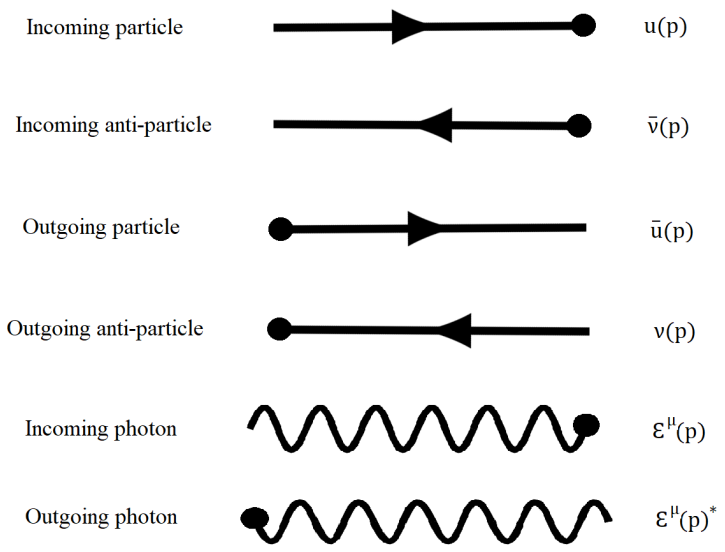

Fig. 34: Feynman rules for various types of external lines

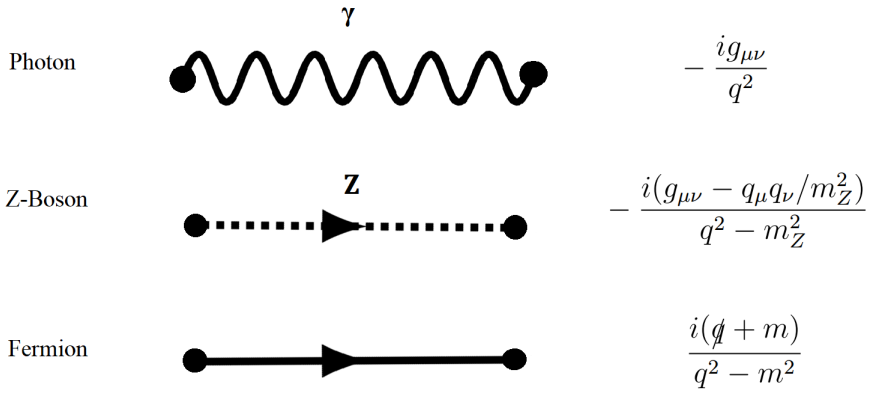

Fig. 35: Feynman rules for various types of internal lines (i.e. propagators)

6.2 Mathematica Code

Essential parts of script used in order to calculate the one-loop asymmetry.

```
<< FeynArts`

FeynArts 3.9 (23 Sep 2015)
by Hagen Eck, Sepp Kueblbeck, and Thomas Hahn

<< FormCalc`

FormCalc 8.4
by Thomas Hahn
last revised 30 Mar 15

(*Generate possible topologies based on interaction
 type and number of loops (adjacencies) included*)
t1tree := CreateTopologies[0, 2 → 2]
t1SE := CreateTopologies[1, 2 → 2,
  ExcludeTopologies → {WFCorrections, Tadpoles, AllBoxes, Triangles}]
t1SECT := CreateCTTopologies[1, 2 → 2,
  ExcludeTopologies → {WFCorrectionCTs, TadpoleCTs, AllBoxCTs, TriangleCTs}]
t1TRI := CreateTopologies[1, 2 → 2,
  ExcludeTopologies → {WFCorrections, Tadpoles, AllBoxes, SelfEnergies}]
t1TRICT := CreateCTTopologies[1, 2 → 2,
  ExcludeTopologies → {WFCorrectionCTs, TadpoleCTs, AllBoxCTs, SelfEnergyCTs}]

(*Insert desired fields into the topology list,
based on the interacting particle types and the underlying model files*)
t2tree := InsertFields[t1tree, {F[2, {1}], P[1]} → {F[2, {1}], P[1]},
  InsertionLevel → {Particles}, ExcludeParticles → {S, V[3]},
  Model → "SM_Proton", GenericModel → "Lorentz_Proton"]
t2SE1 := InsertFields[t1SE, {F[2, {1}], P[1]} → {F[2, {1}], P[1]},
  InsertionLevel → {Particles}, ExcludeParticles → {},
  Model → "SM_Proton", GenericModel → "Lorentz_Proton"]
t2SE := DiagramDelete[t2SE1, {108 ...  111}]
t2SECT := InsertFields[t1SECT, {F[2, {1}], P[1]} → {F[2, {1}], P[1]},
  InsertionLevel → {Particles}, ExcludeParticles → {},
  Model → "SM_Proton", GenericModel → "Lorentz_Proton"]
t2TRI1 := InsertFields[t1TRI, {F[2, {1}], P[1]} → {F[2, {1}], P[1]},
  InsertionLevel → {Particles}, ExcludeParticles → {},
  Model → "SM_Proton", GenericModel → "Lorentz_Proton"]
t2TRI := DiagramDelete[t2TRI1, {1 ...  5}]
t2TRICT := InsertFields[t1TRICT, {F[2, {1}], P[1]} → {F[2, {1}], P[1]},
  InsertionLevel → {Particles}, ExcludeParticles → {},
  Model → "SM_Proton", GenericModel → "Lorentz_Proton"]

(*Set various options to suit the desired interaction*)
SetOptions[InsertFields, InsertionLevel → {Particles}]
SetOptions[CalcFeynAmp, FermionChains → Chiral, FermionOrder → None]

InsertFieldsHook[tops_, V[1] → V[1]] :=
```

```
 InsertFields[tops, V[1] → V[1], ExcludeParticles → {P[1]}]
InsertFieldsHook[tops_, V[1] → V[2]] :=
 InsertFields[tops, V[1] → V[2], ExcludeParticles → {P[1]}]
InsertFieldsHook[tops_, V[2] → V[2]] :=
 InsertFields[tops, V[2] → V[2], ExcludeParticles → {P[1]}]

(*Generating the complete expression
 for Feynman amplitudes of selected diagrams*)
amptree = CreateFeynAmp[t2tree];
ampSE = CreateFeynAmp[t2SE];
ampSECT = CreateFeynAmp[t2SECT];
ampTRI = CreateFeynAmp[t2TRI];
ampTRICT = CreateFeynAmp[t2TRICT];

(*Calculation and algebraic simplification of the Feynman amplitudes*)
stufftree = CalcFeynAmp[amptree];
stuffSE = CalcFeynAmp[ampSE];
stuffSECT = CalcFeynAmp[ampSECT];
stuffTRI = CalcFeynAmp[ampTRI];
stuffTRICT = CalcFeynAmp[ampTRICT];

(*Calculation of the modulus squared tree level amplitude and the next-to-leading-
 order one-loop corrections (quadratic corrections not included). Replacement
  of subexpressions and abbreviations in the final form*)
(*Set helicity of all particles for unpolarized, R or L*)
Hel[1] = 0;
Hel[2] = 0;
Hel[3] = 0;
Hel[4] = 0;
Mog2tree = SquaredME[stufftree, stufftree] //.
     HelicityME[stufftree, stufftree] //. Subexpr[] //. Abbr[];
Mog2SE = SquaredME[stufftree, stuffSE] //. HelicityME[stufftree, stuffSE] //.
    Subexpr[] //. Abbr[];
Mog2SECT = SquaredME[stufftree, stuffSECT] //. HelicityME[stufftree, stuffSECT] //.
    Subexpr[] //. Abbr[];
Mog2TRI = SquaredME[stufftree, stuffTRI] //. HelicityME[stufftree, stuffTRI] //.
    Subexpr[] //. Abbr[];
Mog2TRICT = SquaredME[stufftree, stuffTRICT] //.
     HelicityME[stufftree, stuffTRICT] //. Subexpr[] //. Abbr[];

(*Calculating and simplifying the
 renormalization constants for the counter terms*)
renconstSE = CalcRenConst[ampSECT];
renconstTRI = CalcRenConst[ampTRICT];

(*Implement FormCalc tool for kinetics,
and install LoopTools to evaluate integrals*)
<< /home//Desktop/FeynInstall/FormCalc-8.4/tools/kin2to2.m
```

```
Install["LoopTools"]

(*Final calculation of the cross section, in distinct parts. *)
sigma0tree := Mog2tree
sigma0SE := Mog2SE + Mog2SECT //. renconstSE;
sigma0TRI := Mog2TRI + Mog2TRICT //. renconstTRI;

sigma0 := sigma0tree * (1 + B) + 2 * Re[sigma0SE] + 2 * Re[sigma0TRI]

(*Calculation of the parity-violating asymmetry*)
(*R and L indicate right and left polarized incident electrons in the calculation
 (helicity set to 1 or -1 respectively, 0 indicates unpolarized elections*)
SetMudim[10^0]
SetLambda[10^0]
SetDelta[10^0]
```

$$\text{AsymmB} = 10^9 * 4 * \frac{\text{sigmaRtree} - \text{sigmaLtree}}{2 * 4 * \text{sigma0tree}}$$

$$\text{Asymm1} = 10^9 * 4 * \frac{\text{sigmaR} - \text{sigmaL}}{2 * 4 * \text{sigma0}}$$

$$\text{sigma0e} = \text{sigma0tree} * E\text{^}\left(\frac{\text{sigma0}}{\text{sigma0tree}} - 1\right)$$

$$\text{sigmaRe} = \text{sigmaRtree} * E\text{^}\left(\frac{\text{sigmaR}}{\text{sigmaRtree}} - 1\right)$$

$$\text{sigmaLe} = \text{sigmaLtree} * E\text{^}\left(\frac{\text{sigmaL}}{\text{sigmaLtree}} - 1\right)$$

$$\text{Asymm1e} = 10^9 * 4 * \frac{\text{sigmaRe} - \text{sigmaLe}}{2 * 4 * \text{sigma0e}}$$

```
(*Bremsstrahlung calculation for soft-
 photon approximation in centre of mass reference-frame*)
(*No bremstrahlung contribution from hadronic current*)
Charge[1] := -1
Charge[2] := 0
Charge[3] := -1
Charge[4] := 0
kn[n_] := Vec[k[n]]
dE := 0.05 (*photon cut-off*)

xx[i_, j_] := Pair[kn[i], kn[j]]
x[i_] := Pair[kn[i], kn[3]] + Pair[kn[i], kn[4]]
Λ := m[3]^2 + m[4]^2 + 2 * Pair[kn[3], kn[4]]

R[i_, j_] := 2 * Pi / γ[i, j] * (A1[i, j] + B2[i, j])

A1[i_, j_] := Log[α[i, j] * m[i] / m[j]] * Log[4 * dE^2 / GetLambda[]]

B2[i_, j_] := Log[β[i] / (m[i] * Sqrt[Λ])]^2 - Log[β[j] / (m[j] * Sqrt[Λ])]^2 +
   PolyLog[2, 1 - β[i] * l[i, j] / (Λ * γ[i, j])] + PolyLog[2, 1 - m[i]^2 * l[i, j] / (β[i] * γ[i, j])] -
   PolyLog[2, 1 - β[j] * l[i, j] / (α[i, j] * Λ * γ[i, j])] - PolyLog[2, 1 - m[j]^2 * l[i, j] / (α[i, j] * β[j] * γ[i, j])]

α[i_, j_] := (xx[i, j] + γ[i, j]) / m[i]^2

l[i_, j_] := α[i, j] * x[i] - x[j]

β[i_] := x[i] + Sqrt[x[i]^2 - m[i]^2 * Λ]

γ[i_, j_] := Sqrt[xx[i, j]^2 - m[i]^2 * m[j]^2]

Z[1, 1] := 2 * Pi / m[1]^2 * (Log[4 * dE^2 / GetLambda[]] - 2 * x[1] / Sqrt[x[1]^2 - m[1]^2 * Λ] * Log[β[1] / (m[1] * Sqrt[Λ])])

Z[2, 2] := 2 * Pi / m[2]^2 * (Log[4 * dE^2 / GetLambda[]] - 2 * x[2] / Sqrt[x[2]^2 - m[2]^2 * Λ] * Log[β[2] / (m[2] * Sqrt[Λ])])

Z[3, 3] := 2 * Pi / m[3]^2 * (Log[4 * dE^2 / GetLambda[]] - 2 * x[3] / Sqrt[x[3]^2 - m[3]^2 * Λ] * Log[β[3] / (m[3] * Sqrt[Λ])])

Z[4, 4] := 2 * Pi / m[4]^2 * (Log[4 * dE^2 / GetLambda[]] - 2 * x[4] / Sqrt[x[4]^2 - m[4]^2 * Λ] * Log[β[4] / (m[4] * Sqrt[Λ])])
```

$$B = \frac{Alfa}{(2 * Pi)^2} * \left[-Charge[1]^2 * Mass2[1] * Z[1, 1] - Charge[2]^2 * Mass2[2] * Z[2, 2] - Charge[3]^2 * Mass2[3] * Z[3, 3] - Charge[4]^2 * Mass2[4] * Z[4, 4] + 2 * (Charge[1] * Charge[3] * Pair[kn[1], kn[3]] * R[1, 3] + Charge[1] * Charge[4] * Pair[kn[1], kn[4]] * R[1, 4] + Charge[2] * Charge[3] * Pair[kn[2], kn[3]] * R[2, 3] + Charge[2] * Charge[4] * Pair[kn[2], kn[4]] * R[2, 4] - Charge[3] * Charge[4] * Pair[kn[3], kn[4]] * R[3, 4] - Charge[1] * Charge[2] * Pair[kn[1], kn[2]] * R[1, 2]) \right]$$

```
(*Particle masses in GeV*)
MN := 0.938272081
mp := MN
MPP := MN
ME := 0.000510998928
MZ := 91.1876
MW := 80.379
MH := 125.6
MU := 4.3 * 10^-3
MD := 7.5 * 10^-3
MM := 105.658357 * 10^-3
ML := 1777.03 * 10^-3
MC := 1.25
MB := 4.2
MT := 174.3
MS := 0.125

(*Relevant constants*)
Elab := 1.154 (*0.155*)
ecms := Sqrt[Mass[1]^2 + Mass[2]^2 + 2 * Mass[2] * Elab]

CW := Sqrt[CW2]
CW2 := MW2 / MZ2
SW := Sqrt[SW2]
SW2 := 1 - (MW2 / MZ2)
tau := -T / (4 * MN2)
Alfa := 1 / 137.035999
Alfa2 := Alfa * Alfa
Acc = 20;


(*Electric form factor of the proton*)
SetPrecision[pe1 = -0.4980, Acc];
SetPrecision[pe2 = 5.4592, Acc];
SetPrecision[pe3 = -34.7281, Acc];
SetPrecision[pe4 = 124.3173, Acc];
SetPrecision[pe5 = -262.9808, Acc];
SetPrecision[pe6 = 329.1395, Acc];
SetPrecision[pe7 = -227.3306, Acc];
SetPrecision[pe8 = 66.6980, Acc];
GPE := (1 - T / (0.71))^(-2)
 (**(1-pe1*T+pe2*(T)^2-pe3*T^3+pe4*T^4-pe5*T^5+pe6*T^6-pe7*(T)^7+pe8*T^8)*);

(*Magnetic form factor of the proton*)
SetPrecision[pm1 = 0.2472, Acc];
```

```
SetPrecision[pm2 = -4.9123, Acc];
SetPrecision[pm3 = 29.7509, Acc];
SetPrecision[pm4 = -84.0430, Acc];
SetPrecision[pm5 = 129.3256, Acc];
SetPrecision[pm6 = -111.1068, Acc];
SetPrecision[pm7 = 49.9753, Acc];
SetPrecision[pm8 = -9.1659, Acc];
GPM := 2.792847356 * (1 - T / (0.71)) ^ (-2)
 (**(1-pm1*T+pm2*T^2-pm3*T^3+pm4*T^4-pm5*T^5+pm6*T^6-pm7*T^7+pm8*T^8))*);

(*Electric form factor of the neutron*)
SetPrecision[ne1 = 2.28409, Acc];
SetPrecision[ne2 = 4.41942, Acc];
GNE := (-ne1 * T / 4 / mp^2 / (1 - ne2 * T / 4 / mp^2)) * (1 - T / (0.71)) ^ (-2);

(*Magnetic form factor of the neutron*)
SetPrecision[nm1 = -1.9147, Acc];
SetPrecision[nm2 = 6.47767, Acc];
SetPrecision[nm3 = -17.32918, Acc];
SetPrecision[nm4 = 31.80021, Acc];
SetPrecision[nm5 = -37.18707, Acc];
SetPrecision[nm6 = 27.52359, Acc];
SetPrecision[nm7 = -12.81713, Acc];
SetPrecision[nm8 = 3.63457, Acc];
SetPrecision[nm9 = -0.57277, Acc];
SetPrecision[nm10 = 0.03843, Acc];
GNM := nm1 - nm2 * T + nm3 * T^2 - nm4 * T^3 +
    nm5 * T^4 - nm6 * T^5 + nm7 * T^6 - nm8 * T^7 + nm9 * T^8 - nm10 * T^9;

(*Strangeness form factors*)
(* Pate et al., PRC78, taken from P. Larin, BA, section 5.3 *)
SetPrecision[ps = -0.071, Acc];
SetPrecision[GSM0 = 0.053, Acc];
GSE1 := -ps * T / 4 / mp^2;
GSM1 := GSM0;
(* Wang et al, PRC79, taken from P. Larin, BA, section 5.3 *)
GSE2 := -0.32267 * T / 4 / mp^2 / (1 - 4.686 * T / 4 / mp^2) * (1 - T / 0.71) ^ (-2);
GSM2 := 0.044 - 0.93 * T;
(* Choose one option: GS*1 or GS*2 *)
GSE := GSE2;
GSM := GSM2;

(*Dirac and Pauli form factors*)
F1proton := (tau * GPM + GPE) / (1 + tau)

F2proton := (GPM - GPE) / (1 + tau)
```

```
F1neutron := (tau * GNM + GNE) / (1 + tau)

F2neutron := (GNM - GNE) / (1 + tau)

F1strange := (tau * GSM + GSE) / (1 + tau)

F2strange := (GSM - GSE) / (1 + tau)

F1Zproton :=
  4 * (((1/2 - SW2) * (F1proton - F1neutron)/2 - SW2 * (F1proton + F1neutron)/2 - 1/4 * F1strange))

F2Zproton :=
  4 * (((1/2 - SW2) * (F2proton - F2neutron)/2 - SW2 * (F2proton + F2neutron)/2 - 1/4 * F2strange))

G1proton := 1.267 * (1 - T / (1.014) ^ 2) ^ (-2)

(*Proton couplings corresponding to model file*)
GLG := F1proton
GRG := F1proton
F2G := F2proton / 2 / MN / 2
F2Z := -F2Zproton / (2 * MN) / 4 / SW / CW / 2
GLZ := -(F1Zproton + G1proton) / (4 * SW * CW)
GRZ := -(F1Zproton - G1proton) / (4 * SW * CW)

(*Additional Z' coupling parameters and input parameters*)
F1ZZproton := eps * F1proton + epsZZ * 4 *
    (((1/2 - SW2) * (F1proton - F1neutron)/2 - SW2 * (F1proton + F1neutron)/2 - 1/4 * F1strange)) /
     (4 * SW * CW)

F2ZZproton := eps * F2proton + epsZZ * 4 *
    (((1/2 - SW2) * (F2proton - F2neutron)/2 - SW2 * (F2proton + F2neutron)/2 - 1/4 * F2strange)) /
     (4 * SW * CW)

G1ZZproton := epsZZ * G1proton / (4 * SW * CW)

F2ZZ := -F2ZZproton / (2 * MN) / 2
GLZZ := -(F1ZZproton + G1ZZproton)
GRZZ := -(F1ZZproton - G1ZZproton)
```

```
epsZZ := del * MZZ / MZ
del := Sqrt[3 * 10^-5]

MZZ = 1;
```

$$\text{eps} = \sqrt{3 * 10^{-6}}\ ;$$

6.3 One-loop Feynman diagrams

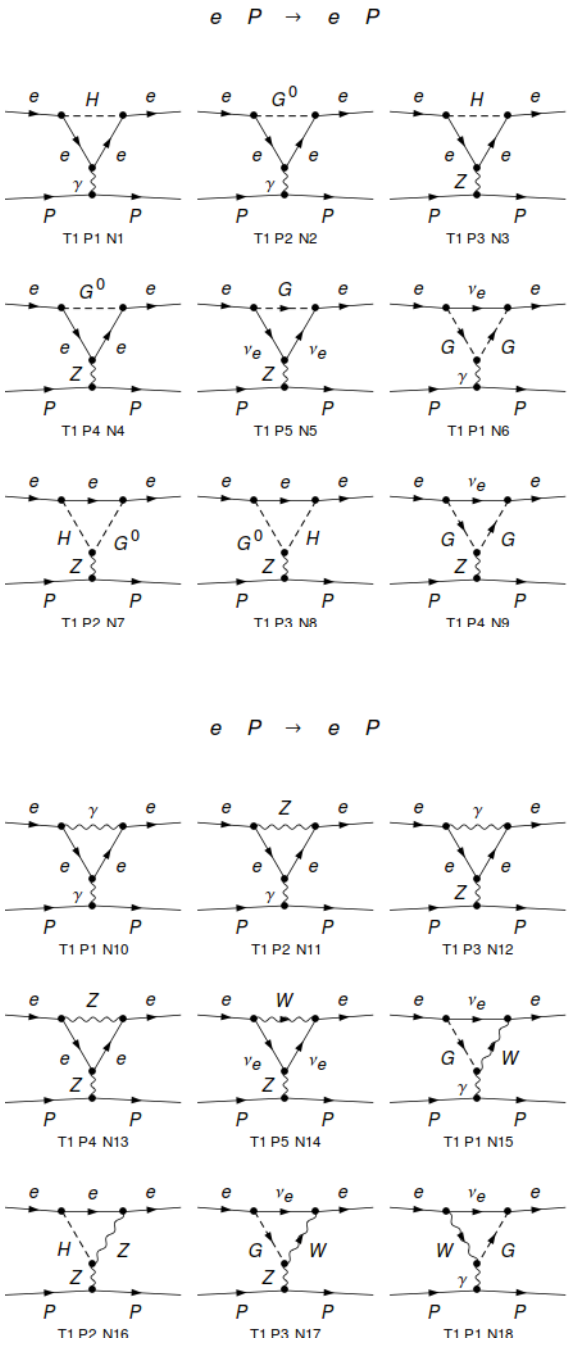

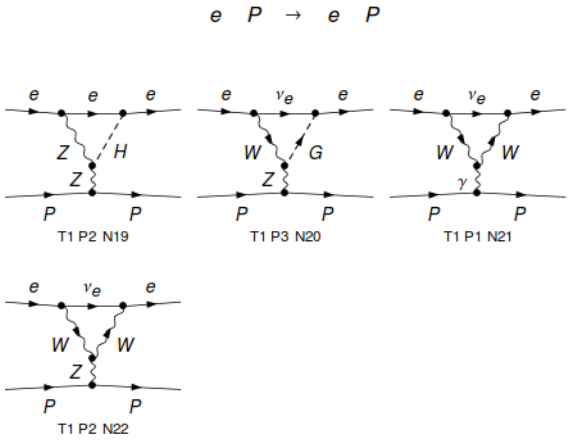

Fig. 36: Lepton vertex triangle diagrams

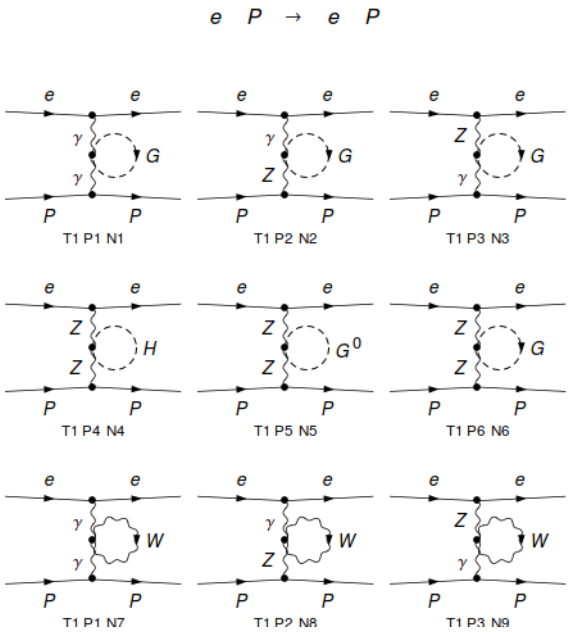

$e\ P \rightarrow e\ P$

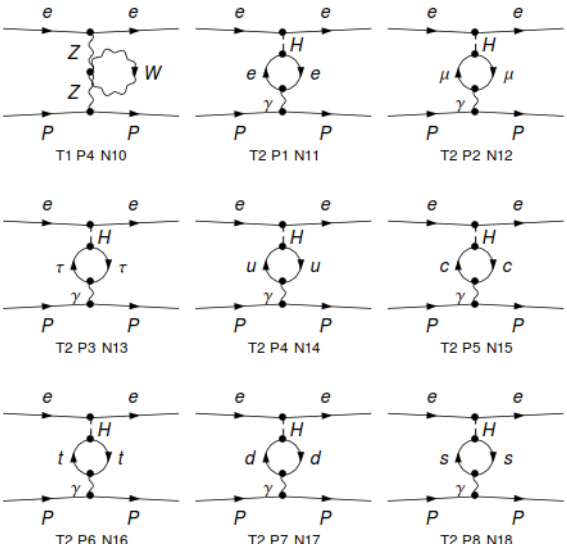

$e\ P \rightarrow e\ P$

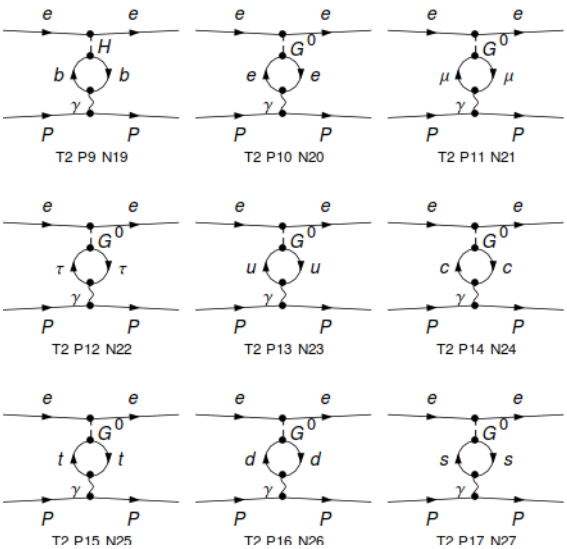

$e\ P \rightarrow e\ P$

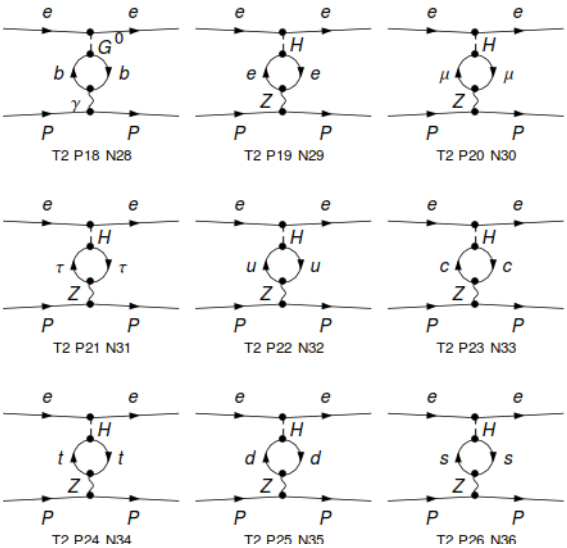

$e\ P \rightarrow e\ P$

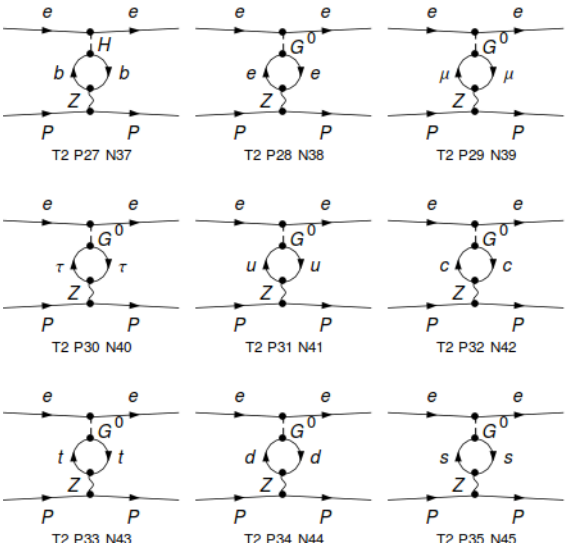

$e \quad P \quad \rightarrow \quad e \quad P$

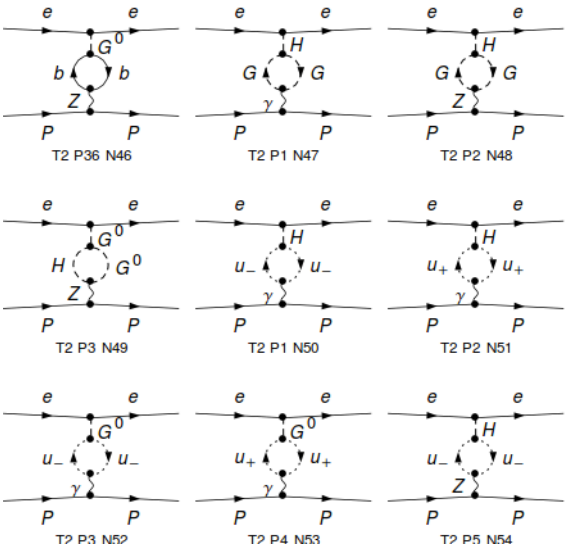

$e \quad P \quad \rightarrow \quad e \quad P$

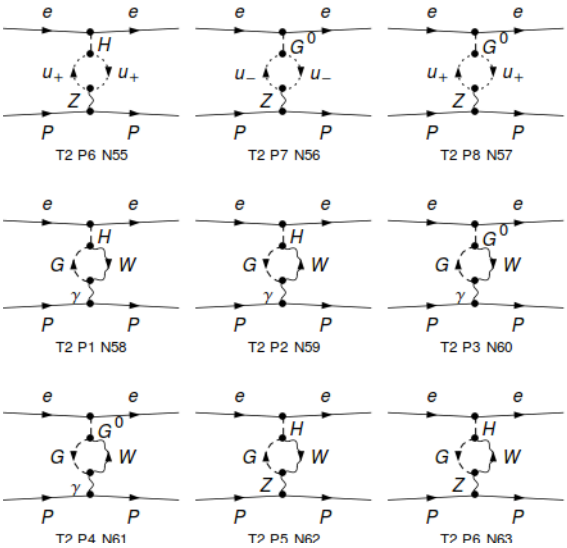

$e\ P \rightarrow e\ P$

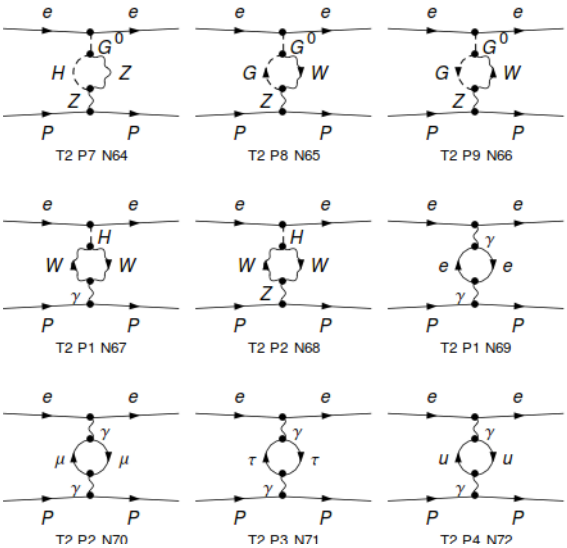

$e\ P \rightarrow e\ P$

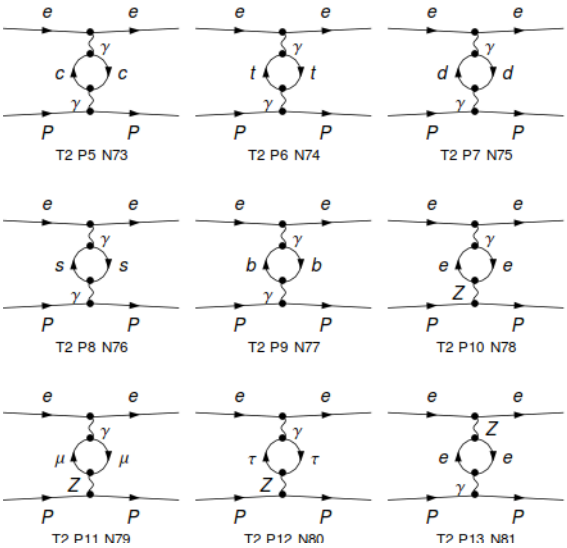

$e\ P \rightarrow e\ P$

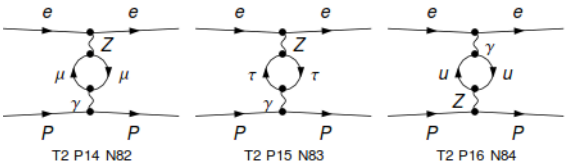

T2 P14 N82 T2 P15 N83 T2 P16 N84

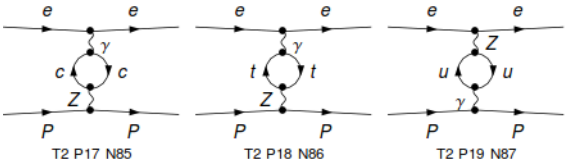

T2 P17 N85 T2 P18 N86 T2 P19 N87

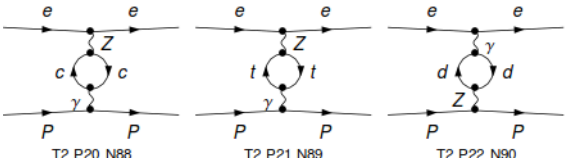

T2 P20 N88 T2 P21 N89 T2 P22 N90

$e\ P \rightarrow e\ P$

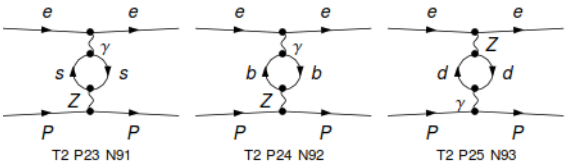

T2 P23 N91 T2 P24 N92 T2 P25 N93

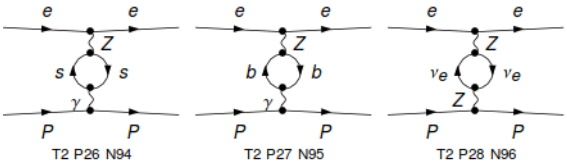

T2 P26 N94 T2 P27 N95 T2 P28 N96

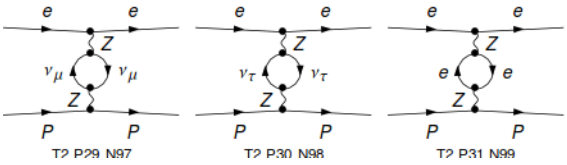

T2 P29 N97 T2 P30 N98 T2 P31 N99

$e\ P \to e\ P$

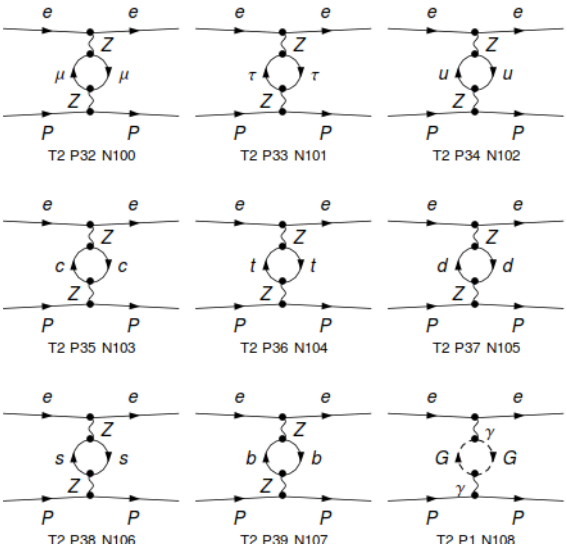

$e\ P \to e\ P$

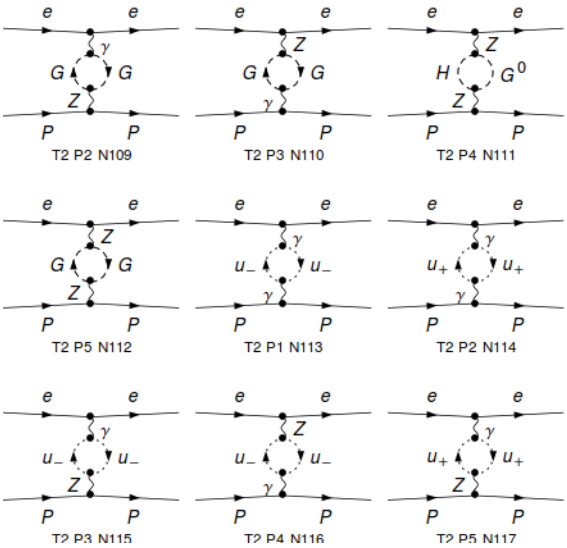

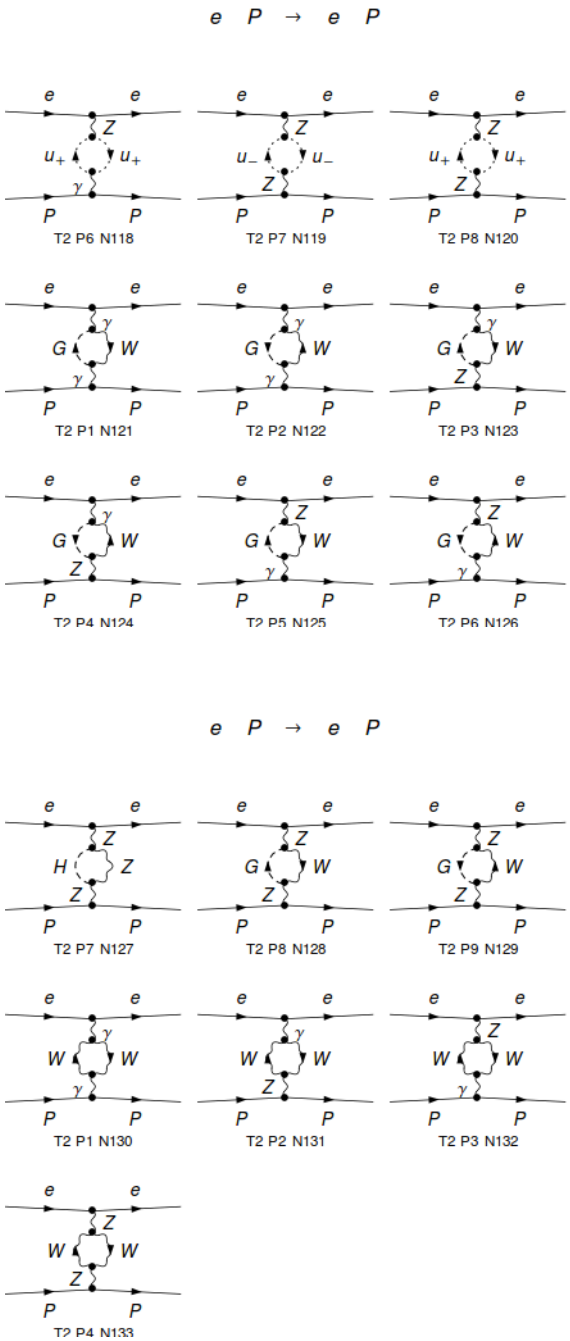

Fig. 37: Boson self-energy diagrams

7 References

[1] The Jefferson Lab Qweak Collaboration, "Precision measurement of the weak charge of the proton," *Nature*, vol. 557, pp. 207–211, may 2018.

[2] N. L. Hall, P. G. Blunden, W. Melnitchouk, A. W. Thomas, and R. D. Young, "Quark-hadron duality constraints on γZ box corrections to parity-violating elastic scattering," *Physics Letters, Section B: Nuclear, Elementary Particle and High-Energy Physics*, vol. 753, pp. 221–226, 2016.

[3] Particle Data Group, M. Tanabashi, *et al.*, "Review of particle physics," *Phys. Rev. D*, vol. 98, p. 030001, Aug 2018.

[4] L. W. Mo and Y. S. Tsai, "Radiative Corrections to Elastic and Inelastic e-p and u-p Scattering," *Reviews of Modern Physics*, vol. 41, pp. 205–235, jan 1969.

[5] L. C. Maximon and J. A. Tjon, "Radiative corrections to electron-proton scattering," *Physical Review C - Nuclear Physics*, vol. 62, no. 5, p. 17, 2000.

[6] J. Erler, A. Kurylov, and M. J. Ramsey-Musolf, "Weak charge of the proton and new physics," *Physical Review D*, vol. 68, p. 016006, jul 2003.

[7] S. Barkanova, A. Aleksejevs, and P. G. Blunden, "Radiative corrections and parity-violating electron-nucleon scattering," pp. 1–21, dec 2002.

[8] J. Erler and S. Su, "The weak neutral current," *Progress in Particle and Nuclear Physics*, vol. 71, pp. 119–149, jul 2013.

[9] A. Denner, "Techniques for the calculation of electroweak radiative corrections at the one-loop level and results for W-physics at LEP200," *Fortschritte der Physik/Progress of Physics*, vol. 41, pp. 307–420, sep 2007.

[10] N. Kaiser, "Radiative corrections to leptonlepton scattering revisited," *Journal of Physics G: Nuclear and Particle Physics*, vol. 37, p. 115005, nov 2010.

[11] A. Aleksejevs, S. Barkanova, Y. Kolomensky, E. Kuraev, and V. Zykunov, "Quadratic electroweak corrections for polarized Møller scattering," *Physical Review D - Particles, Fields, Gravitation and Cosmology*, vol. 85, no. 1, 2012.

[12] A. Aleksejevs, S. Barkanova, P. Blunden, and N. Deg, "Electroweak Hard Photon Bremsstrahlung in Electron-Nucleon Scattering," jul 2007.

[13] C. S. Epstein and R. G. Milner, "QED radiative corrections to low-energy Møller and Bhabha scattering," *Physical Review D*, vol. 94, p. 033004, aug 2016.

[14] P. Blunden, W. Melnitchouk, and J. Tjon, "Two-photon exchange in elastic electron-proton scattering," *The European Physical Journal A*, vol. 24, pp. 59–63, feb 2005.

[15] H. Q. Zhou, C. W. Kao, and S. N. Yang, "Two-Photon-Exchange and γ Z-Exchange Corrections to Parity-Violating Elastic Electron-Proton Scattering," *Physical Review Letters*, vol. 99, p. 262001, dec 2007.

[16] A. G. Aleksejevs, S. G. Barkanova, Y. M. Bystritskiy, E. A. Kuraev, and V. A. Zykunov, "Two-loop electroweak vertex corrections for polarized Møller scattering," *Physics of Particles and Nuclei Letters*, vol. 13, pp. 310–317, may 2016.

[17] A. Aleksejevs, S. Barkanova, and V. Zykunov, "Two-Loop Effects in Low-Energy Electroweak Measurements," *Nuclear and Particle Physics Proceedings*, vol. 273-275, pp. 2259–2264, 2016.

[18] A. Afanasev, P. Blunden, D. Hasell, and B. Raue, "Two-photon exchange in elastic electronproton scattering," *Progress in Particle and Nuclear Physics*, vol. 95, pp. 245–278, jul 2017.

[19] D. Becker *et al.*, "The P2 Experiment - A future high-precision measurement of the electroweak mixing angle at low momentum transfer," feb 2018.

[20] J. Erler and R. Ferro-Hernndez, "Weak Mixing Angle in the Thomson Limit," *JHEP*, vol. 03, p. 196, 2018.

[21] A. G. Aleksejevs, S. G. Barkanova, A. N. Ilyichev, Y. G. Kolomensky, and V. A. Zykunov, "One-loop electroweak corrections for polarized Møller scattering at

different renormalization schemes and conditions," *Physics of Particles and Nuclei*, vol. 44, pp. 161–174, mar 2013.

[22] H. Spiesberger, R. Bucoveanu, and M. Gorchtein, "Precision Measurement of $\sin^2\theta_w$ at MESA," in *Proceedings of Loops and Legs in Quantum Field Theory PoS(LL2016)*, (Trieste, Italy), p. 061, Sissa Medialab, oct 2016.

[23] K. Kumericki, "Feynman Diagrams for Beginners," pp. 11–21, feb 2016.

[24] M. E. Peskin and D. V. Schroeder, *An Introduction to quantum field theory*. Reading, USA: Addison-Wesley, 1995.

[25] D. Griffiths, *Introduction to Elementary Particles*. Physics textbook, Wiley, 2008.

[26] J. C. Bernauer, *Measurement of the elastic electron-proton cross section and separation of the electric and magnetic form factor in the Q2 range from 0.004 to 1 (GeV=c)2*. Dissertation, 2010.

[27] P. Larin, *Voruntersuchungen fur ein neues Prazisionsexperiment zur Messung der schwachen Ladung des Protons*. Bachelor thesis, 2011.

[28] A. Denner and S. Dittmaier, "Reduction schemes for one-loop tensor integrals," *Nuclear Physics B*, vol. 734, no. 1-2, pp. 62–115, 2006.

[29] G. 't Hooft and M. Veltman, "Scalar one-loop integrals," *Nuclear Physics B*, vol. 153, pp. 365–401, jan 1979.

[30] A. Freitas, "Numerical multi-loop integrals and applications," *Progress in Particle and Nuclear Physics*, vol. 90, pp. 201–240, 2016.

[31] G. Passarino and M. Veltman, "One-loop corrections for e+e annihilation into μ+μ in the Weinberg model," *Nuclear Physics B*, vol. 160, pp. 151–207, nov 1979.

[32] A. C. Genz and A. A. Malik, "Remarks on algorithm 006: An adaptive algorithm for numerical integration over an N-dimensional rectangular region," *Journal of Computational and Applied Mathematics*, vol. 6, no. 4, pp. 295–302, 1980.

[33] L. C. Maximon, "The dilogarithm function for complex argument," *Proceedings of the Royal Society A: Mathematical, Physical and Engineering Sciences*, vol. 459, no. 2039, pp. 2807–2819, 2003.

[34] S. Mandelstam, "Determination of the Pion-Nucleon Scattering Amplitude from Dispersion Relations and Unitarity. General Theory," *Physical Review*, vol. 112, pp. 1344–1360, nov 1958.

[35] M. Benhamou and G. Mahoux, "Multiplicative renormalization of continuous polymer theories, in good and θ solvents, up to critical dimensions," *Journal de Physique*, vol. 47, no. 4, pp. 559–568, 1986.

[36] T. Hahn, "Generating Feynman diagrams and amplitudes with FeynArts 3," *Computer Physics Communications*, vol. 140, pp. 418–431, nov 2001.

[37] J. Küblbeck, M. Böhm, and A. Denner, "Feyn arts computer-algebraic generation of Feynman graphs and amplitudes," *Computer Physics Communications*, vol. 60, pp. 165–180, sep 1990.

[38] T. Hahn, *FeynArts 3.9 User ' s Guide*. 2015.

[39] T. Hahn, S. Paβehr, and C. Schappacher, "FormCalc 9 and Extensions," *Journal of Physics: Conference Series*, vol. 762, p. 012065, oct 2016.

[40] T. Hahn and T. Hahn, "FormCalc 9.3," 2016.

[41] T. Hahn and M. Pérez-Victoria, "Automated one-loop calculations in four and D dimensions," *Computer Physics Communications*, vol. 118, pp. 153–165, may 1999.

[42] A. Aleksejevs, S. Barkanova, S. Wu, and V. Zykunov, "New Physics Search with Precision Experiments: Theory Input," *Nuclear and Particle Physics Proceedings*, vol. 273-275, pp. 2249–2252, 2016.

[43] H. Davoudiasl, H. S. Lee, and W. J. Marciano, ""Dark" Z implications for parity violation, rare meson decays, and Higgs physics," *Physical Review D - Particles, Fields, Gravitation and Cosmology*, vol. 85, no. 11, 2012.